Australian Government

ansto

Nuclear-based science benefiting all Australians

Research Selections

2009

The Australian Nuclear Science and Technology Organisation (ANSTO) is the home of Australia's nuclear science expertise. This unique expertise is applied to radiopharmaceutical production and research, climate change research, water resource management, materials engineering, neutron scattering and a range of other scientific research disciplines.

ANSTO is a Federal Government agency and operates Australia's only nuclear reactor OPAL – used for research and isotope production. ANSTO applies nuclear science in a wide range of areas for the benefit of all Australians.

Accelerators are used to analyse materials – often using extremely small samples – to determine their elemental composition and age. ANSTO currently has two accelerators, ANTARES and STAR, both of which are used in ion beam analysis and accelerator mass spectrometry. Over the next four years, ANSTO will be establishing a Centre for Accelerator Science including adding two new accelerators, putting ANSTO at the forefront of this field worldwide. The new accelerators are a low energy multi-isotope accelerator mass spectrometer and a new medium-energy tandem accelerator.

ANSTO has also become a partner in a national accelerator collaboration – Australian Collaboration for Accelerator Science (ACAS) – aimed at maintaining state-of-the-art accelerator-based facilities and a world-class pool of accelerator scientists in Australia.

Table of Contents

Foreword

The important thing in science is not so much to obtain new facts as to discover new ways of thinking about them. *William Lawrence Bragg*

Each day at the Australian Nuclear Science and Technology Organisation (ANSTO) is an opportunity to do just that. The chance to see the world and play a role in shaping that world through the prisms of our science. To build on existing knowledge, discovered knowledge, shared knowledge, all offering profound insights into issues as fundamental as the deepest laws of nature through to the basic human factor of everyday issues including food, water and health.

And it is because of those everyday issues that impact ordinary people that ANSTO exists. ANSTO scientists and their collaborators have and continue to discover new information about the way the world works ranging from biology and health through to physics and material science. These discoveries allow for new ways to approach healthcare, our environment and our safety. Through state-of-the-art facilities ANSTO and the international research community advance and contribute to knowledge of how the world works, at the atomic level.

A quarter of ANSTO's employees are involved in research across a variety of fields

In the area of health, radiopharmaceutical and radiolabelling, techniques are being developed to diagnose and treat diseases such as cancer, and disorders such as Alzheimer's, Parkinson's and schizophrenia. Neutron and X-ray scattering methods are used to investigate and determine the structure of food-based systems, such as proteins, with direct applications to food processing and human nutrition. In materials science, researchers are aiming to design safer, smarter materials and examining the lifetime and integrity of existing materials in major infrastructure projects. They are also involved in national security, including forensics research. In the environmental arena, ANSTO scientists use nuclear-based techniques to understand and track climate change to provide practical, science based advice to decision makers.

Understanding the future means unlocking the past

For example, radiocarbon dating is one of the most reliable and well-established methods for dating artefacts from the past 50,000 years. The radiocarbon age of a sample is determined by measuring its ^{14}C concentration and by assuming a known level of atmospheric ^{14}C through time. Reporting high-precision, high-resolution atmospheric ^{14}C record from a Huon pine in Tasmania for improved radiocarbon calibration for the early Younger Dryas has provided insights into the implications for radiocarbon calibration and abrupt climate change.

Quality of life

In our life sciences work we are making advancements in understanding the neurobiological mechanisms involved in the onset of epilepsy through investigating the neuroinflammatory processes. Using our in-house radiotracer (^{18}F-PBR111), which is highly specific for receptors reflecting inflammatory tissue, has allowed us to map and quantify neuro-inflammation *in vivo*, and to correlate it with a full *in vitro* assessment of the neuroinflamation pattern.

Elucidating the role of the neurotransmitter dopamine through small-angle X-ray scattering, we have mapped a further step in the study of brain diseases such as Parkinson's. ANSTO has also shown how understanding complex food structures is essential in providing new insights into diet-related diseases.

Taking it to extremes

In the materials world, we have a new understanding of materials that shrink on heating. Through the study of the structure and dynamics of a metal organic framework compound, using neutron scattering and modelling methods, we find a new mechanism in which molecular groups twist locally, rather than collectively, offering the possibility of tuning the molecular mechanism to obtain the desired thermal-expansion characteristics.

ANSTO's quest for new knowledge is supported by collaboration, partnerships and state-of-the-art facilities to ensure that, as a public research organisation, we fulfill our mandate.

The following pages offer a cross selection of our research to illustrate how seriously we take our responsibility.

Dr Adi Paterson,
Chief Executive Officer
ANSTO

Climate and Environment

Climate and Environment

ANSTO is a centre of excellence in understanding how environmental systems function and interact and the impact that humans are having on the environment.

Our ability to understand, mitigate and adapt to climate change requires robust measurements and objective analysis. Our scientists collaborate with national and international partners in using nuclear and isotopic techniques to understand the role of natural variability and human impacts on water, air and Earth systems.

ANSTO has some of the best instruments in the world to do this work. These instruments are capable of showing us what the Earth was like millions of years ago, helping us to model and predict future climate change, manage our limited water resources and monitor air pollution and its effect on human health.

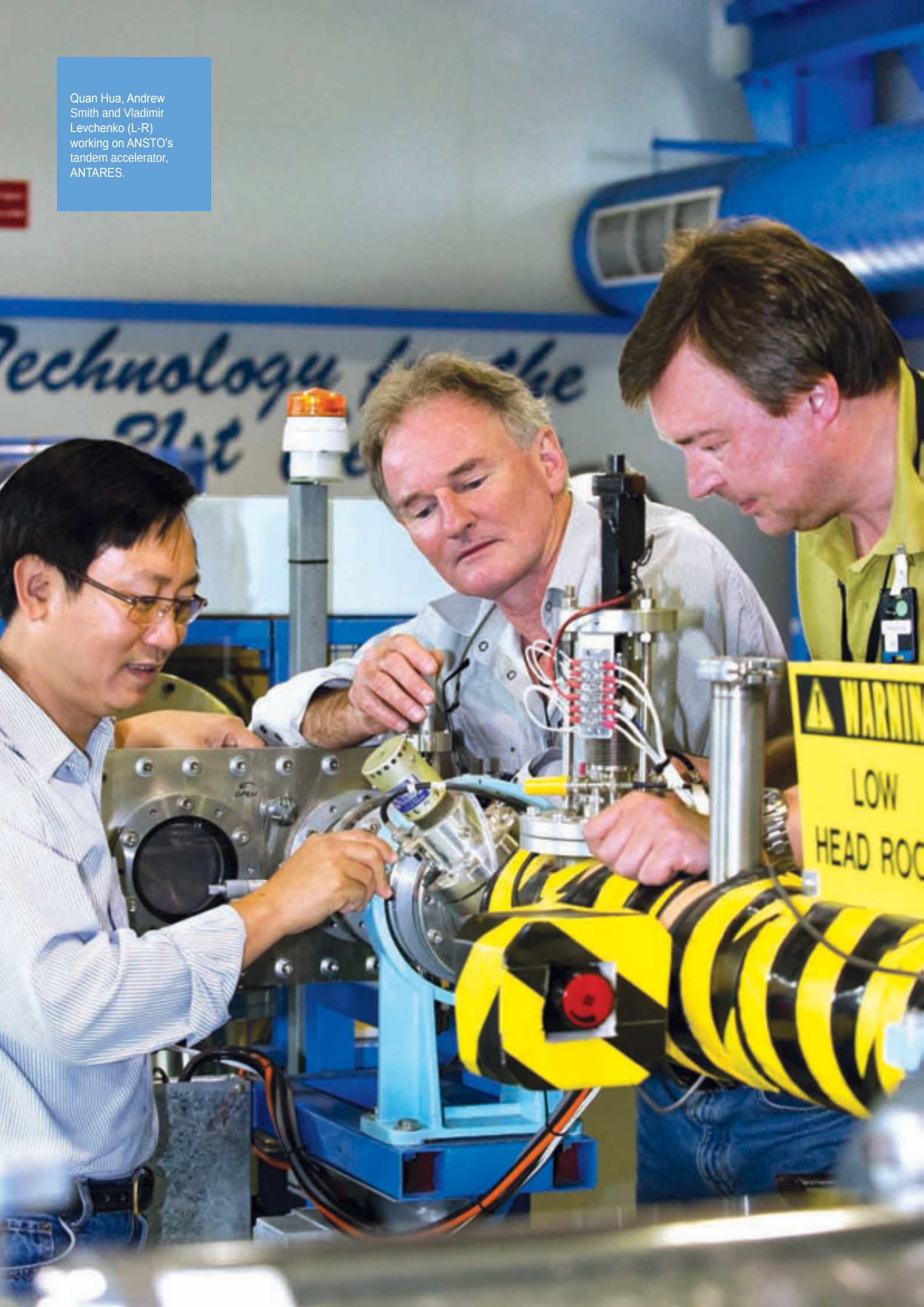

Quan Hua, Andrew Smith and Vladimir Levchenko (L-R) working on ANSTO's tandem accelerator, ANTARES.

Radiocarbon in Tasmanian Huon pine and its implications for radiocarbon calibration and abrupt climate change

Quan Hua, David Fink, Vladimir Levchenko, Andrew Smith and Fiona Bertuch
ANSTO

Radiocarbon dating is one of the most reliable and well-established methods for dating the past ~50,000 years. Radiocarbon age of a sample is determined by measuring its ^{14}C concentration and by assuming a constant level of atmospheric ^{14}C through time. However, not long after the establishment of the radiocarbon dating method (in the late 1940s), it was recognised that the ^{14}C concentration of the atmosphere in the past has not been constant. Here, we report the high-precision, high-resolution atmospheric ^{14}C record from a Huon pine in Tasmania for improved radiocarbon calibration for the early Younger Dryas. Our study also allows for a critical evaluation of mechanisms of atmospheric ^{14}C variations and abrupt climate change during the Last Deglaciation, ~20,000 – 11,600 calendar years before present.

Radiocarbon calibration

Variations in atmospheric ^{14}C concentrations are mainly due to variations in the rate of radiocarbon production in the atmosphere, caused by changes in the Earth's magnetic field, variability in solar activity, and changes in the carbon cycle. The result is that radiocarbon and calendar ages are not identical, and the radiocarbon ages have to be converted to calendar ages using a calibration curve, which describes the atmospheric ^{14}C concentration in the past measured in precisely and independently dated materials.

The internationally ratified calibration curve for IntCal04 terrestrial samples (e.g. woods, charcoals and macro-fossils) covers the past 26,000 years [1]. This curve is reliably based on dendrochronologically dated for the period 12,400 – 0 calendar years before present (BP). For the remaining period 26,000 – 14,000 calendar years BP, the curve is derived from independently dated marine samples such as corals and foraminifera in varved marine sediments. However, these archives may not be ideal for radiocarbon calibration because they are subject to uncertainties in varve counting and in the assumption of a constant marine reservoir age correction (a ^{14}C age offset due to upwelling of old carbon from the ocean interior) applied for each marine sampling site, which may not be valid for intervals of rapid climate change during the Last Deglaciation (~20,000 – 11,600 years ago).

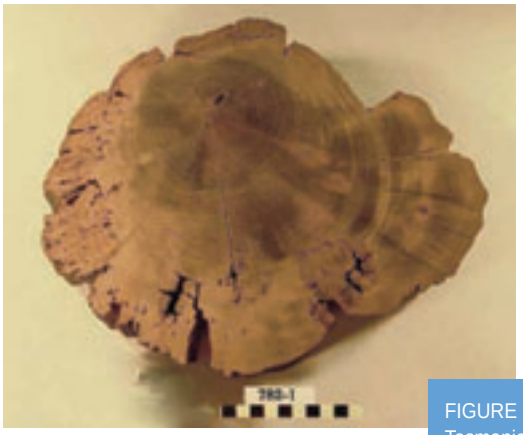

FIGURE 1
Tasmanian Huon pine log

Figure 1 - One of the 4 sub-fossil Tasmanian Huon pine used for AMS analysis. This log, SRT-782, contains 350 rings.

Excavation of sub-fossil Huon pine logs

Tasmanian Huon-pine logs

We have studied four sub-fossil logs of Huon pine with clearly defined and measured annual tree rings which were excavated from alluvial sediments along Stanley River in north-western Tasmania, Australia, at 41°41'S, 145°18'E. These logs are quite well preserved and contain several hundreds of tree rings each (Figure 1). We performed radiocarbon measurements on sequential decadal samples from each of the logs. A total of 137 samples were pre-treated to alpha-cellulose, converted to CO_2 and then graphite for Accelerator Mass Spectrometry ^{14}C analysis using the ANTARES facility at ANSTO [2]. Final total analytical ^{14}C measurement precision for most samples ranged from 0.3 to 0.4% (24 – 32 ^{14}C years) obtained after a 1-hour runtime. Based on ring-width information and radiocarbon results, we have successfully constructed a floating 617-ring Huon pine chronology, covering an age range from 10,350 to 10,760 ^{14}C years BP.

New tree-ring ^{14}C record and its implications

The ^{14}C age range and patterns of the older part and middle portion of the Huon pine record are similar to those of the younger part of a 1382-ring Late Glacial Pine chronology from Europe [3], and to those of the older portion of extended European absolute chronologies [4], respectively. This allowed us to link our Huon pine ^{14}C record to the floating Late Glacial Pine record and anchor it to the absolute tree-ring timescale (calendar years), by ^{14}C wiggle matching (Fig. 2). This resulted in a continuous and reliable atmospheric ^{14}C record based on tree rings for the past 14,000 cal BP (Fig. 3) for improved radiocarbon calibration. Large differences of up to 400 years between tree-ring radiocarbon ages and those of marine samples during the early Younger Dryas from 13,000 to 12,600 calendar years BP (Fig. 3) indicate that marine-derived ^{14}C records do not faithfully represent atmospheric ^{14}C during periods of abrupt climate change, due to possibly large changes in marine reservoir age which were not accounted for in these records.

In addition, the availability of the continuous and reliable tree-ring-based atmospheric ^{14}C record for the past 14,000 calendar years BP allows for a critical evaluation of mechanisms of atmospheric ^{14}C variations and abrupt climate change during the Last Deglaciation. In particular, by comparing the tree-ring ^{14}C with marine derived ^{14}C and modelled ^{14}C based on ice-core ^{10}Be fluxes, we conclude that changes in ocean circulation were mainly responsible for the onset of the Younger Dryas cold reversal, while a combination of changes in ocean circulation and ^{14}C production rate were responsible for atmospheric ^{14}C variations for the remainder of the Younger Dryas [4].

Our work, together with previous studies, indicates that investigations of atmospheric radiocarbon variations over time can deliver crucial information about climate change and changes in ocean circulation in the past. It demonstrates that marine-based ^{14}C records, which can be affected by changes in ocean circulation during abrupt climate change, are not ideal for radiocarbon calibration.

References

[1] Reimer P.J., Baillie M.G.L., Bard E. et al., *Radiocarbon 46* (2004) 1029.

[2] Fink D., Hotchkis M.A.C., Hua Q. et al., *Nuclear Instruments and Methods B 223-224* (2004) 109.

[3] Kromer B., Friedrich M., Hughen K.A.et al., *Radiocarbon 46* (2004) 1203.

[4] Hua Q., Barbetti M., Fink D. et al., *Quaternary Science Reviews 28* (2009) 2982.

[5] McCormac F.G., Reimer P.J, Hogg A.G. et al., *Radiocarbon 44* (2002) 641.

FIGURE 2

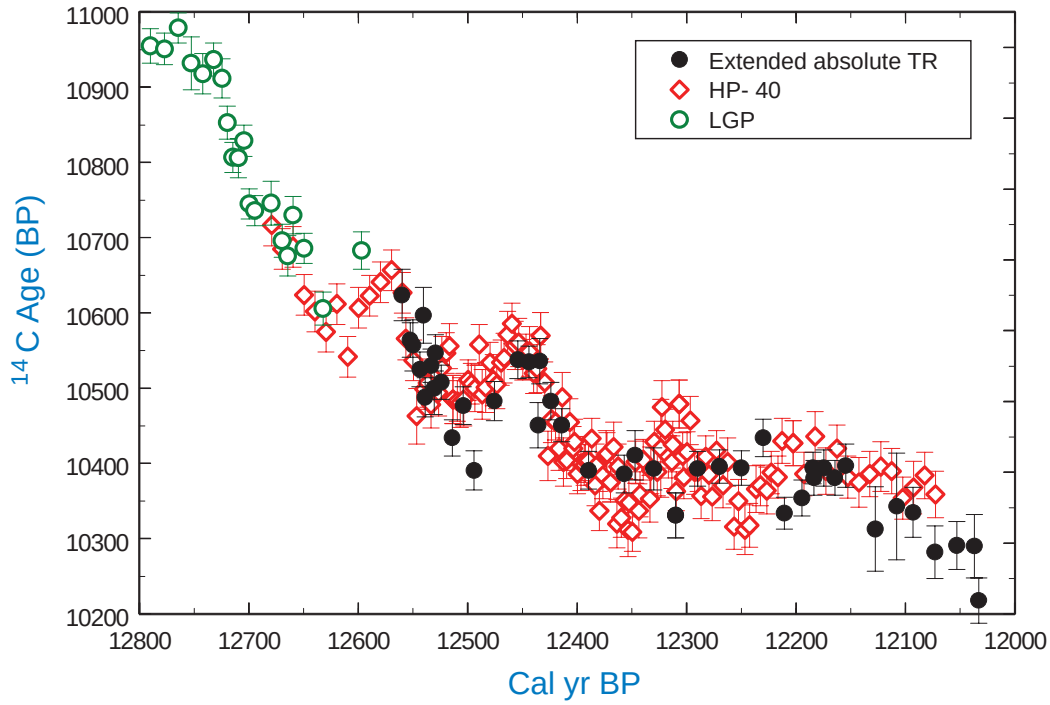

Figure 2 - Linkage of the floating Huon pine ^{14}C record to the floating Late Glacial Pine (LGP) and extended absolute tree-ring chronologies. The Huon pine ^{14}C ages (from the Southern Hemisphere (SH)) were subtracted by 40 years before being linked to those of extended absolute tree-ring and the floating LGP chronologies (from the Northern Hemisphere (NH)) because tree rings from the SH were on average 40 ^{14}C years older than contemporaneous NH samples for the last millennium [5].

FIGURE 3

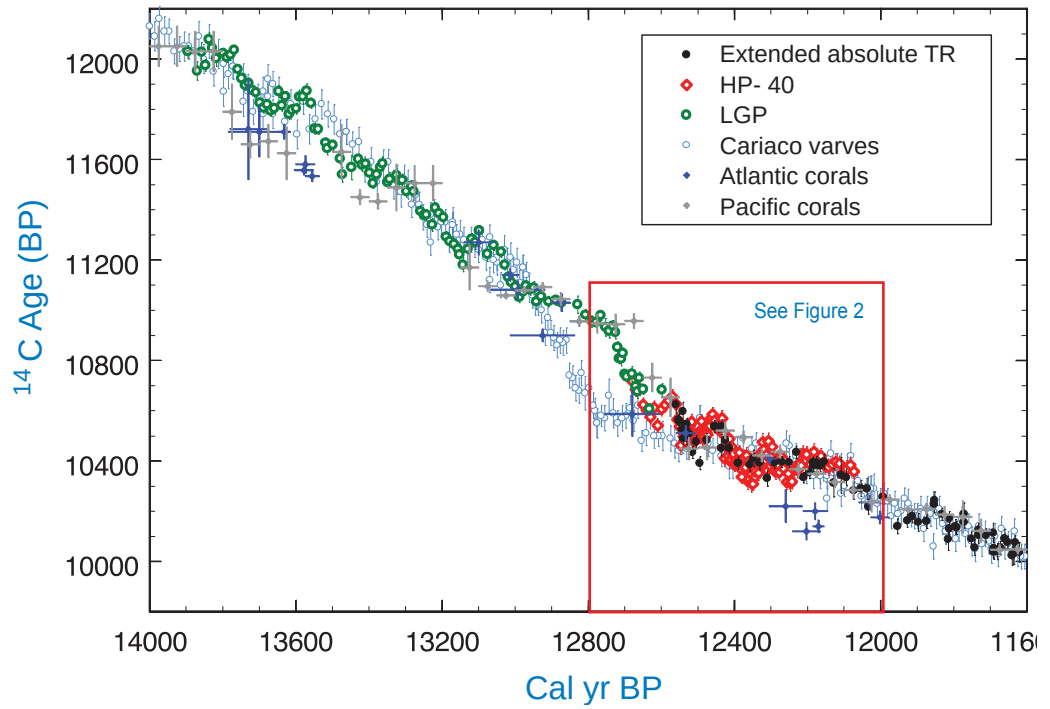

Figure 3 - Tree-ring ^{14}C vs marine-derived atmospheric ^{14}C for the period 14,000 – 11,600 calendar years BP. These marine-based ^{14}C records were used for the reconstruction of the IntCal04 calibration curve beyond 12,400 calendar years BP [1].

Stalagmites and stalactites (pictured) are being studied in ANSTO's climate change research.

Key to past climates lies in understanding cave-formation growth

Chris Waring[1], Stuart Hankin[1], David Griffith[2], Stephen Wilson[2] and Samantha Hurry[2]
[1]ANSTO and [2]University of Wollongong, Australia

Studying cave environments and their formation provides a unique insight into our prehistoric climate and is an important step towards a quantitative interpretation of palaeo climate. In our field campaign to the Jenolan Caves in New South Wales, we monitored air gases and drip water through the year, using isotope techniques for our measurements. A detailed picture of seasonal cave formation (speleothem) emerged, illustrating growth patterns of stalactites and stalagmites, and thus helped to further the interpretation of palaeo-climate records.

Why we study caves

Evidence for global warming and Earth's climatic history comes from long continuous Greenland and Antarctic ice-core records [1,2]. These palaeo-climate records from the poles show the Earth experienced four major cycles of glaciation with short intervening periods of relative warmth over the preceding 500,000 years. At present, Earth is in a warm inter-glacial period. This global pattern of glacial cycles has contrasting and divergent impact in different regions across the globe because of the influence of changing ocean currents, atmospheric weather circulation patterns, and latitude. If we want to better understand regional impacts of global warming on our weather long high-resolution palaeo-climate records from mid and low latitudes are required. Cave formations (speleothems) are long, widespread, continental palaeo-climate archives. At issue is the quantitative translation of speleothem isotopic and trace element abundances into reliable records of past temperature and rainfall. Studies of modern speleothem growth linked to weather and climate records are used to improve speleothem translation.

Whilst there are many good qualitative speleothem palaeo-climate records, a universal quantitative transfer function from external weather / climate to speleothem record is elusive. Studies of cave environments and speleothem growth are an important step towards quantitative speleothem palaeo-climate interpretation. The growth looks at the net accumulation of $CaCO_3$ (speleothem growth), but in order to interpret this we need to understand the Gas-Aqueous-Solid equilibrium conditions in the cave environment (dissolved ions in water, temperature T, pressure P, carbon-dioxide concentration in air pCO_2). The largest change to equilibrium conditions in a ventilated cave environment causing speleothem growth is fluctuating carbon-dioxide concentration as a response to the cave-air exchange, driven by external temperature. Figure 1 shows the cycle and summarises isotope tracing in speleothems. The scheme also indicates that the cave ventilation system, i.e. the location of the speleothem, will influence carbon-dioxide concentration - quantative measurements (pCO_2) are shown in Figure 2 - and therefore influence speleothem growth pattern and palaeo-climate records.

Field campaign in Jenolan Caves

Continuous CO_2 monitoring records from different caves at Jenolan (NSW, Australia) show different ventilation patterns ranging from slow drainage at week-month long time-scales (cave opening "Temple of Baal" one opening without through-air flow) to large daily (diurnal) fluctuations ("Katie's Bower" chamber between a top and bottom opening) dependent upon the configuration of cave openings, see Figure 1 [3]. Seasonal differences are also apparent at Katie's Bower with summer peak CO_2 reaching 5,000 ppm compared to a winter range from 400 ppm to 1,000 ppm.

An intense 3-week field campaign in May (winter) continuously measured (5 min) trace gases (CO_2, CH_4, N_2O) H_2O and isotopic contributions of $CO_2\delta^{13}C_{CO2}$ using a Fourier Transform Infrared (FTIR) spectrometer. Simultaneous drip-water pH, air flow, temperature, pressure, and relative humidity were logged by sensors in the cave together with external rainfall, temperature, pressure, and relative humidity.

FIGURE 1

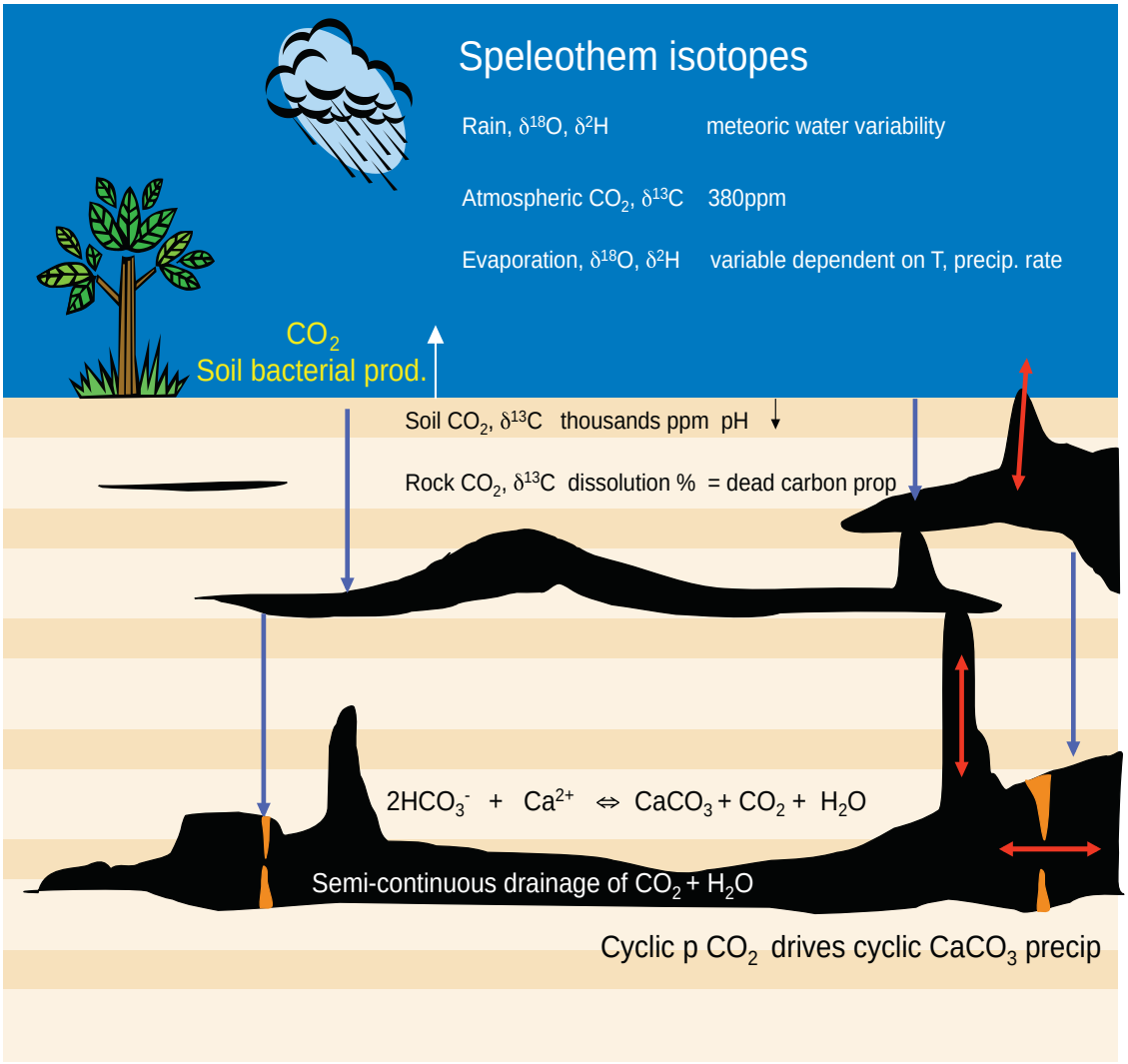

Figure 1 - Schematic diagram showing the proposition; cyclic pCO_2 drives cyclic $CaCO_3$ precipitation. Links cave atmosphere $\delta^{13}CCO_2$ and CO_2 outgassing = speleothem growth timing in the diurnal cycle. Similarly there will be a strong seasonal bias to speleothem growth rates. By implication speleothem isotopes will have a seasonally biased record towards max growth in summer (highest CO_2) and summer isotopes.

Drip water was sampled twice daily, coinciding with CO_2 maxima and minima (Figure 3 shows dissolved inorganic carbonate (DIC), $\delta^{13}C_{DIC,}$ dissolved organic carbonate (DOC),$\delta^{13}C_{DOC}$, alkalinity, anions, and cations). Further spot samples were taken for drip-water stable isotopes, $^{14}C_{DIC}$, and ^{3}H. Our results on soil and drip water and their isotopic constraints are shown in Figure 3 – they imply that speleothem $\delta^{13}C$ is largely influenced by prior calcite precipitation, and hence factors that change speleothem growth will have a consequent impact on speleothem $\delta^{13}C$ in palaeo-climate records.

At Katie's Bower with a strong ventilation pattern, speleothem growth rate varies through the diurnal cycle and between seasons (Figure 4). Low pCO_2 in the morning, cave air causes rapid speleothem growth with CO_2 exsolved to the cave atmosphere lowering drip-water pH. pCO_2 increases to an evening maxima and slows speleothem growth before early morning temperature-induced ventilation decreases pCO_2. We find, see Figure 4, that (i) $\delta^{13}C_{CO2}$ has an antithetic relationship with CO_2, (ii) drip-water remains constant throughout the winter experiment. This suggests that CO_2 is not re-dissolving into drip-water to dissolve speleothems nor complicate interpretation of speleothem $\delta^{13}C$ palaeo-climate records. Summer speleothem growth may have a different $\delta^{13}C$ incorporation pattern from a higher diurnal peak CO_2 (up to 5,000 ppm).

Current climate records start from the assumption of a regular annual growth rate for the speleothem and a formation age error plus or minus decades at best. However, our study shows that the growth patterns of speleothems have a diurnal and seasonal component as large as the climatic range. This means climate records need much more fine-tuning since the growth rate not only varies over years, but also within a year. High-resolution speleothem records can also take advantage of the seasonal isotopic variations to provide annual markers, thereby allowing high-resolution chronology and growth rates, similar to ice-core and tree-ring analysis. We plan to demonstrate the linkage between weather records and speleothem isotopes with high-resolution (monthly) analysis of a speleothem grown at Jenolan between 1938 and 1998 on a wire strung across a chamber.

Weather station at Jenolan

FIGURE 2

CO_2 a guide to ventilation pattern

Diurnal

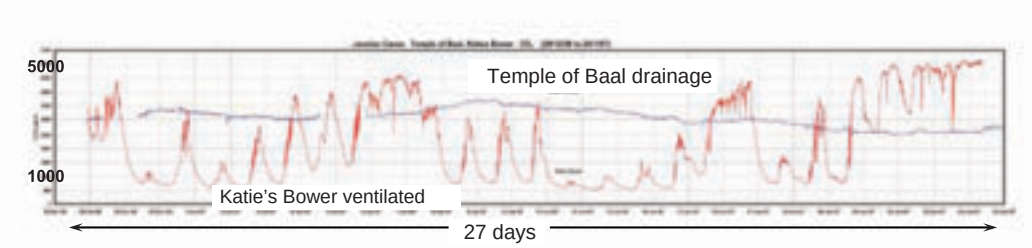

Summer peak CO_2 Winter peak δ^{13}_{co2}

Seasonal

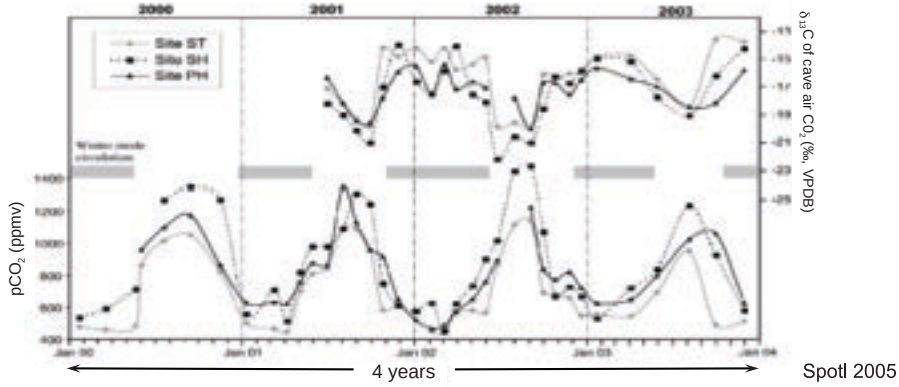

Figure 2 - At Jenolan, different caves have different ventilation patterns, respond (or not) to external weather. This data shows the two-end members, only one has a strong diurnal pattern. Katie's Bower has a top and bottom entrance allowing free through-flow in response to T-differences inside the cave vs outside, whereas Temple of Baal is isolated. Note, diurnal pattern is also present in winter but amplitude is less; summer range to 5,000 ppm; winter range to 1,000 ppm. Many caves will have some component of diurnal ventilation.

FIGURE 3

Soil and drip water $\delta^{13}C_{DIC}$ $+^{14}C$ quantifies prior calcite precipitation

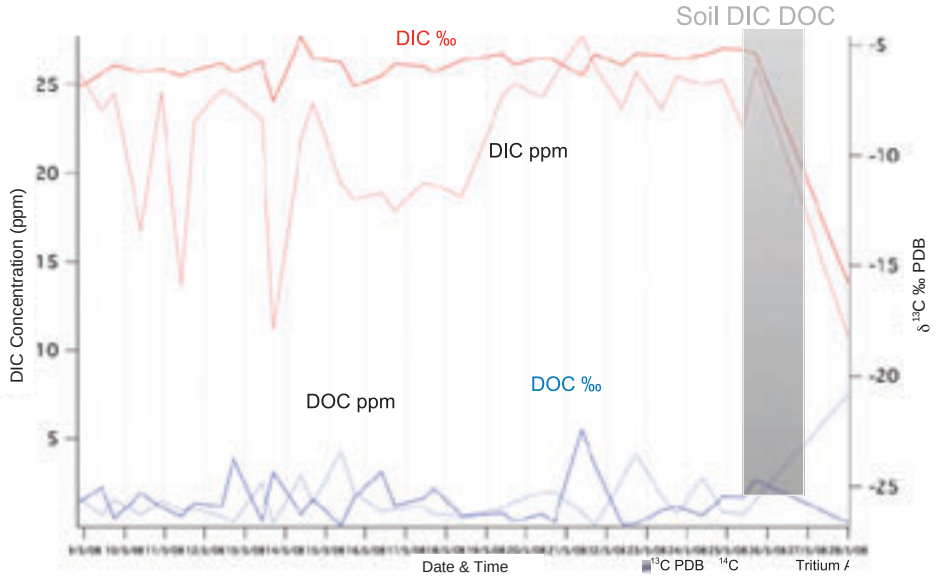

	δ13C PDB ‰	14C PMC	Tritium / TU
Stalactite Drip water, FOB, 09-May-08, 10:00	-6.00	105.52	3
Stalactite Drip water, FOB, 14-May-08, 12:00	-4.50	105.29	3.03
Stalactite Drip water, FOB, 20-May-08, 17:00	-6.30	105.48	3.01
Stalactite Drip water, FOB, 23-May-08, 09:30	-5.80	104.76	2.84

Figure 3 - The soil water DIC $\delta^{13}C$ shift from δ-15‰ (per mil) to speleothem drip water -5‰ must be due to prior calcite precipitation where lighter $\delta^{13}C$ CO_2 (9‰ equilibrium fractionation at 13° C) is evolved progressively during speleothem formation. The 10‰ shift to heavier DIC $\delta^{13}C$ would normally be interpreted as interaction with marine limestone, however the drip water ^{14}C rules out any significant inheritance of dead carbon from limestone. We took twice daily drip water samples at approx 10am (min CO_2) and 6-9pm (max CO_2) for DIC and DOC plus $\delta^{13}C$ of each. On 4 occasions larger samples 1L were taken for ^{14}C ($+\delta^{13}C$) and ^{3}H. Drip water DIC $\delta^{13}C$ is very consistent at -5 to -6 per mil except for minor excursion when door was left open for 24 hrs on 13/5/08. Soil DIC $\delta^{13}C$ is -15‰ (already higher than expected -20 to -25‰).

FIGURE 4

CO_2 $\delta^{13}C$ signatures

Possible sources

- atmospheric $\delta^{13}C_a$ = -8.5‰
- biogenic $\delta^{13}C_b$ = -29‰
- degassing of drip-water $\delta^{13}C_c$ = -14.5‰ (speleothem growth)

$$\delta^{13}C_{obs} = a\delta^{13}C_a + b\delta^{13}C_b + c\delta^{13}C_c$$

$$\delta^{13}C_{obs} = a(-8.5) + b(-29) + (1 - a - b)(-14.5)$$

$$b = \left(\frac{\delta^{13}C_{obs} - 6.0a + 14.5}{-14.5} \right)$$

Therefore:

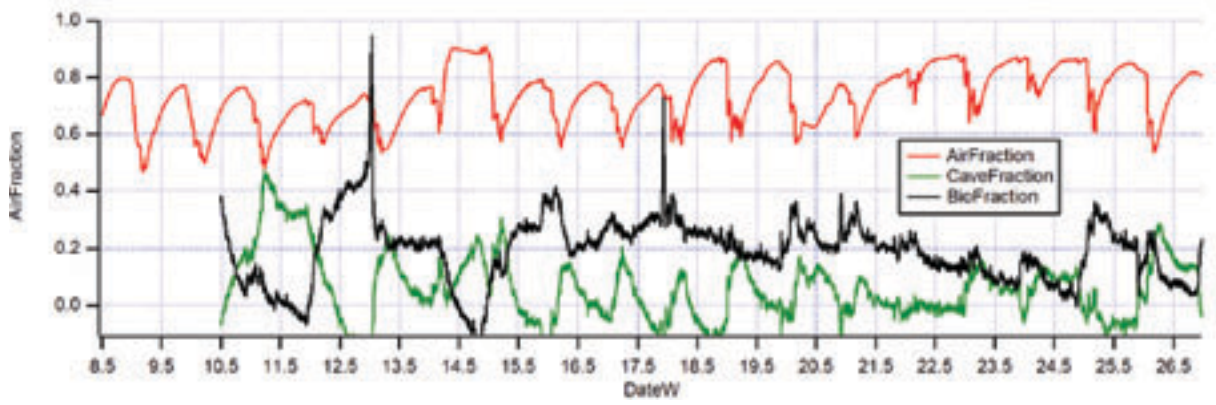

Figure 4 - $\delta^{13}C_{CO2}$ may be partitioned to its sources: -8.5‰ PDB is normal air; -29‰ PDB is biogenic air or air derived from biological respiration, which could be trees outside cave or bacteria in the cave. -14.5‰ PDB is derived from drip water DIC $\delta^{13}C$ at -5.5 minus 9‰ fractionation factor for CO_2 gas at 13° C. Note, speleothem growth is not constant during the day: $\delta^{13}C_{CO2}$ has an antithetic relationship with CO_2, with low pCO_2 morning air the highest $\delta^{13}C_{CO2}$ at -8‰. A special analysis provides the proportion of external air drawn into the cave and CO_2 produced from speleothem formation through the diurnal cycle. Drip-water $\delta^{13}C_{DIC}$ remains constant at -5 to -6‰ throughout the winter experiment. By implication in summer when CO_2 reaches 5,000 ppm speleothem growth is likely to make up the bulk of the CO_2 if external air conc is fixed.

References

[1] Augustin et al., *Nature, 429* (2004) 623-628.

[2] Anderson et al., *Nature, 431* (2004) 147-151.

[3] Spotl et al., *Geochimica Cosmochimica Acta, 69* (10), (2005) 2451-2468.

Fresh groundwater lenses identified within salty groundwater

Dioni I. Cendón[1,2], Josh R. Larsen[1,2], Brian G. Jones[2], Gerald C. Nanson[2] and Stuart I. Hankin[1]
[1]ANSTO and [2]University of Wollongong, Australia

Surface water resources in the Australian interior are unreliable and scarce. However, they are vital in supporting the vegetation along and near river channels and in maintaining a delicate ecological balance along the waterholes "billabongs". Our research has identified and described shallow groundwater of low salinity forming freshwater lenses up to 1 km wide. These are located directly adjacent to major waterholes, and overlying the otherwise widespread saltier regional groundwater along the Cooper Creek floodplain near Ballera (south-west Queensland).

Why we study the Cooper Creek

Cooper Creek (Fig. 1), with a total catchment area of 306,000 km^2 is the longest and probably most ecologically important dryland river in Australia [1]. It starts at the confluence of the Barcoo and Thomson Rivers and is fed largely by the Australian summer monsoon rainfalls along the north-western slopes of the Great Dividing Range. Its middle to lower course is characterised by a multiple channel floodplain where interacting aeolian and fluvial sedimentation and gradually reducing river discharges over the Late Quaternary have resulted in a unique stratigraphic and geomorphic setting [2,3]. Local geomorphic features such as remnant dunes, mud-capped waterholes and floodplain, combined with large hydrological variability, result in huge uncertainties in recharge and groundwater evolution processes. The Cooper Creek catchment provides a non-disturbed analogue to understand how other presently wetter regions, particularly those along the Murray-Darling Basin, could evolve in the future if their climate and hydrology becomes even more variable. Furthermore, this research could be applied to understand the effects on dry-land rivers of artificially depleted natural flooding cycles and their impacts on shallow groundwater.

Defining fresh water lenses

Fresh water lenses were defined after piezometers had been installed and groundwater analysed for major-element chemistry, water stable isotopes (δ^2H and δ^{18}O) and dissolved sulfate stable isotopes (sulfate δ^{34}S and δ^{18}O) along a floodplain transect. This research identified shallow groundwater of low salinity forming freshwater lenses, directly adjacent to major waterholes, and overlying the otherwise widespread saltier regional groundwater. The groundwater is recharged through the base of the waterholes at times of flood scour, but not through the impermeable floodplain mud. Total dissolved solids rise with distance from the waterhole and stable water isotopes confirm that recharge is consistent with and dependant on, monsoonal flooding events. Our findings at Cooper Creek have coincided with the recent description of similar lenses in the Murray River [4]. While the Murray lenses are still within a predominantly gaining stream (watertable above the base of the stream), the Cooper Creek lenses are below the base of the waterholes and is therefore a hydrologically losing stream.

The freshwater lenses we found

The freshwater lenses are asymmetrical and directly related to the size of the nearby waterhole. The lenses spread downstream with total-dissolved solids <5000 mg/L for distances of up to ~300 m from the waterholes, mixing progressively with saline regional groundwater and increasing total dissolved solids between 5000 and 15000 mg/L at 1000 m (Fig. 1b). Higher total-dissolved solids concentrations in groundwater are found farther south in central areas of the floodplain. Complete mixing with regional saline groundwater is not achieved in the Goonbabinna-Chookoo transect as shown by sulfate-δ^{34}S and -δ^{18}O of groundwater between waterholes, with generally more enriched isotopic values than regional groundwater (Fig. 1c).

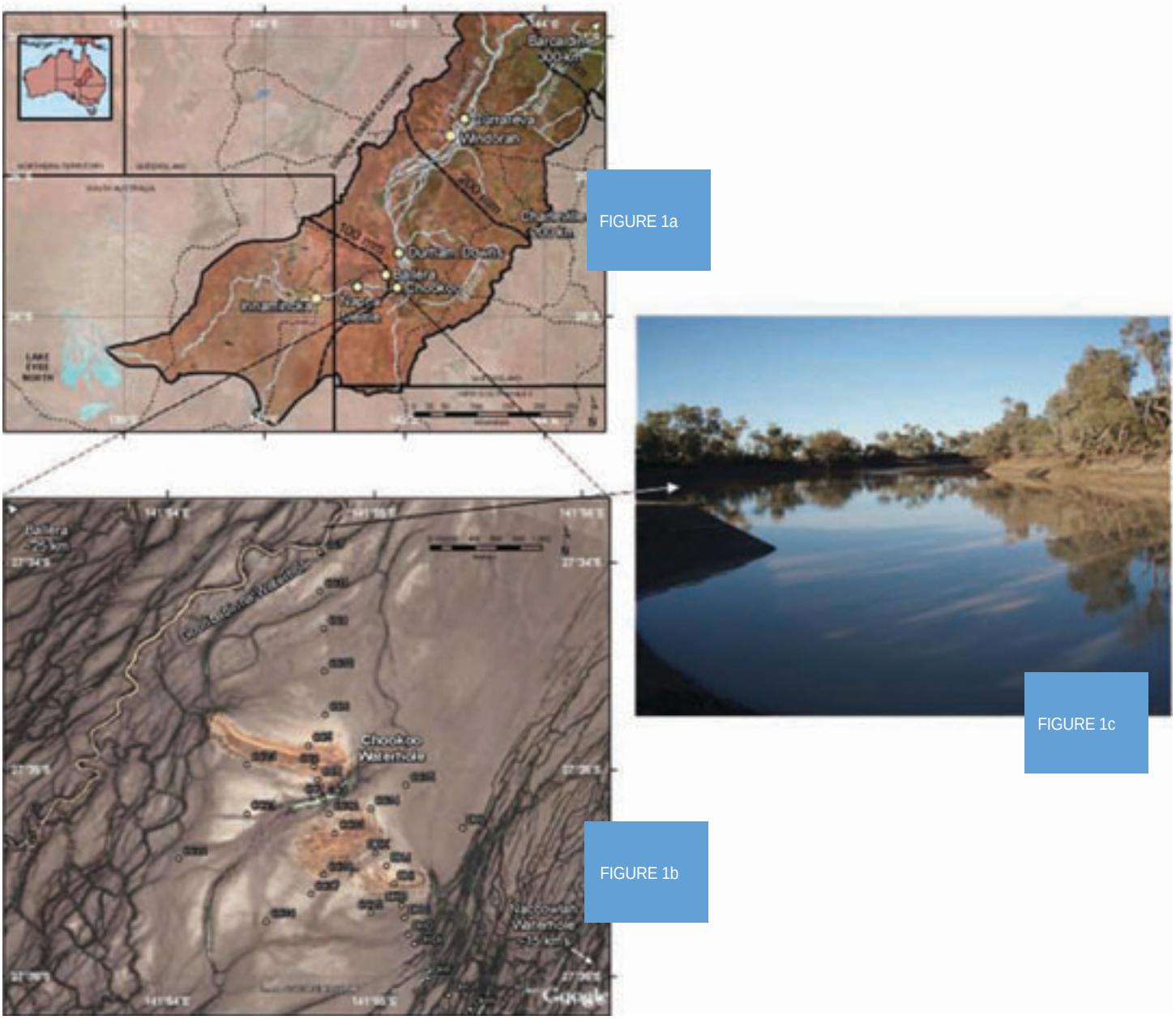

Figure 1a - General satellite photograph of the southern section of the Cooper Creek basin showing projected isohyets of mean rainfall (This map contains data from Commonwealth, Copyright © Geoscience Australia). **Figure 1b** - Detailed satellite photograph showing a section of the Cooper Creek floodplain with piezometer locations, the Goonbabinna and Chookoo waterholes and sand dune complex. **Figure 1c** - Detailed photograph of the Goonbabinna waterhole near sample location CC7.

ANSTO has undertaken work at numerous water testing sites across Australia.

FIGURE 2

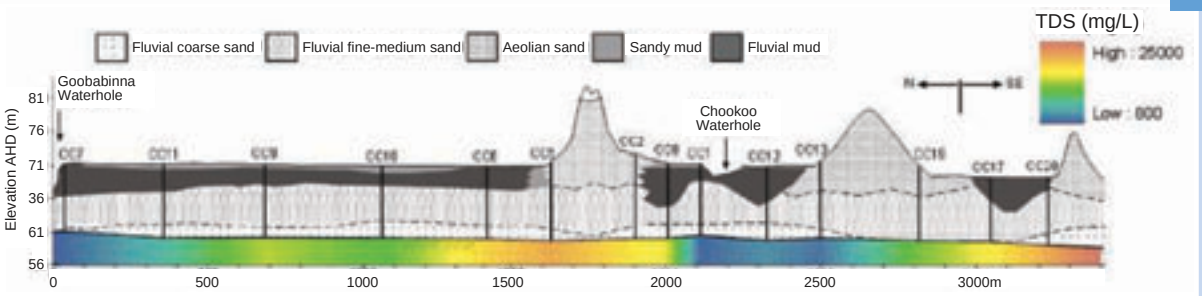

Figure 2 - Variations of total dissolved solids in the groundwater across the transect from the Goonbabinna waterhole to the sand dunes (see satellite photo Fig.1b). The line above the colourer section indicates the level of the watertable. Floodplain stratigraphy and lithologies are also depicted.

The hydrochemical information suggests that some degree of communication between waterholes and the underlying groundwater exists. This is greatest during recharge episodes facilitated by channel scour and direct water contact with underlying sands and is minimised during no flow conditions due to clay settling from the receding flood waters. All conservative major and minor ions analysed in groundwater show a progressive increase in concentrations farther from waterholes, regardless of the presence of sand dunes (Fig. 2, 3). This trend would not be possible unless freshwater was being supplied from the waterholes and slowly mixing with the regional saline groundwater. It also suggests there is little or no significant contribution of freshwater through the dunes, despite being comprised of porous sands and stratigraphically connected to the underlying fluvial sands.

Water stable isotopes indicate that the shallow groundwater within the Cooper Creek floodplain is recharged by water with a homogeneous isotopic signature, during major flooding events. Sulfate stable isotopes reveal a limited connection between the Chookoo waterhole and the regional shallow groundwater. In the proximity of the waterhole sulfate -$\delta^{18}O$ shifts towards enriched values, probably as the result of hyporheic redox processes within the waterhole sediments, and suggests diffuse leakage to the underlying watertable may occur during no flow conditions.

The limited extent of freshwater lenses surrounding the waterholes may have important controls on the floodplain vegetation ecology, despite the ability of these trees to tolerate highly saline ground and soil water. The ground and surface water dynamics investigated may also

FIGURE 3

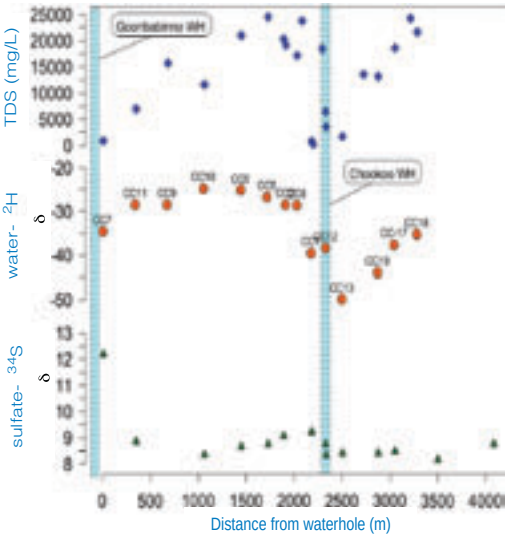

Figure 3 - (A) Evolution of total-dissolved solids, water-δ^2H and sulfate-$\delta^{34}S$ with increasing distance from Goonbabinna waterhole. Vertical bars represent the position of the waterholes (see Fig.1b for location of samples).

provide a possible analogue for other Australian rivers that are expected to experience more ephemeral flow regimes under changing climatic and anthropogenic conditions.

Future work

A new piezometer transect has been installed and sampled with four monitoring piezometers left to investigate seasonal fluctuations in groundwater level. The new samples are being analysed at ANSTO for other naturally occurring isotopes (14-Carbon, Tritium), these results will define the time scales involved in the formation of the fresh water lenses.

References

[1] Kingsford R.T., Curtin A.L. and Porter J., *Biological Conservation, 88* (1999) 231-248.

[2] Nanson G.C., Price D.M., Jones B.G., Maroulis J.C., Coleman M., Bowman H., Cohen T.J., Pietsch T.J. and Larsen J.R. *Geomorphology, 101* (2008) 109-129.

[3] Maroulis J.C., Nanson G.C., Price D.M. and Pietsch T, *Quaternary Science Reviews, 26* (2007) 386-404.

[4] Cartwright I., Weaver T. R., Simmons C. T., Fifield L. K., Lawrence C. R, Chisari R. and Varley S., *Journal of Hydrology 380* (2010), 203-221.

David Cohen's research is helping identify the sources and origins of fine-particle pollution across the Asian region.

Understanding long-range fine-particle pollution in Asia

David Cohen, Eduard Stelcer and Jagoda Crawford
ANSTO

Fine-particle pollution in Asia is generally very high compared with internationally accepted health goals. Much of this fine-particle pollution is produced by motor vehicles, fossil-fuel combustion, industrial processes and even windblown soils from desert regions. As part of a long-term project in the Asian region we have been using nuclear techniques not only to characterise fine-particle pollution, but also to quantify their sources and origins across 15 countries in the region.

Monitoring air pollution in the Asian region

In 2002, the International Atomic Energy Agency (IAEA) established a Regional Cooperative Agreement (RCA) project with 14 member states, including Australia, Bangladesh, China, India, Indonesia, Korea, Malaysia, Mongolia, New Zealand, Pakistan, Sri Lanka, Thailand and Vietnam, to monitor, characterise and quantify sources of fine-particle pollution in each of these countries. This is a unique study as each country uses the same stacked filter samplers and has sampled at the same time twice a week for at least 5 years.

The data obtained are unique for the region and will be picked up by a range of environmental agencies controlling and managing air pollution in each of the member states as well as non-government organisations like the World Bank and the Asian Development Bank. They will be used to correlate medical conditions related to lung disease and heart conditions with high pollution days, with sources of air pollution and with hospital admissions. Even for relatively pollution-free countries like Australia, estimates show that generally more people are dying each year from air-pollution related issues than are killed on the roads. In these Asian regions the air-pollution levels are above World Health Organisation (WHO) recommended guidelines most of the time, and hence the health effects are much more significant.

Fig.1 shows the average, media, and distribution of fine-particle air pollution as measured in this IAEA project between 2002-08. In this box and whisker plot the hatched boxes contain 25%-75% of the measurements for each country, the vertical whiskers from each box cover the 95% confidence interval, the (+) signs are the means and the horizontal bars the median values for each country. The remaining points outside the box and whiskers represent extreme values. The red horizontal bar at 35 $\mu g/m^3$ is the current US EPA 24 hour maximum fine particle goal and the green horizontal bar at 15 $\mu g/m^3$ is annual average goal. Clearly most Asian countries exceed both US EPA goals for fine particles most of the time.

Fine-particle characterisation

Fine particles in ambient air are defined as those particles with aerodynamic diameters less than 2.5 µm in diameter. Particles in this size range can be directly absorbed into the blood stream from the lungs, are most efficient at absorbing and scattering visible light and can travel thousands of kilometres from their original source emission points. A full characterisation of these particles, their sources and their origins will help regulators better understand air-pollution issues in their countries.

Each filter has been analysed using four nuclear techniques (Particle induced X-ray and gamma ray emission and nuclear scattering and recoil methods) for between 20-30 different chemical species [1]. This broad range of chemical species, together with the long-time series and extensive area covered by the data collection allowed a comprehensive dataset of source fingerprints and source contributions to be compiled across a very broad area of Asia.

The current US EPA (Environmental Protection Agency) fine-particle health goal is 15 $\mu g/m^3$ (green line) annual average and 35 $\mu g/m^3$ 24 hr maximum (red line). Clearly many countries exceed these two goals.The current database (established by the IAEA/RCA project) contains more than 8,400 individual sampling days. Each analysed for more than 20 different elements from hydrogen to lead.

Studying the trajectories of fine particles

Statistical techniques such as Positive Matrix Factorisation [2] can be applied to this database to obtain source fingerprints and their contributions to the total fine-particle mass. Fig. 2 shows the major desert regions and the larger coal-fired power stations in eastern China, north of Hanoi. It is well known that the Taklamakan and Gobi Desert regions produce large dust storms between March and April each year which may travel across Korea and Japan [3].

By applying standard back trajectory techniques [4] we can determine source 'fetch regions' for major Soil and Coal events from the Hanoi site. Figs. 3 and 4 show two such seven-day back trajectories for a high Soil event on 5 March 08 and a high Coal event on 10 Feb 08 at the Hanoi site.These back trajectory methods can be extended to look at all extreme events (over a long period of time) whose back trajectories intersect with known source regions such as the Taklamakan or Gobi Deserts or the coal-fired power stations in eastern China.

FIGURE 1

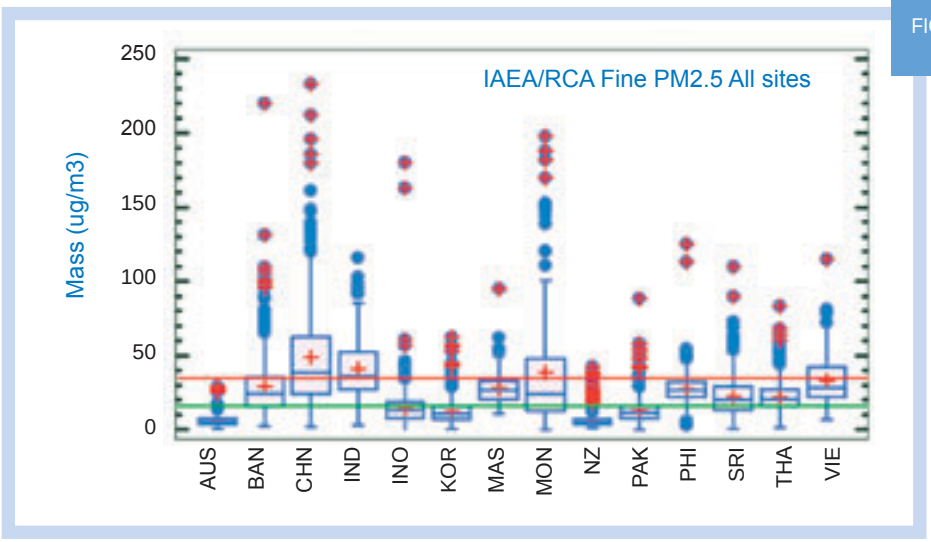

Figure 1 - Box and whisker plot of average fine particle masses for 14 Asian countries between 2002-08. (+) are means, horizontal bars are the medians.

FIGURE 2

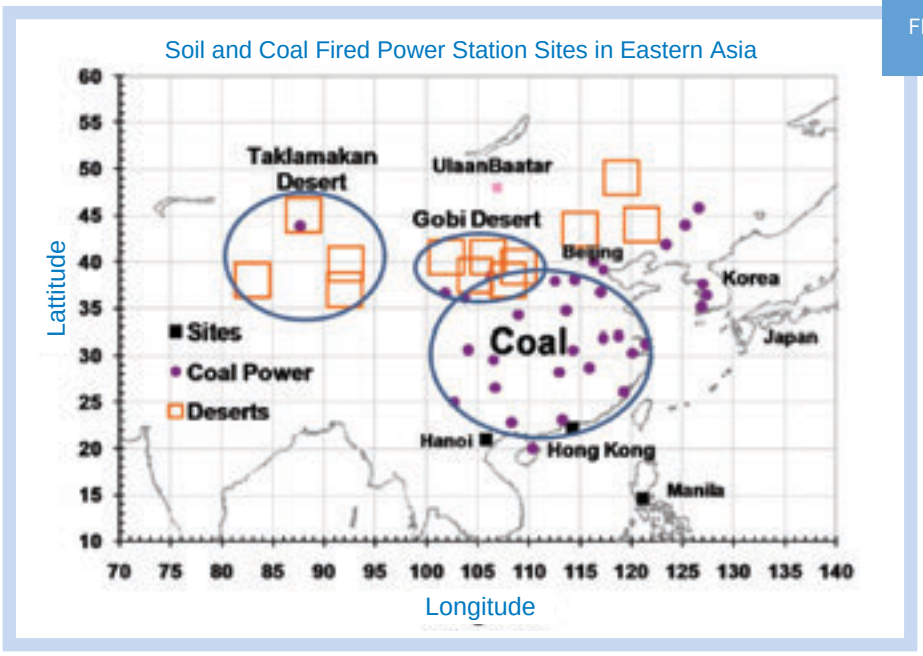

Figure 2 - Map of the desert regions (boxes) and major coal fired power stations (dots) in China.

Acknowledgements

We would like to acknowledge the help of staff at the Vietnamese Institute of Nuclear Sciences and Technologies and the International Atomic Energy Agency RCA Program for financial assistance and support throughout this work.

FIGURE 3

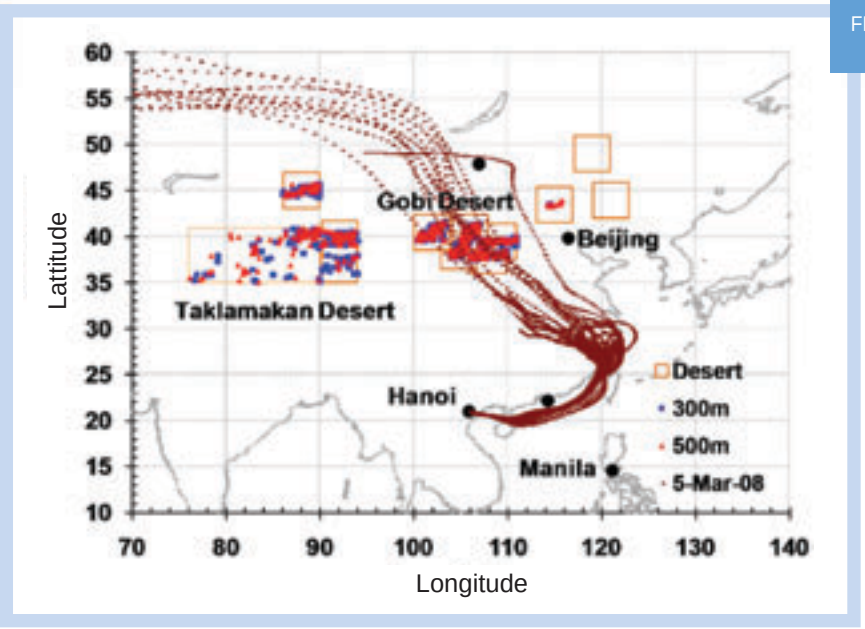

Figure 3 - Back trajectory plots and intersections for extreme Soil events between 2001-08.

The symbols within the desert regions (boxes) of Fig. 3 and the coal-fired power stations open circles) of Fig. 4 represent the number of trajectory intersections that impacted the Hanoi site between April 2001 and December 2008 with Soil levels above 6 µg/m^3 and Coal levels above 30 µg/m^3.

FIGURE 4

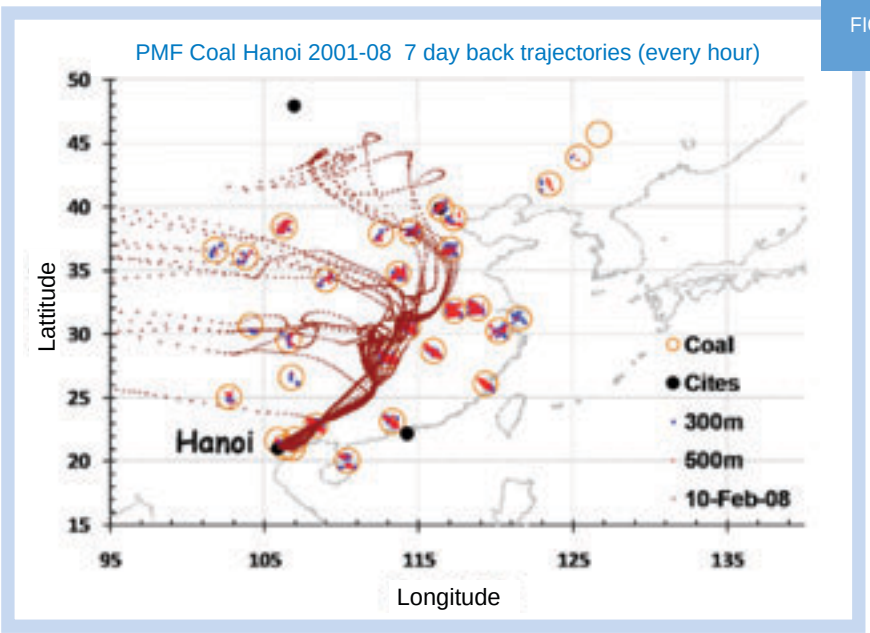

Figure 4 - Back trajectory plots and intersections for extreme.

Fig. 4 shows Coal events between 2001-08. Clearly, the Gobi and Taklamakan deserts impact the Hanoi site as do several major coal-fired power stations in eastern China. These source sites represent long-range transport of fine-particle pollution some hundreds and even thousands of kilometres into Hanoi.

References

[1] Cohen D.D., Stelcer E., Hawas O., Garton D., IBA Methods for Characterisation of Fine Particulate Atmospheric Pollution: A local, regional and global research problem. *Nuclear Instruments and Methods in Physics Research, Section B 219-220*, (2004) 145-152.

[2] Paatero P., Tapper U., Positive Matrix Factorisation: A non-negative factor model with optimal utilisation of error estimates of data values, *Environmetrics Vol 5* (1994) 111-126.

[3] Cohen D.D., Garton D., Stelcer E., Wang T., Poon S., Kim J., Oh S.N., Shin H., Ko M., Uematsu M., 2004a. Multielemental analysis and characterisation of fine aerosols at several key ACE Asia sites. *Journal of Geophysical Research,* 109 (2004) D19S12, doi:10.1029/2003JD003569.

[4] Draxler R. R., Rolph G.D, 2003. *HYSPLIT* (HYbrid Single-Particle Lagrangian Integrated Trajectory) Model access via NOAA ARL READY Website http://www.arl.noaa.gov/ready/hysplit4.html) NOAA Air Resources Laboratory, Silver Spring, MD.

Life Sciences

Life Sciences

ANSTO's life sciences research utilises nuclear and isotopic techniques to probe the fundamental properties of living matter to gain insights that will benefit individuals and society.

Our life sciences function operates within interdisciplinary teams using a range of technology platforms to investigate intractable biological issues such as disease prevention and treatment, environment and climate change.

ANSTO develops radiopharmaceuticals for imaging and treating diseases such as cancer, Alzheimer's and Parkinson's disease and utilises a suite of cutting-edge instruments, including the Bragg Institute's neutron-scattering instruments which are already used to study the structure/function relationships in food-based systems with direct applications to food processing and human nutrition.

With its life sciences studies, ANSTO has the imprimatur to ask the big biological questions and to provide education and training to improve outcomes and the public understanding of science.

Mapping the early inflammation process that leads to epilepsy in rodents

Paul Callaghan, Stefanie Dedeurwaerdere, Marie Gregoire, Tien Pham and Andrew Katsifis
ANSTO

Imaging of the living brain using Positron Emission Tomography (PET), a non-invasive, sensitive and quantitative imaging methodology, allows us to investigate neurobiological mechanisms involved in the onset of the neurological disease. Our work has focused on investigating the pre-symptomatic neuroinflammatory processes (called epileptogenesis) that lead development of chronic seizures, in an animal model of epilepsy. We have used our in-house radiotracer (18F-PBR111) which is highly specific for receptors expressed in the inflammatory response within the brain. Performing pre-clinical PET imaging with this radioligand allowed us to map and quantify neuroinflammation *in vivo*, and to correlate this with full *in vitro* assessment of the neuroinflamation response. The *in vivo* ligand binding patterns highly correlate with the structures involved in the generation of seizures, and these data reflect the *in vitro* data, illustrating that the PET binding represents true neuroinflammation. Thus, longitudinal PET studies will be possible in order to follow-up the evolution of the inflammatory regions during the onset of the disease, and test new preventive therapies that modulate this disease process.

Why PET in epilepsy research?

A fundamental goal of epilepsy research is to prevent the development of chronic seizures through the treatment of the initiating causative disease process. The use of nuclear medicine imaging techniques such as Positron Emission Tomography (PET) may allow detection of epileptogenesis in patients, after brain injuries such as stoke or head trauma, to allow preventative pharmacotherapies to stop or reduce the severity of epilepsy progression at the earliest stage of disease.

As shown in Figure 1, the onset of the disease occurs long before seizure activity is seen clinically or in animal models. In the human, this process, known as epileptogenesis, often occuring years before symptoms presenting [1].

We have used preclinical PET imaging with our in-house radiotracer, ^{18}F-PBR111, to map the response of the brain's immune system (neuroinflammation) to an insult that potentially leads to epilepsy (epileptogenesis, see Figure 1). This radiotracer has shown high affinity for the translocator protein in a previous study on acute brain lesion [2].

In order to check whether the PET images accurately reflect the neuroinflammation, we first correlated these results with post-mortem analysis. If the PET quantification was accurate, repeated PET imaging would allow us to follow up the evolution of the brain inflammation in the same animal during the full epileptogenesis, until the occurrence of the seizures, and maybe lead to a very early diagnostic tool. It will be used to assess the brain response to new preventive therapies in animal models first, then in clinical environment.

Our findings

PET imaging with ^{18}F-PBR111 was performed seven days after intra-peritoneal administration of kainic acid (treated rats which will become epileptic within 1 month, see Figure 1) or saline (control rats). The PET data of the treated group showed significant increases in radiotracer binding compared to the control group in several brain regions that are intrinsically involved in epileptogenesis: the amygdala, hippocampus and thalamus showed increases in receptor density (see Figure 2). *In vitro* binding on the same brains showed significant increases in translocator-protein density in the same brain regions including hippocampus, piriform cortex and basolateral/medial amygdala, in each case strongly associated with OX42 (indicator of activated microglial cells) signal. Figure 2 also shows the spatial correlation between the *in vivo* index (Volume of distribution), the *in vitro* translocator-protein density and the microglial activation, thus neuroinflammation.

FIGURE 1

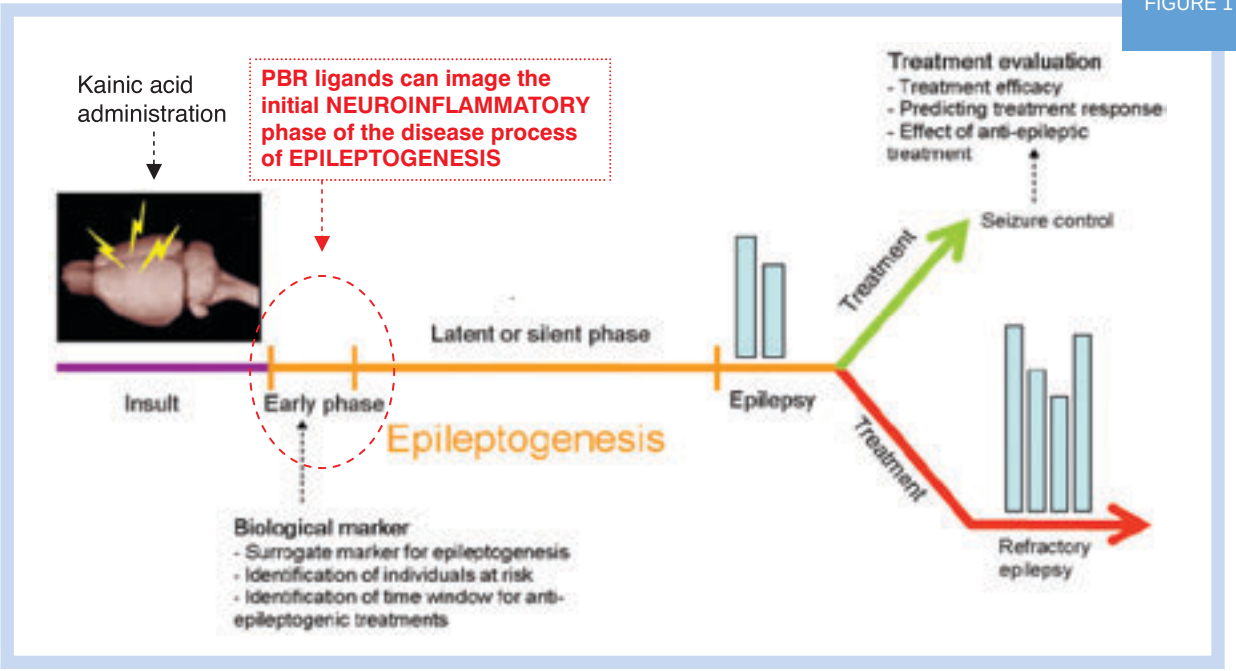

Figure 1 - Disease progression in the development of epilepsy. Usually an initial brain insult, such as a head injury, inducing seizure activity, initiates a range of physiological changes in the brain that can result in a proportion of the population developing chronic spontaneous seizures (known as epilepsy). These causal alterations in neurobiological processes are known as epileptogenesis, which is characteristically associated with no seizure activity. However once the brain has entered the epileptic state, only the symptoms of epilepsy can be treated with anti-epileptic drugs. Our goal is to use molecular imaging with TSPO radiotracers (a biological marker of neuroinflammation) to image this initial epileptogenesis period. Treatment of epileptogenesis (the efficacy of which can be assessed also with imaging) during this period of the disease offers the potential to be able to prevent the development of epilepsy in the future.

Our tools: from *in vivo* animal to cellular imaging

Our radiotracer has already shown a high affinity for the translocator protein, which is a receptor that immune cells of the brain - activated microglia - significantly over-express in response to brain injury [1-3]. We have utilised an extensively characterised animal model of epilepsy, where an initiating brain injury is induced using the excitotoxin, kainic acid [3]. Epilepsy symptoms are not seen in this model until a period of one or more months after this treatment.

A complex imaging protocol was required that allowed the assessment of density of translocator protein and radioligand affinity in the brain structures of interest. Once anaesthetised, the rats were injected intravenously with three different masses of ^{18}F-PBR111 while in the PET camera, and imaged for three-hours. Arterial blood samples were collected during the scan for quantification of radiotracer pharmacokinetics. For each rat, a CT scan was performed just before the PET scan, providing us with anatomical information. After the scan, each rat was sacrificed and its brain was kept for post-mortem confirmation of neuroinflammation .

Co-registration of a neuroanatomical atlas to the CT image of the animal allowed us to outline 20 different brain structures of interest. By using a non-linear compartmental model, translocator -protein density could be calculated in all the brain structures of interest.

A more global index called Volume of Distribution (VD), which reflects the binding of the radiotracer to the receptor, has been derived for each pixel and parametric maps could be calculated (Figure 2). *In vitro* analyses of brain sections from the animals that had been imaged were performed to determine relative translocator protein density changes (autoradiography) and assess microglial activation (immunohistochemistry) between experimental conditions.

ANSTO scientists working on a component of the ANSTO LifeSciences *in vivo* imaging platform, the Siemens INVEON microPET/CT camera.

FIGURE 2

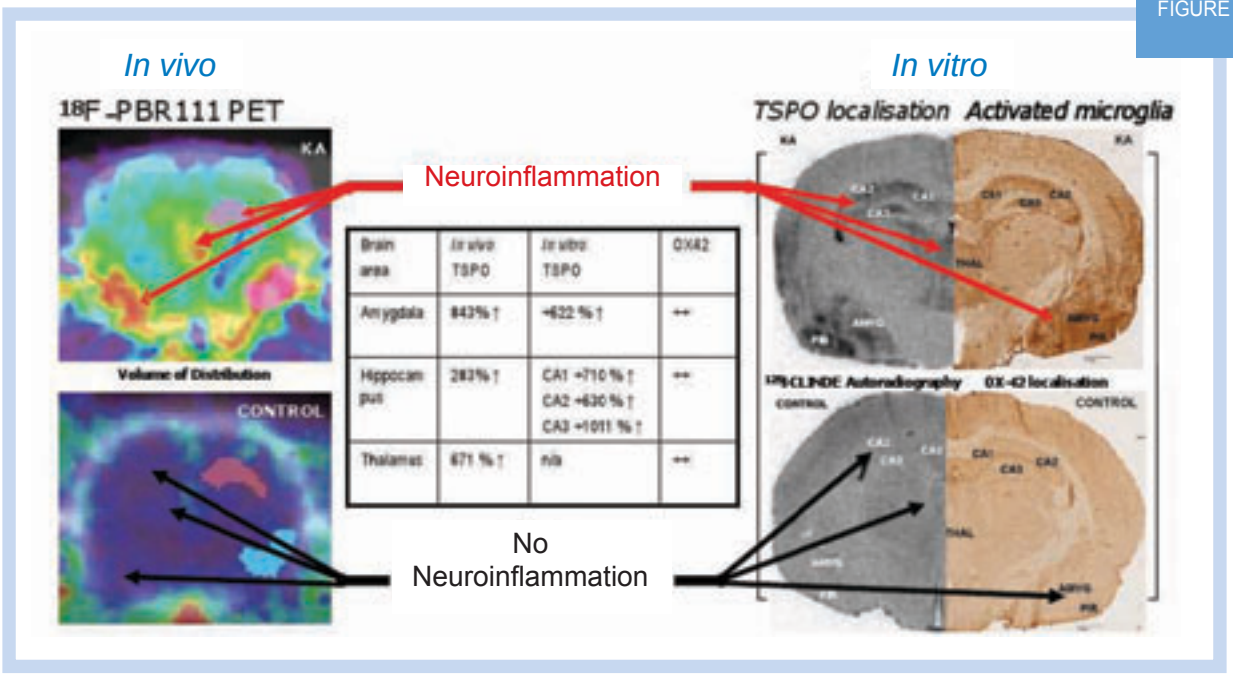

Figure 2 - *Correlation of in vivo PET ^{18}F-PBR111 uptake with in vitro biomarkers of neuroinflammation and translocator protein density.* Left, *in vivo* mapping of the Volume of Distribution is displayed in rainbow color, from blue (lower) to red (higher values) and fused with CT data. The arrows point at the most significant increases in radiotracer VD in pre-epileptic animals compared to controls. The same brain post mortem analysis, on the right, also show increases in OX42 immunoreative labelling (neuroinflammation-microglial activation) and translocator-protein (TSPO) receptor density (^{125}I-CLINDE autoradiography. Abbreviations: KA, Kainic acid treatment group; CA1-3, hippocampal subregions; THAL, thalamus; PIR, piriform cortex; AMYG, Amygdala

References

[1] Sauvageau A., Desjardins P., Lozeva V., Rose C., Hazell A.S., Bouthillier A., Butterworth R.F. *Metabolic Brain Disease*, 17 (2002) 3.

[2] Van Camp N, Boisgard R, Kuhnast B, Thézé B, Viel T, Grégoire MC, Chauveau F, Boutin H, Katsifis A, Dollé F, Tavitian B. *European Journal of Nuclear Medicine Molecular Imaging.* 2010, Jan 13.

[3] Hellier J.L., Patrylo P.R., Buckmaster P.S., Dudek F.E. *Epilepsy Research, 31* (1998) 73.

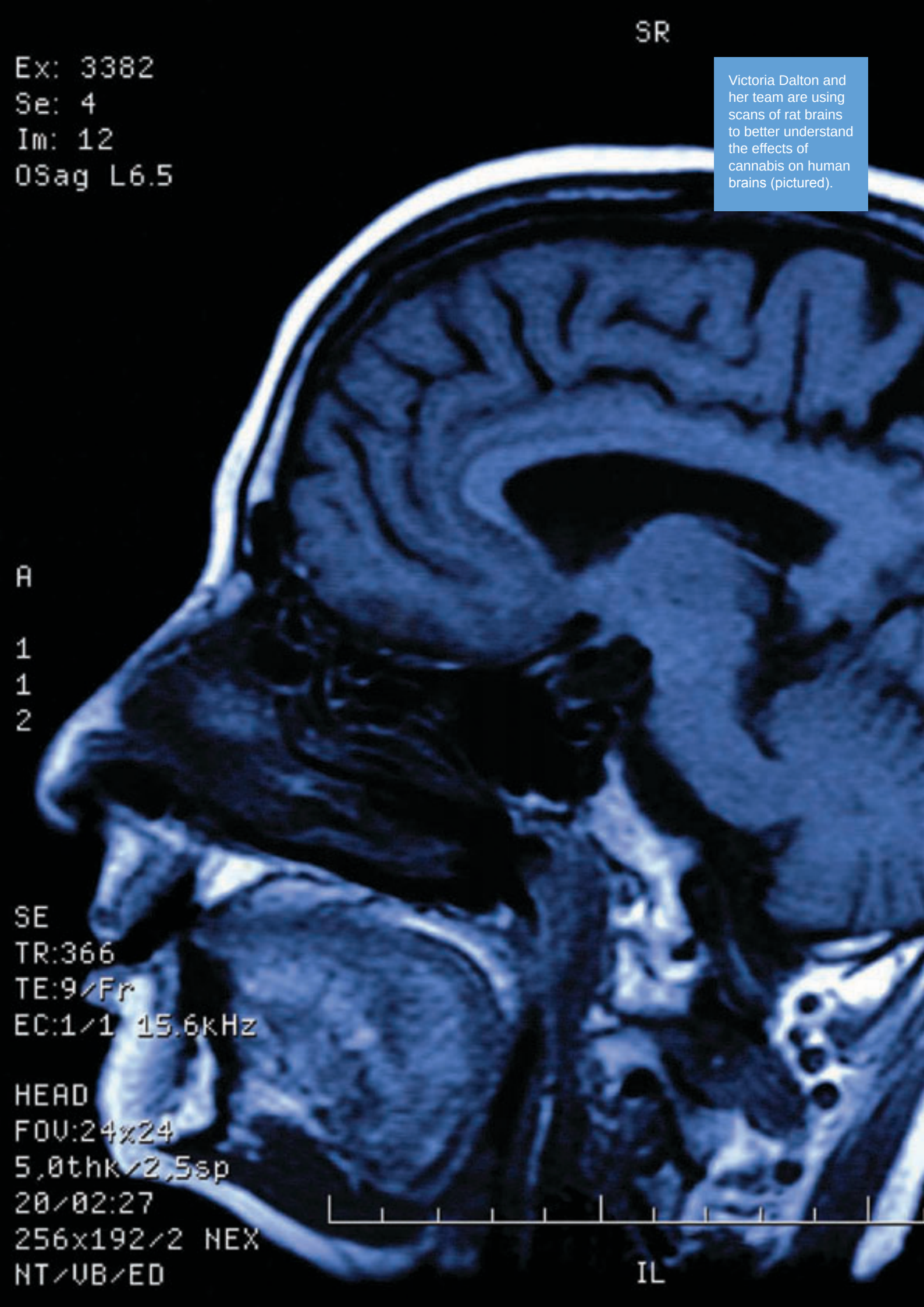

Victoria Dalton and her team are using scans of rat brains to better understand the effects of cannabis on human brains (pictured).

What is happening in the adolescent brain after exposure to cannabinoids?

Victoria S. Dalton[1,2] and Katerina Zavitsanou[1,2].
[1] ANSTO and [2] Schizophrenia Research Institute, Sydney, Australia

Cannabis use in teenagers can result in the development of drug dependence and has the potential to trigger psychosis and schizophrenia in vulnerable individuals. Aiming to investigate the age-specific responses in the brain following cannabinoid exposure, we treated adolescent and adult rats with a synthetic cannabinoid for 14 days. Comparing the levels of the cannabinoid CB1 receptor (the main target of both synthetically produced cannabinoids as well as marijuana) by using *in vitro* autoradiography, we found that adult rats adapted to excess cannabis exposure. Interestingly, in adolescent rats this adaptation was smaller. The reduced adaptive response to cannabinoid drug treatment that we observed in adolescent rats may account in part for the behavioural effects, decreased response to other drugs and adverse psychological consequences following cannabinoid exposure during adolescence.

Effects of cannabis use during adolescence

Cannabis is one of the most widely used street drugs worldwide by adolescents, but cannabis use during teenage years is linked to the development of drug dependence, impairments in memory and thought processing, and psychoses including schizophrenia in later life. Adolescence is an important time for brain maturation when many connections between nerve cells are being made as well as eliminated and fluctuations are occurring in levels of brain chemicals. It is likely that cannabis use, which can alter levels in brain chemicals and affect the formation of connections between nerve cells [1], may adversely influence the developmental processes taking place in the adolescent brain. Behavioural studies in animal models show that adolescent and adult rodents respond differently to cannabinoids in the short and long term with adolescents showing less anxiety, more movement and deficiencies in memory and attention which mirror some aspects of schizophrenia. Despite these studies though, few groups have examined the underlying changes that take place in adolescent brain chemical systems that drive the different age-specific behavioural responses to cannabinoid exposure.

Age-specific difference in response to cannabinoid exposure

We observed age-specific differences in the adaptive, compensatory response to long–term cannabinoid drug treatment in the adolescent and adult rat brain.

In brain regions involved in movement, memory, anxiety and drug response, for example, adolescents showed a smaller adaptive response than adults (i.e. a smaller reduction in cannabinoid CB1 receptor number compared to adults). These age-specific differences may account in part for the different short term behavioural responses to cannabinoids seen in adolescent and adult animals in this study [2,3,4] and reported by others [5,6]. We also noted a decreased compensatory response to treatment in adolescents in brain areas such as nucleus accumbens and amygdala, which are important in producing the rewarding effects or “high” associated with drugs of abuse. This decreased response may in turn encourage further drug consumption to achieve the desired high, may account in part for the decreased adolescent reaction to other drugs of abuse such as morphine, cocaine and amphetamine [7] and perhaps increase the risk of drug dependence in later life.

In the long term, the lessened compensatory response in adolescents, in brain regions important in memory (hippocampus), thought processing and attention (cortex) may have an adverse impact on the developmental changes taking place in various neurochemical systems in these brain areas during adolescence. The consequences of disrupting these developmental changes may include problems in learning, memory and attention, and the development of psychosis in later life.

Methods: Treatment of adolescent and adult rats with the synthetic cannabinoid, HU210.

We treated groups of adult [2] and adolescent [3,4] rats with a potent synthetic cannabinoid, HU210, which binds to the naturally occurring cannabinoid receptor in the brain, the CB1 receptor. We examined the effect of HU210 treatment on levels of the CB1 cannabinoid receptor. Adolescent and adult male rats were treated daily with low, medium or high doses of HU210 for 14 days. CB1 receptor numbers (densities) were investigated in brain regions that are important in functions such as cognition (cortex), control of movement (basal ganglia), drug response (nucleus accumbens) and memory (hippocampus). A technique called *in vitro* autoradiography was used whereby a radioactively labelled molecule, [^{3}H] CP55,940, targeted towards the receptor of interest (CB1) is applied to the brain tissue and binding of the labelled molecule is visualised using photographic film (Figure 1) and quantified.

HU210 treatment caused a region specific, dose-dependent decrease in CB1 receptor levels in the adult and adolescent brains (Figure 1 and 2). In the adult brain, decreases ranged from 35-90%, with the highest dose of HU210 causing the greatest decline in receptor number (Figure 1). Regions where the largest reductions (78-88%) in binding took place included the hippocampus and hypothalamus (Figure 1). Smaller reductions (51-76%) were seen in the basal ganglia and a major information integration centre of the brain, the thalamus (Figure 1).

The compensatory responses (i.e. alterations in receptor levels) to HU210 treatment were different however in the adolescent and adult brain (Figure 2). The treatment caused a dose-dependent decrease in CB1 receptor levels which was smaller by up to 28% in adolescents than in adults (Figure 2).

What is next?

Future studies will focus on the effects of cannabis in animal models of psychosis (e.g. animals made vulnerable to develop psychosis like behaviour due to environmental or genetic manipulations) using *in vitro* and *in vivo* imaging techniques. This research will provide an insight into the mechanisms by which cannabis is involved in triggering psychosis in vulnerable individuals. Furthering our understanding of these processes will aid in identifying targets for treatment of both drug dependence and psychosis.

References

[1] Schlicker E, Kathmann M, Modulation of transmitter release via presynaptic cannabinoid receptors. *Trends in Pharmacological Sciences, 22(11), (2001) 565-572.*

[2] Dalton VS, Wang H, Zavitsanou K; HU210-induced downregulation in cannabinoid CB1 receptor binding strongly correlates with body weight loss in the adult rat. *Neurochemical Research, 34(7), (2009)1343-1353.*

[3] Dalton VS, Zavitsanou K. Cannabinoid effects on CB1 receptor density in the adolescent brain: an autoradiographic study using the synthetic cannabinoid HU210. Synapse (2010), in press (DOI: 10.1002/syn.20801).

[4] Dalton V S, Zavitsanou K. Adolescent rats show a reduced neurochemical reaction compared to adults in response to cannabinoid administration. Schizophrenia Research 117(2010) 388.

[5] Schramm-Sapyta N.L, Cha Y.M, Chaudhry S, Wilson W.A, Swartzwelder H.S, Kuhn C.M Differential anxiogenic, aversive, and locomotor effects of THC in adolescent and adult rats, *Psychopharmacology (Berlin)* 191: (2007) 867-77.

[6] Quinn H.R, Matsumoto I, Callaghan P.D, Long L.E, Arnold J.C, Gunasekaran N, Thompson M.R, Dawson B, Mallet P.E, Kashem M.A, Matsuda-Matsumoto H, Iwazaki T, McGregor I.S Adolescent Rats Find Repeated Delta(9)-THC Less Aversive Than Adult Rats but Display Greater Residual Cognitive Deficits and Changes in Hippocampal Protein Expression Following Exposure. *Neuropsychopharmacology* 33, (2008) 1113-26.

[7] Pistis M, Perra S, Pillolla G, Melis M, Muntoni AL, Gessa GL; Adolescent exposure to cannabinoids induces long-lasting changes in the response to drugs of abuse of rat midbrain dopamine neurons. *Biological Psychiatry* 56(2), (2004) 86-94.

FIGURE 1

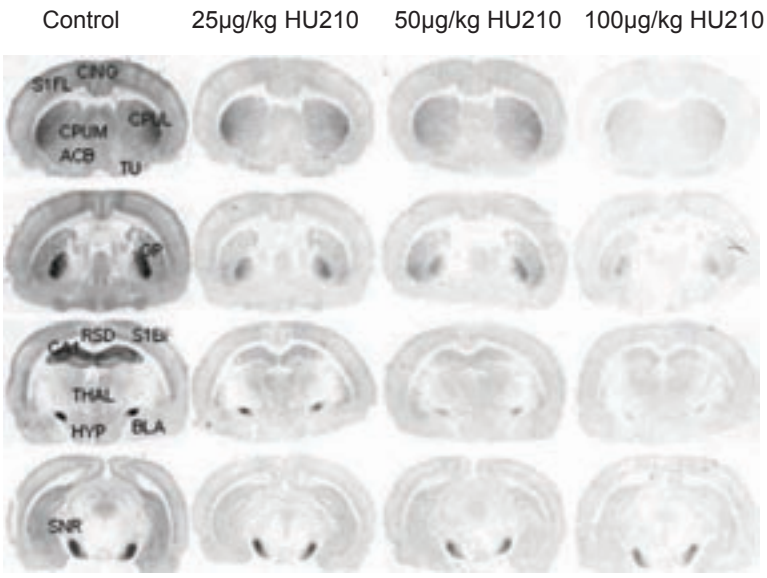

Figure 1 - Typical autoradiographs showing CB1 receptor density ([^{3}H] CP55,940 binding) in adult control rats treated with drug vehicle or rats treated with 25 (low), 50 (medium) or 100 µg/kg (high) doses of HU210 for 14 days. A dose dependent decrease in CB1 receptor density was seen with the highest dose of HU210 causing the greatest decrease in receptor number. Abbreviations: ACB: nucleus accumbens, BLA: basolateral amygdala, CA1: CA1 region of the hippocampus, CING: cingulate cortex, CPUL: lateral caudate putamen, CPUM: medial caudate putamen, GP: globus pallidus, HYP: hypothalamus, RSD: retrospenial cortex, S1BF: primary somatosensory cortex (barrel field), S1FL: primary somatosensory cortex (forelimb field), SNR: substantia nigra, THAL: thalamus, TU: olfactory tubercle nucleus.

FIGURE 2

Figure 2 - Percentage decrease in cannabinoid CB1 receptor ([^{3}H] CP55,940) binding density from control levels in adolescent (Adol) and adult rats after 14 days treatment with the highest dose of HU210, 100 µg/kg, in cortical regions (A), the basal ganglia (B) and other brain regions (C). Statistical analysis revealed that all decreases in binding were significant ($P<0.01$) except in TU in adult animals. The decrease in CB1 receptor levels was smaller by up to 28% in adolescents than in adults. See Figure 1 for other abbreviations.

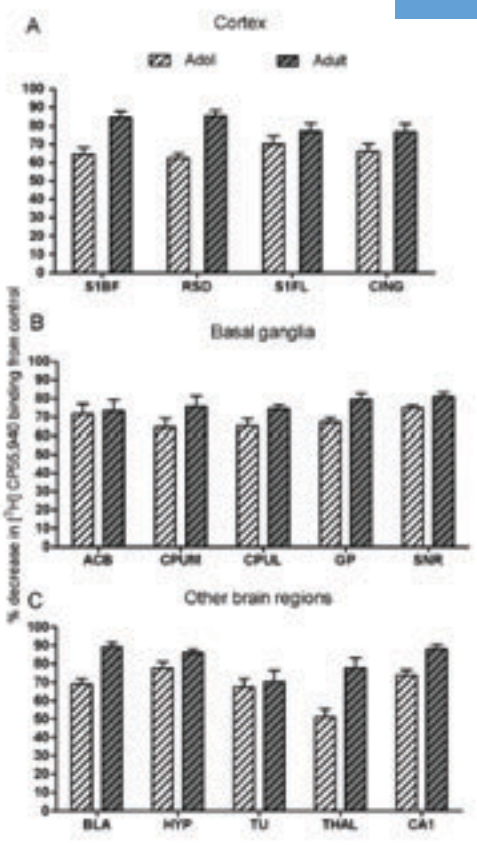

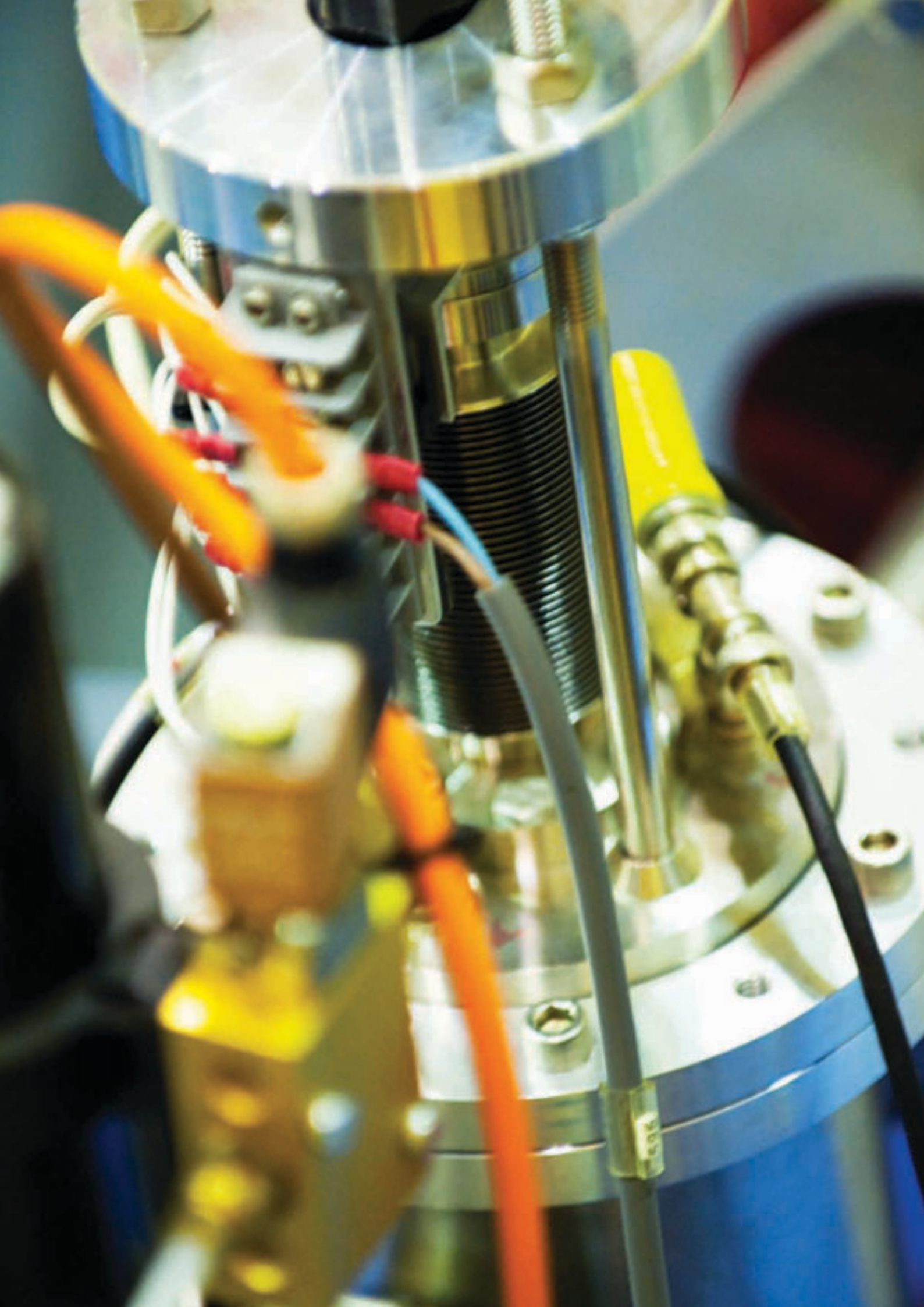

Improving radiation dosimetry in aviation, space sciences and high-energy physics

Dale Prokopovich[1], Mark Reinhard[1], Anatoly Rosenfeld[2], Iwan Cornelius[2] and Graeme Taylor[3]
[1]ANSTO, [2]University of Wollongong, Australia, [3]National Physical Laboratory, UK

Radiation transport simulations were compared with experimental measurements obtained at the High Energy Reference Field facility at CERN (European Organization for Nuclear Research, Geneva, Switzerland) to provide an improved understanding of this complex mixed radiation-field used in the calibration and testing of dosimetry instrumentation. In addition, a performance evaluation of a recently developed solid-state microdosimeter was completed. Both aspects of this study contribute to radiation-biology research and improved radiation-protection practises for commercial aviation, space sciences and high-energy physics.

The CERN - EU (European Union) High Energy Reference Field facility

In order to improve radiation protection for air crew and astronauts we combine radiation transport simulations and experimental measurements to further the understanding of the complex mixed radiation-field at the High Energy Reference Field (CERF) facility [1]. An improved understanding of the complex radiation field allows greater accuracy of dosimetry equipment calibrated at the facility. In addition, we tested a new solid-state microdosimeter device developed in Australia for performing radiation-protection measurements in unknown mixed radiation fields.

The CERF facility generates a radiation field with the characteristics of a cosmic-ray generated background found in the upper atmosphere. A neutron-dominated field of similar spectral characteristics is produced via the interaction of a high energy 120 GeV/c mixed hadron beam with a thick copper target and subsequent transport of the secondary particle production through thick concrete walls to simulate the cascade of secondary particles through the upper atmosphere. CERF is predominantly used in the calibration of radiation-dosimetry instrumentation for applications in aviation, space and high-energy physics and for the evaluation of new dosimetry instrumentation and measurement techniques.

The complex environment of CERF was simulated, using the Monte Carlo-based GEANT4 toolkit [1], to recreate the particle-energy fluence of the radiation field at different positions of interest within the facility. Figure 1a-d displays the various components of the particle-energy fluence from the mixed-particle radiation field at the CERF facility irradiation position CS1, consisting of high-energy particles including neutron, proton, muon, pion, electron, positron and gamma-ray components. The mixed-radiation field is dominated by a broad energy spectrum of neutrons and similarly gamma radiation, as shown in Figure 1a. Knowledge of these two components is well understood. In particular the dominant neutron component compared well with data obtained from simulations [2] using the FLUKA Monte Carlo transport-code, and from published experimental Bonner sphere measurements [3].

Of considerable interest is the non-negligible presence of a charged-particle component not previously considered relevant to the calculation of dosimetry calibrations factors employed at the facility. The current simulations revealed a significant fluence component of electrons, positrons (Figure 1b) and protons (Figure 1a) in addition to other charged particles, pions (Figure 1d) and muons (Figure 1c), at lesser fluence. Prior to these simulations the charged-particle component was considered negligible in terms of the contribution to the measurable dose rate. These results suggest the importance of including the charged-particle component into the facility's dosimetry calibration factors.

Microdosimeters

Microdosimetry provides a means to obtain a radiological hazard assessment of complex mixed radiation-fields. Conventionally, this is performed using a Tissue Equivalent Proportional Counter (TEPC) filled with a tissue equivalent gas at low pressure (0.4 - 1 kPa). As an alternative we developed a solid-state detector using a silicon-on-insulator (SOI) microdosimeter with the advantages of low weight, low voltage of operation, low power consumption and low maintenance, while being able to monitor a wide range of particles and energies [4]. The SOI Microdosimeter device possesses an array of human cell sized (30 x 30 x 10μm^3) sensitive detection volumes used to measure the spectrum of lineal energy deposit events when exposed to the field of interest. Lineal energy is the ratio of the energy deposited in a volume of tissue to the average chord length of that volume (measured in units of $keV\mu m^{-1}$). Using the regional microdosimetry approach [5] the lineal energy deposition spectrum, along with radiobiological data, is used to estimate the radiological hazard.

Comparison measurements using both a commercial TEPC (HAWK) and the SOI Microdosimeter were undertaken at identical positions within the CERF field. In the case of the SOI Microdosimeter, data were acquired using both a bare device and additionally with an over layer of low-density polyethylene to produce recoil protons from the neutron component of the field. The SOI Microdosimeter spectra were adjusted using a geometric tissue equivalence scaling factor for silicon to tissue dose conversion of ζ=0.63 [6] and a correction for charge collection efficiency of 80% at the 10 V operating bias employed [7].

Suitability of a silicon-on-insulator microdosimeter

Figure 2 shows a good agreement between the TEPC and the SOI Microdosimeter measurements over the full range of lineal energies. This indicates that the SOI Microdosimeter is suitable for use in the radiation environment encountered at the CERF facility in comparison with conventional TEPC microdosimetry techniques. The SOI Microdosimeter response to the CERF radiation field was also simulated (using GEANT4) for the various field components. The experimental measurement and the simulated response of the combined radiation field components compare well for the range of lineal energies covered, as shown in Figure 3. Using our simulations we can show that the majority of the contribution for the mid-range of lineal energies comes from the charged-particle component of the field. By comparing the results for the SOI Microdosimeter, the TEPC and the GEANT4 simulation, it can be demonstrated that the charged-particle component contributes significantly to the microdosimetric spectrum. The contribution of this charged-particle component was not recognised in previous microdosimetry measurements.

Conclusions

GEANT4 simulations of CERF have revealed the non-negligible presence of a charged-particle component of the radiation field. The accurate calibration and testing of dosimetry equipment undertaken at the facility requires that the dose contributions of the charged-particle component are properly taken into account.

Testing of a new solid-state microdosimeter device demonstrated comparable performance to existing TEPC instruments. The SOI Microdosimeter is a small, low weight, battery operable device which does not require a gas supply and can provide a true on-line measurement of the microdosimetric properties of any arbitrary mixed radiation field. It is highly suited as a portable instrument for radiation protection applications in high-energy mixed radiation fields for aviation dosimetry and related applications in space sciences and high-energy physics.

A new generation of SOI Microdosimeter is currently under development (Australian Research Council grant between University of Wollongong, University of New South Wales and ANSTO). This new generation of SOI Microdosimeter will provide the capability of online personal dosimetry in radiation-protection applications such as nuclear reactors, high-energy accelerators as well as aviation and space applications. As soon as the development is completed, the new devices will be tested at the CERF facility.

FIGURE 1

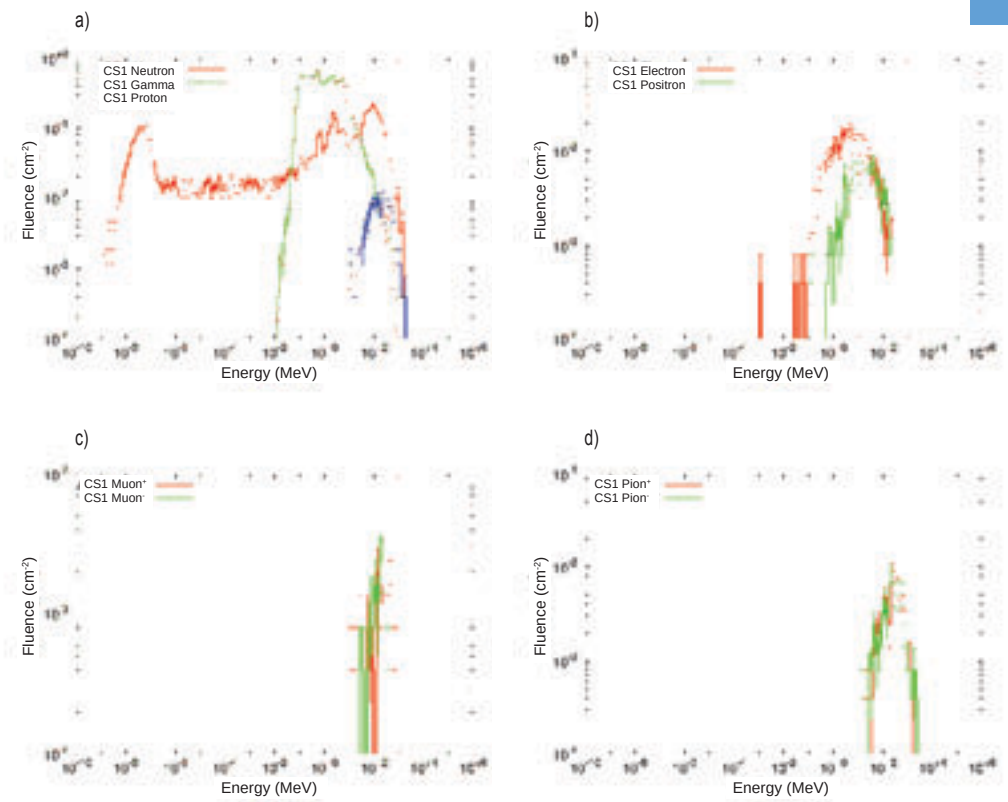

Figure 1 - Simulation of the particle fluence distributions (using the GEANT4 toolkit) of the radiation field at CERF with respect to energy at one of the irradiation position (CS1).

a) Neutron, gamma and proton

b) Electron and positron

c) Positive and negative muon

d) Positive and negative pion components.

References

[1] Agostinelli et al., *Nuclear Instruments and Methods in Physics Research A*, 506, (2003) 250-303.

[2] Mitaroff A and Silari M, *Radiation Protection Dosimetry*, 102(1), (2002) 7–22.

[3] IAEA, *Technical Reports Series*, No. 403, (2001) ISBN 92–0–102201–8.

[4] Rosenfeld A. B and Bradley P. D, *Radiation Protection Dosimetry*, 85(1-4), (1999) 385-388.

[5] Rossi H.H and Zaider M, Springer (1996) ISBN 3-54058541-9.

[6] Bradley P. D and Rosenfeld A. B, *Medical. Physics*, 25, (1998) 2220–2225.

[7] Cornelius I, Rosenfeld A, Siegele R, and Cohen D, *IEEE Transactions on Nuclear Science*, 50, (2003) 2373–2379.

FIGURE 2

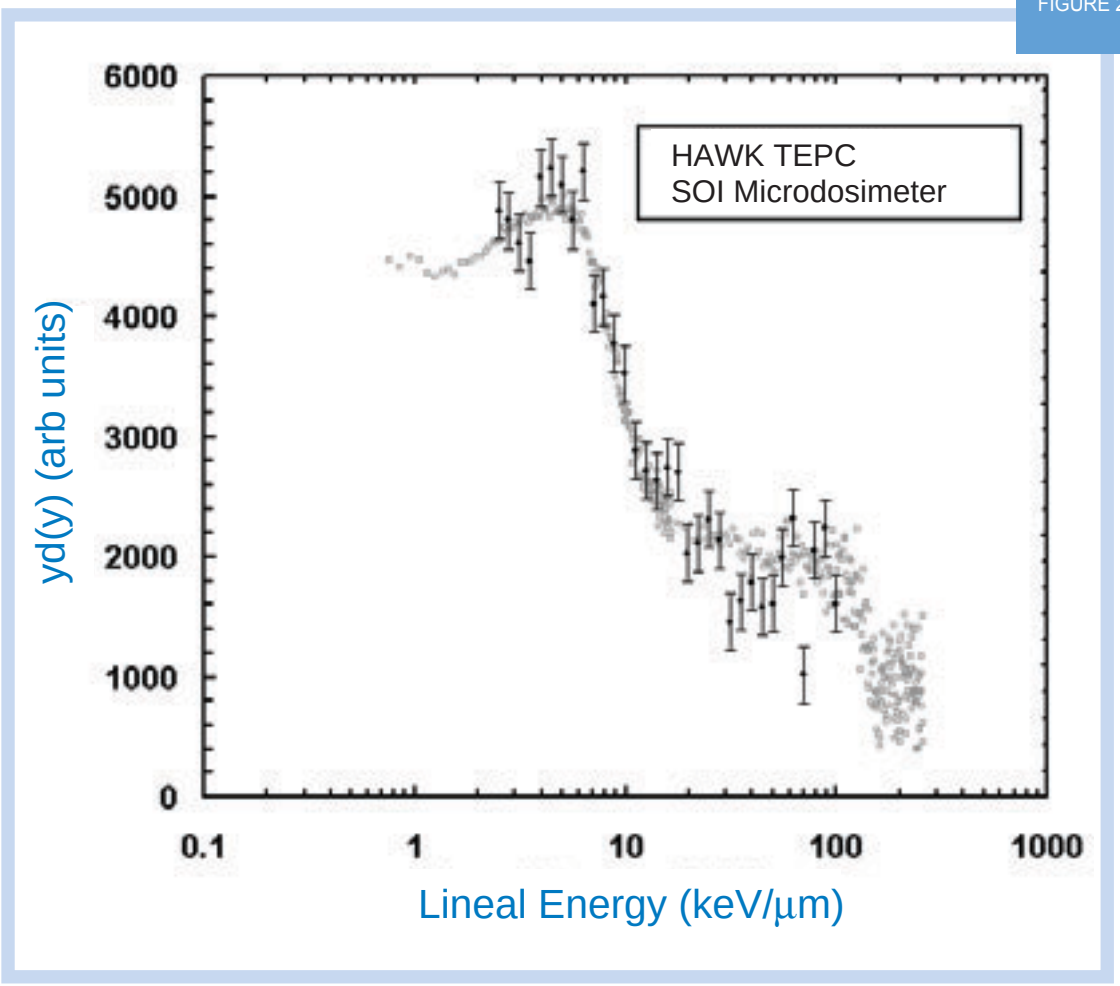

Figure 2 - Comparison of the lineal energy spectra as obtained with the SOI Microdosimeter and commercial HAWK TEPC.

FIGURE 3

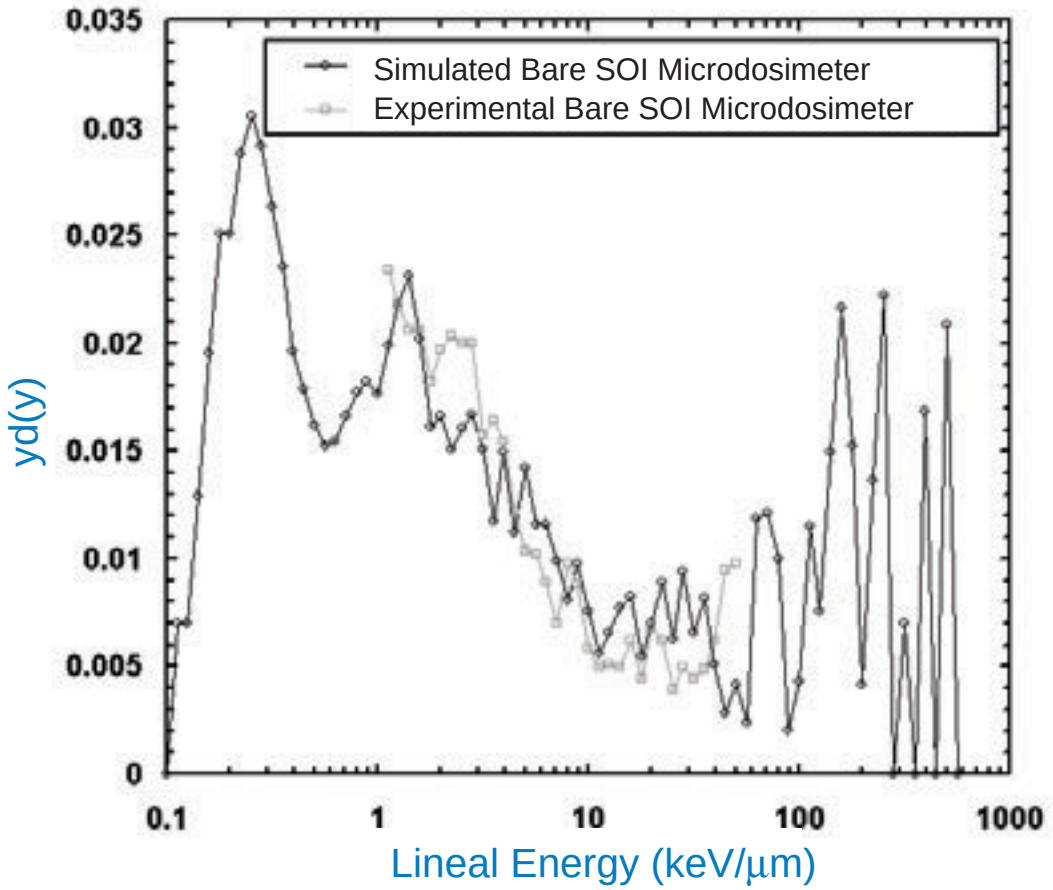

Figure 3 - Comparison of the simulated and experimentally measured bare SOI Microdosimeter lineal energy spectra.

ANSTO's neutron beam hall features state-of-the-art neutron beam instruments including the small-angle scattering instrument, Quokka, (pictured in foreground) which will be used in the next stage of ANSTO's dopamine research.

Elucidating the role of the neurotransmitter dopamine - a further step in the study of brain diseases

Agata Rekas[1], Robert K. Knott[1], Anna Sokolova[1], Kevin J. Barnham[2], Keyla Perez[2], Colin L. Masters[2], Simon C. Drew[2], Roberto Cappai Cyril C. Curtain[2] and Chi Le Lan Pham[2]
[1]ANSTO and [2]University of Melbourne

A major class of brain diseases called 'synucleinopathies', is characterised by the abnormal deposition of the protein α-synuclein (α-syn) in nerve cells (neurons). The most important member of this group is Parkinson's disease where α-synuclein aggregates are found in dopamine-producing neurons. These dopamine-producing neurons are gradually lost, eventually leading to the clinically observed inability to control movement. α-Syn in the presence of dopamine forms non-fibrillar oligomers, a molecule containing the two components, here denoted α-syn:dopamine.

These α-syn:dopamine oligomers have a variety of sizes (shown by electron microscopy), but there is no information about their supra-molecular structure and therefore, mode of association. Using small-angle X-ray scattering we could characterise shapes of α-syn:dopamine oligomers, an important part of understanding their physiological effects (e.g. neurotoxicity), and thus elucidating the role of dopamine and oligomeric α-syn in Parkinson's disease, potentially leading to new preventive and therapeutic strategies.

Why we study α-syn with dopamine

Many neurodegenerative disorders, which include Alzheimer's, Parkinson's, Huntington's and Creutzfelt-Jakob diseases, involve misfolding (abnormal structuring) and aggregation of certain proteins in the brain. One of such proteins is α-syn whose normal function in a healthy brain has not yet been established, however its ability to form elongated polymers, so-called amyloid fibrils, was found associated with dementias (e.g. Parkinson's disease, dementia with Lewy bodies and multiple-system atrophy). Despite the presence of fibrillar material in the affected brain tissue, evidence suggests that the neurotoxic agents might be smaller soluble oligomers of α-syn. Dopamine is a neurotransmitter produced by particular neurons, whose death is a significant consequence of Parkinson's disease. *In vitro*, α-syn in the presence of dopamine forms small soluble oligomers which do not lead to fibrillar structures [1,2].

What we found

In our study we looked closely at untreated α-syn and small α-syn:dopamine species: monomer and trimer. We used small angle X-ray scattering (SAXS), a technique that gives information on particle size and shape in solution. While the size information is directly derived from the SAXS data, shapes of molecules and their complexes are obtained by computational modelling [3,4] and can be validated with other techniques, such as sedimentation velocity analysis, circular dichroism spectroscopy, mass spectrometry and electron spin resonance spectroscopy.

The size (expressed as 'radius of gyration', a different measure than linear dimensions) of α-syn monomer oxidised by dopamine (37 Å) was similar to that of the untreated monomer (36 Å) which coincides with the similarity of shapes shown in Figure 1A and B.

It was previously known that monomeric α-syn in solution is unstructured, while amyloid fibrils contain structural elements called β-sheets. We found that α-syn:dopamine trimers of ~ 50 Å have more β-sheet and turn structure than monomers. A partly overlapping lateral (rather than end-to-end) arrangement of α-syn chains in the α-syn:dopamine trimer can be inferred from the size and a higher degree of structuring. Figure 2A shows the possible arrangements. Both monomers and trimers have elongated 'worm-like' shapes, as illustrated in Figure 1, which are however more diverse for trimers than monomers. It is possible that the trimers represent a mixture of species with different modes of assembly, see Figure 1C.

Higher-mass oligomers of α-syn:dopamine progressively increased in size to 105 Å for a 26-mer. And as their size increased, these species became more globular in shape, which is consistent with their images under electrone microscope [1].

Conclusions and outlook

In vitro, α-syn in the presence of dopamine forms soluble oligomers which do not lead to fibrillar structures and understanding this process is relevant for developing therapeutic and diagnostic strategies for Parkinson's disease [5]. Our experiments provide further insight into the role of neurotransmitter dopamine in the development of Parkinson's disease and other synucleinopathies and mechanisms of α-syn toxicity to brain cells. Dopamine and/or its products (melanin) oxidize methionine residues in monomeric α-syn, which with time associates to form α-syn:dopamine oligomeric species. Our data indicate that in oligomers, α-syn is bound to polymeric dopamine (melanin) with four of its methionine residues oxidised.

On the basis of these and earlier data, we propose an oxidation-based mechanism of prevention of fibrillation by dopamine. Methionine oxidation in α-syn causes structural changes (including increased propensity for β-sheet formation) which allow cross-linking between chains and stabilization of the resulting oligomer by dopamine/melanin (Figure 2B), also formed as a result of a redox process. Despite these structural changes of α-syn chains in small oligomers, their partly overlapping lateral arrangement can prevent them from directly parallel association into (also β-sheet-structured) amyloid fibrils. In this way, dopamine may be responsible for toxic effects in Parkinson's disease brain. However, from the SAXS models, it is unclear which parts of α-syn interact with dopamine. Small angle neutron scattering (SANS) can distinguish between deuterated and non-deuterated molecules. Thus, our next step will be to use deuterated dopamine in a SANS experiment on instrument Quokka at ANSTO in order to find its binding site on α-syn.

References

[1] Cappai R, Leck SL, Tew DJ, Williamson NA, Smith DP, Galatis D, Sharples RA, Curtain CC, Ali FE, Cherny RA, Culvenor JG, Bottomley SP, Masters CL, Barnham KJ, Hill AF 'Dopamine promotes alpha-synuclein aggregation into SDS-resistant soluble oligomers via a distinct folding pathway', *Faseb Journal, 19*, (2005) 1377-9.

[2] Leong SL, Pham CL, Galatis D, Fodero-Tavoletti MT, Perez K, Hill AF, Masters CL, Ali FE, Barnham KJ, Cappai R, 'Formation of dopamine-mediated alpha-synuclein-soluble oligomers requires methionine oxidation'. *Free Radical Biology and Medicine, 46*, (2009b) 1328-37.

[3] Svergun DI, 'Restoring three-dimensional structure of biopolymers from solution scattering using simulated annealing'. *Biophysical Journal, 76*, (1999) 2879-2288.

[4] Konarev PV, Petoukhov MV, Volkov VV, Svergun DI ATSAS 2.1, a program package for small-angle scattering data analysis. *Journal of Applied Crystallography, 39*, (2006) 277-286.

[5] Conway KA, Rochet JC, Bieganski RM, Lansbury PT, Jr. 'Kinetic stabilization of the α-synuclein protofibril by a dopamine-α-synuclein adduct'. *Science 294*, (2001) 1346-1349.

FIGURE 1

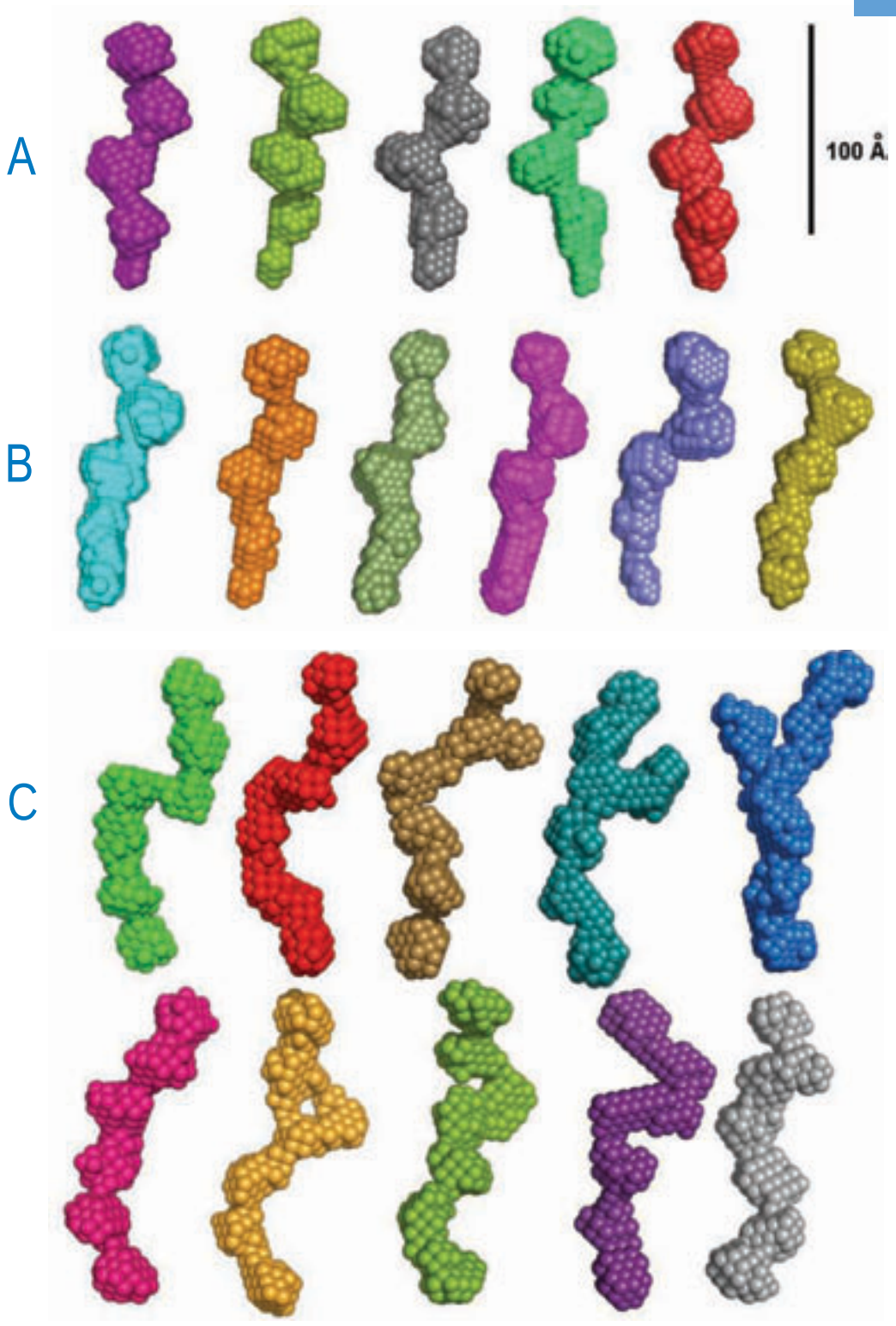

Figure 1 - SAXS shape models of (A), untreated α-syn, (B) dopamine-treated α-syn monomer and (C), α-syn:dopamine trimer Each model represents an equal probability solution.

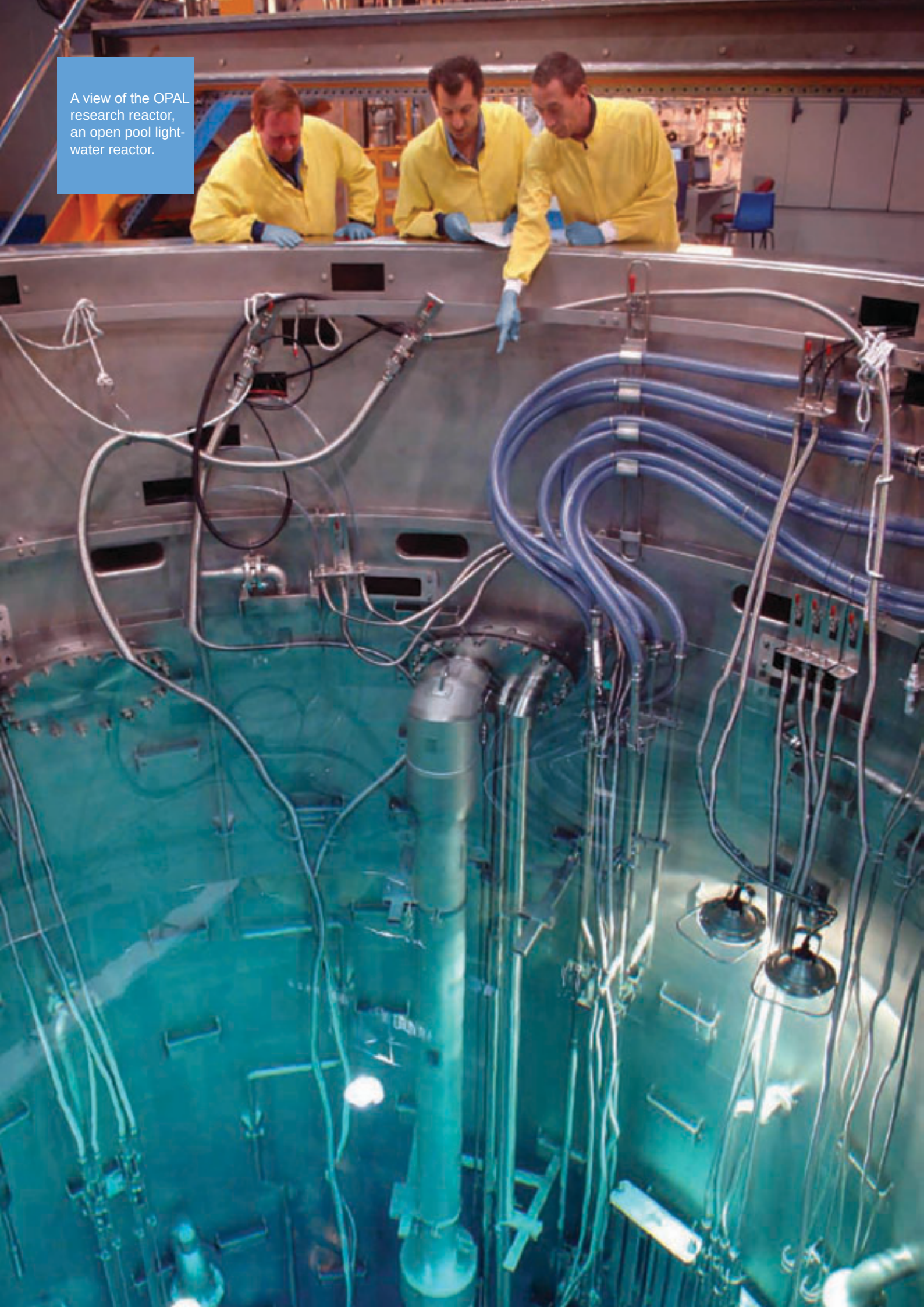

A view of the OPAL research reactor, an open pool light-water reactor.

FIGURE 2

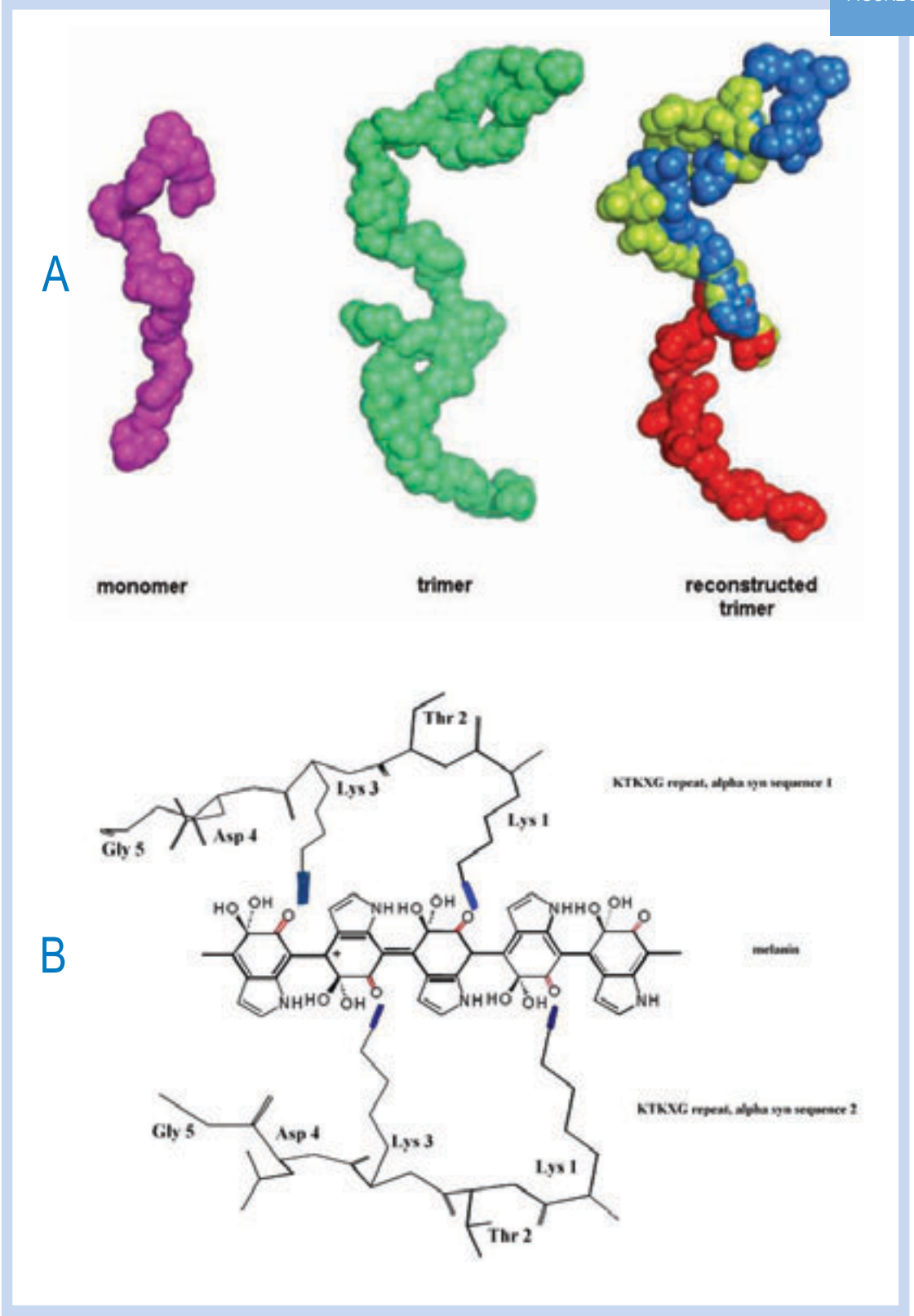

Figure 2 - Proposed interactions of α-syn monomers within a trimer. (A) Possible arrangement of α-syn monomers within SAXS model of α-syn:DA trimer; (B) Potential melanin interaction with the N-terminal region of α-syn.

Elliott Gilbert is leading ANSTO's food research project which, in part, aims to better understand diet-related diseases.

Developing novel and healthy food via scattering methods

Elliot Gilbert[1], Catherine Kealley[2], Amparo Lopez-Rubio[3], Anna Sokolova[1], Jaroslav Blazek[1] and Jitendra Mata[1]
[1]ANSTO, [2]University of Technology, Sydney, Australia and [3]Novel Materials and Nanotechnology Laboratory, Valencia, Spain

The understanding of complex food structures is essential in providing new insights into diet-related diseases and the development of novel foods. Our work focuses on proteins and carbohydrates looking not only at the structural components but also at the dynamics using neutron and X-ray scattering [1]. Demonstrating the capabilities of these techniques, we have recently established a food consortium collaborating with other research institutes and major food companies to investigate a range of food proteins.

Governments around the world are concerned about the spiralling cost of healthcare. In the US, life expectancy is anticipated to decline for the first time, partly due to diet-related diseases such as type-II diabetes. Consumers, too, are becoming increasingly aware of the importance of what they eat and are demanding new products with enhanced nutritional or disease-preventing components. However, changing the composition of the product inevitably leads to a change in the physicochemical properties, which can significantly alter its processing properties, as well as texture and flavour. To develop new food formulations therefore requires a better understanding of how structure at the meso- and nano-scale affects these characteristics. In addition, techniques that cover a broad range of timescales are also necessary to describe food structure from milliseconds to hours (processing) and minutes to months (product stability).

Until relatively recently, structure in foods was considered too complex to be studied with X-ray and neutron scattering techniques. However, with the availability of more intense sources, and advanced instrumentation and computer methods, food-based problems can now be properly addressed. In addition, for neutron scattering, when combined with so-called contrast-variation methods that rely on the sensitivity to the isotopic composition of the material under study, different structural components may be readily distinguished. Neutrons are also capable of penetrating complex sample environments - which opens up the opportunity to study industrially relevant processes in real time. Recently, we have used neutron and X-ray scattering to study structures and dynamics in two important food groups - proteins and carbohydrates [2-4].

Proteins as dried ingredients

Proteins are often incorporated in foods in a dried form. However when re-hydrated, they do not have the same properties as the hydrated protein in its native folded state. The absorption of water may be a relatively slow process due to the formation of a metastable glassy state, during which conformational changes happen only very slowly. Such characteristic structures govern the material properties of the protein and impact on their potential to be processed, in an extruder for example. Through understanding how water impacts on the material properties, the food industry will be able to predict the behaviour of the protein, thus improving the quality of the product and shelf life leading to reduced waste.

To probe these changes, we studied the protein-water interaction in dried glycinin - a protein extracted from soybean and used as a gelling, emulsifying and foaming agent [3-4] (Figure 1). At low levels of hydration, small angle X-ray scattering identified the presence of Bragg peaks associated with the presence of some degree of long-range order in the protein. With increasing moisture content, the intensity and resolution of the scattering peaks decreases significantly. Using neutrons, and deuterated water to improve the scattering contrast, it was possible to demonstrate that hydration causes the peaks to shift to a lower angle, indicating that the intermolecular distances in the structure had expanded (Figure 2). More recently, we employed quasi-elastic neutron scattering methods to follow the moisture-dependent dynamics of the structure and related this behaviour to the macroscopic glass transition behaviour. Using pure proteins as model systems provides the basis for the study of protein mixtures and the influence of additives. Since proteins as ingredients are subject to storage under varying humidity and environmental conditions, the results from these studies will assist food manufacturers in developing new formulations with predictable behaviour. Indeed, this work, in collaboration with CSIRO Food and Nutritional Sciences and The University of Queensland, has resulted in sufficient interest from several major food companies that are providing funding to investigate a range of other food proteins.

FIGURE 1

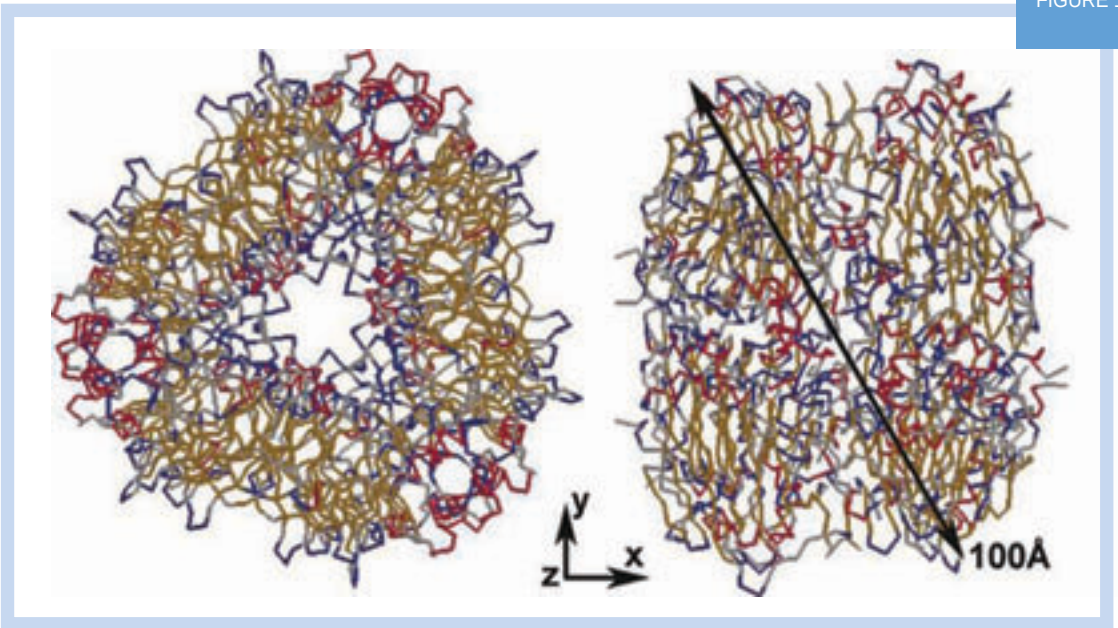

Figure 1 - Structure of the soy protein, glycinin, determined from the Protein Data Bank entry 1od5. The right panel shows the left view rotated by 90 degrees around the Y-axis. Glycinin is a heterogeneous protein with a polymorphic subunit composition, which varies among different cultivars. Five major subunits have been characterized, namely, A1aB2, A1bB1b, A2B1a, A3B4, and A5A4B3. Note that the structure displayed is for the glycinin A3B4 subunit from a soybean mutant line associates into the homohexamer for which all constituent sub-units are identical.

FIGURE 2

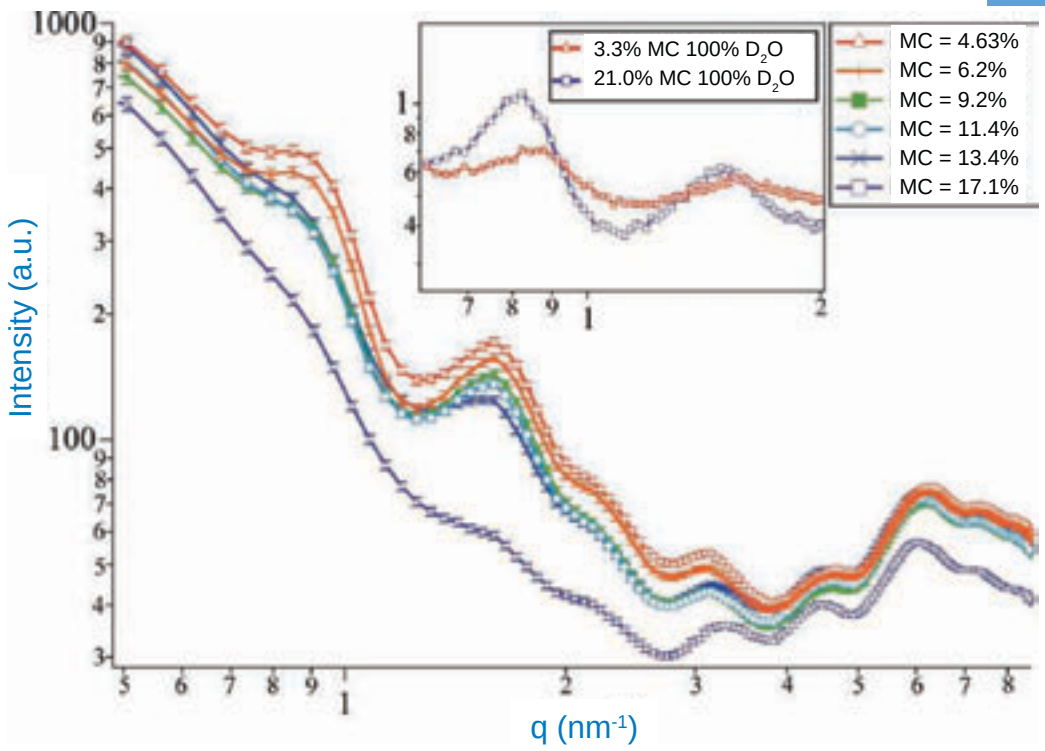

Figure 2 - Small-angle X-ray scattering data from glycinin powder with increasing moisture content. Data collected using small-angle neutron scattering is shown in the inset and for which moisture has been introduced in the form of heavy water instead of light water [3]. The use of such substitution for the SANS experiments enables improved contrast at the higher moisture contents and lowers the contribution from incoherent background scattering. Note the greater clarity in the diffraction peaks at high moisture content.

Combating Disease

Resistant Starch (RS) is a fraction of starch that is not digested in the small intestine of healthy individuals and arrives to the colon where it is fermented into short-chain fatty acids. The latter molecules are beneficial for the correct functioning of the bowel and implicated in disease prevention including colorectal cancer. Furthermore, because its breakdown into glucose is slow, RS has a role to play in combating obesity and type II diabetes. RS in processed food is believed to be formed by one of the constituents of starch, amylose, which forms digestion-resistant crystallites on cooling. We have investigated the structure of starch as a function of amylose content, processing conditions and in-vitro digestion time, with the aim of understanding how RS levels can be enhanced in processed food. Combined X-ray and neutron scattering revealed regions of crystalline material in an amorphous matrix, and allowed us to determine the physical density of the RS fraction (see Figure 2). This provides a unique insight into this extremely important food ingredient.

References

[1] Lopez-Rubio A and Gilbert E. P, Trends in *Food Science and Technology*, 20 (2009) 576.

[2] Htoon A, Shrestha A. K, Flanagan B. M, Lopez-Rubio A, Uthayakumaran S, Chanvrier H, Bird A.R, Gilbert E.P and Gidley M. J, "Effects of processing high amylose maize starches under controlled conditions on structural organization and amylase digestibility.", *Carbohydrate Polymers*, 75 (2009) 236–245.

[3] Kealley C. S, Rout M. K, Dezfouli M. R, Strounina E, Whittaker A. K, Appelqvist I.A.M, Lillford P. J, Gilbert E. P and Gidley M. J, "Solid-State Structure and Molecular Mobility of Native 11S Soy Glycinin as a Function of Moisture Content", *Biomacromolecules*, 9 (2008) 2937-2946.

[4] Kealley C.S, Kearley G.J, Kemner E, Russina M, Faraone A, Hamilton W.A, Gilbert E.P, "Novel Relaxation in Hydrated Solid-State Globular Protein", Biochimica et Biophysica Acta - *Proteins and Proteomics* 1804 (2010) 34–40.

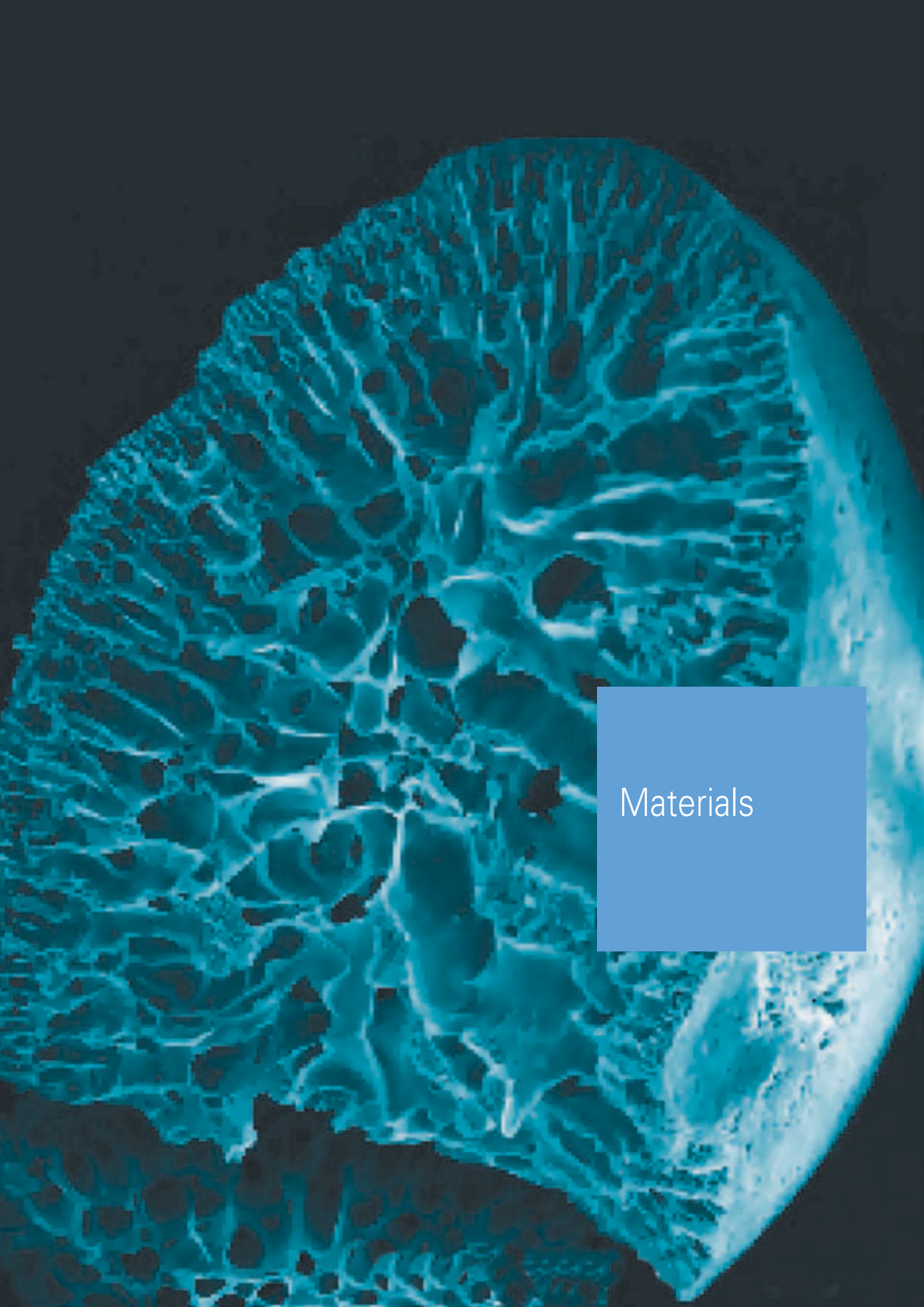

Materials

Materials

ANSTO's state-of-the-art neutron-beam instruments are unlocking the secrets of our modern world's complex materials.

ANSTO scientists use computer modelling to link the output of neutron-scattering experiments to real models, giving a visual representation of 'where atoms are and how they move'.

Among other things, our materials research seeks to gain a better understanding of materials and their life expectancy in order to design new advanced materials which are lighter, stronger and longer lasting under extreme conditions. These discoveries have applications within a diverse range of industries such as aviation and manufacturing.

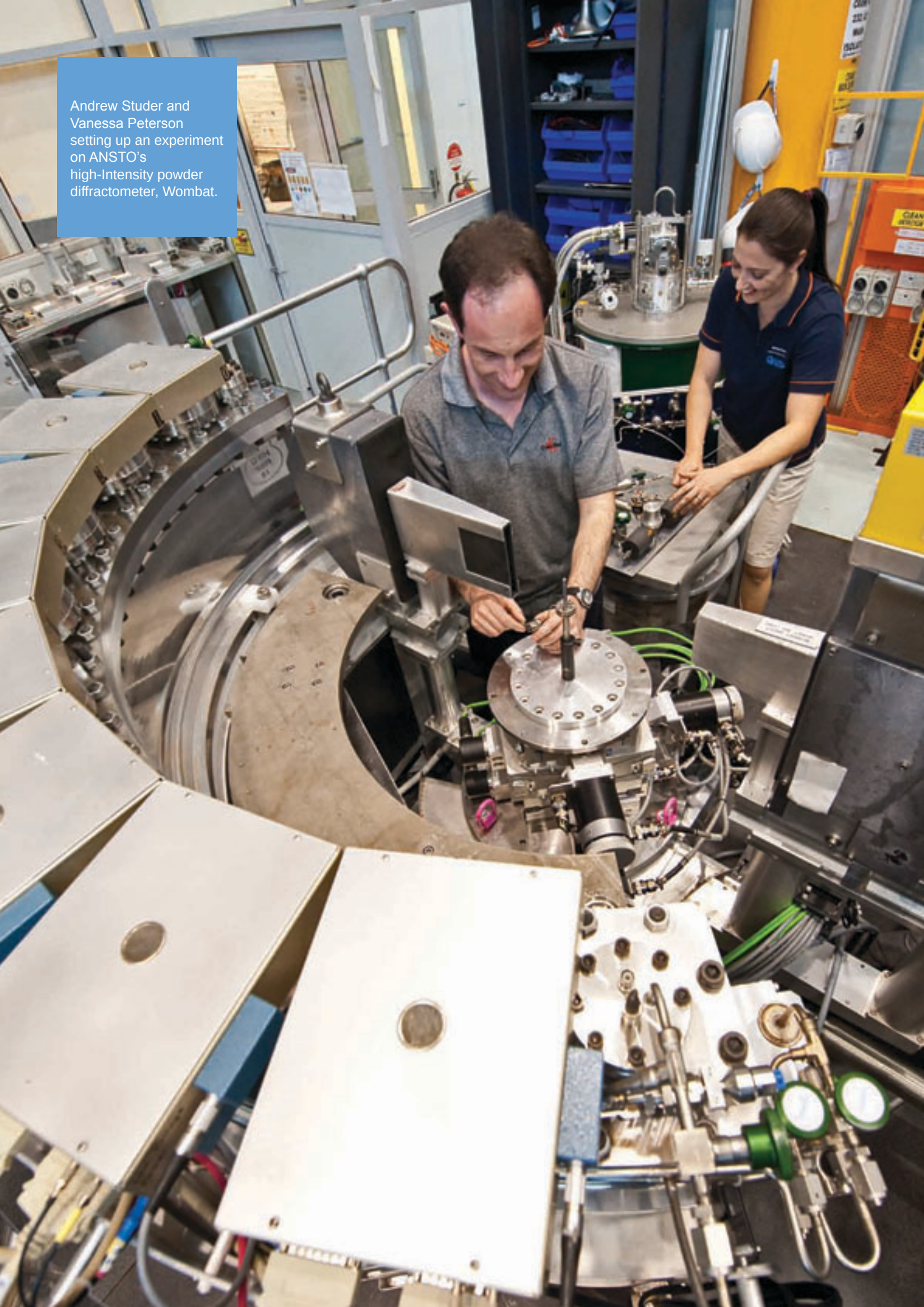

Andrew Studer and Vanessa Peterson setting up an experiment on ANSTO's high-Intensity powder diffractometer, Wombat.

A new understanding of materials that shrink on heating

Vanessa K. Peterson[1], Gordon J. Kearley[1], Cameron J. Kepert[2], Yue Wu[2], Anibal Javier Ramirez-Cuesta[3] and Ewout Kemner[4]
[1]ANSTO, [2]University of Sydney, [3]ISIS, UK, [4]Helmholtz Zentrum Berlin, Germany

We study the structure and dynamics of a metal organic framework compound using neutron scattering and modelling methods in order to understand why this material shrinks when it is heated. Porous metal organic frameworks are being increasingly studied for applications in gas-storage, (including H_2 and CO_2 for environmental applications), catalysis, and gas-separations. The diverse guest-host chemistry supported by these materials arises, in part, due to their flexibility. This flexibility leads to interesting and novel expansion properties, and as is increasingly found, to negative thermal expansion. We find a new mechanism in one material in which molecular groups twist locally, rather than collectively, offering a new way of achieving negative-thermal expansion.

What is negative thermal expansion (NTE)?

The fact that some materials reduce in size when heated seems to be rather bizarre, but this is not as counter-intuitive as it may first appear. Water expands on freezing, as does bismuth (and some of its alloys). The phenomenon is known to occur through a number of mechanisms that include electronic and magnetic transitions [1] and transverse atomic and molecular vibration [2,3].

Among the vibrational systems, there are materials which contain M-O-M' bridges (M represents a metal atom and O is oxygen) that undergo transverse vibration to cause contraction of the M-M' distance [3]. A simple analogy for this is a skipping rope held by two people that when turned quickly pulls-in on both ends. Another material is a diverse family of metal cyanides [4], which contain M-C-N-M' bridges that show an analogous effect but with increased vibrational flexibility. The mechanism proposed for these systems involves the coupling of transverse vibrations into concerted low-energy lattice modes arising from the rotation and/or translation of undistorted metal-coordination polyhedra, known as rigid unit modes [5]. On heating, these modes thermally populate and counteract higher-energy longitudinal modes that cause bond-length expansion and lead to bulk NTE.

NTE is a useful characteristic in a material, and may find applications such as devices that require precision engineering. If we want to optimise smart materials to further reduce their volume on heating or to remain unchanged, we need to understand the NTE mechanisms before these systems can be designed for specific purposes.

FIGURE 1

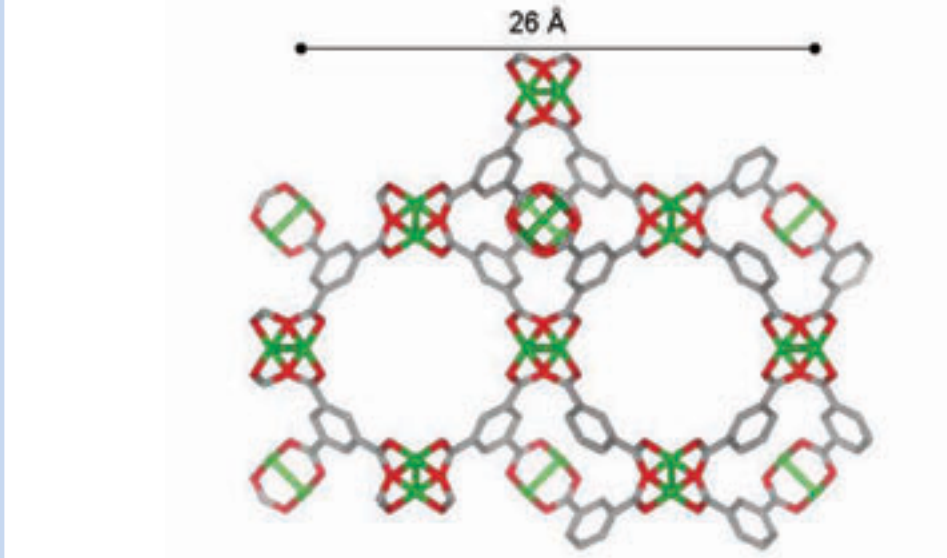

Figure 1 - $Cu_3(btc)_2$. Cu is green, O is red, and C is grey.

Metal Organic Framework Compounds (MOFs)

MOFs are composed of a regular lattice of metal atoms that are held apart by rather larger organic molecules (such as a functionalised benzene), which causes them to have large pores and structural flexibility. MOFs are interesting not only for storing molecules, such as hydrogen which can be used as an energy carrier, or CO_2 to remove this from the atmosphere, but also for NTE. Our interest has been in Cu_3btc_2 [6] which is comprised of a cubic three dimensional (3D) framework of $Cu_2(carboxylate)_4$ 'paddlewheel' units bridged by btc (benzene1,3,5-tricarboxylate) (Fig. 1). The framework's topology (a Pt_3O_4-net) makes it impossible to maintain a perpendicular arrangement of the paddlewheel units and perfectly flat (planar) btc. This causes the material to be geometrically strained, and is a driving force for NTE.

Determining the NTE mechanism

This is a complex system requiring a number of techniques to elucidate the mechanism of NTE. Firstly, we used neutron diffraction on the instrument Echidna at ANSTO to see how the atomic arrangements are modified as the temperature is changed (Fig. 2). Further analysis of the diffraction data enabled determination of the overall amplitude of thermal motion of each atom as a function of temperature. Taken together, these revealed regions of the structure where temperature changes are important. Of particular interest are the paddlewheel units. Using neutron spectroscopy we can measure the frequencies of the thermal motions of the atoms, and by combining this with the structural information and modelling we can "see" how the atoms are moving around at any temperature (data were collected using the instrument TOSCA at ISIS, UK and the instrument NEAT at HZB, Germany). From this we were able to work out which motions lead to the NTE. This resulted in a consistent picture in which a twisting of the paddlewheel is a particularly easy (or soft) motion, partly because of the nature of the bonding to the copper dimer, but also because this motion tends to relieve the geometric frustration of the lattice (see inset, Fig. 2). This twist causes a reduction in the distance between copper dimers and as the amplitude of the twist increases with temperature so the lattice contracts.

Our inelastic neutron-scattering data indicate that the dynamic paddlewheel distortion is localised. Hence, the NTE in $Cu_3(btc)_2$ is achieved through a mechanism that is novel for two reasons - most notably, through contributions from local vibrations rather than concerted modes, and secondly, through transverse vibrations of three-connecting (btc) rather than two-connecting ligands.

FIGURE 2

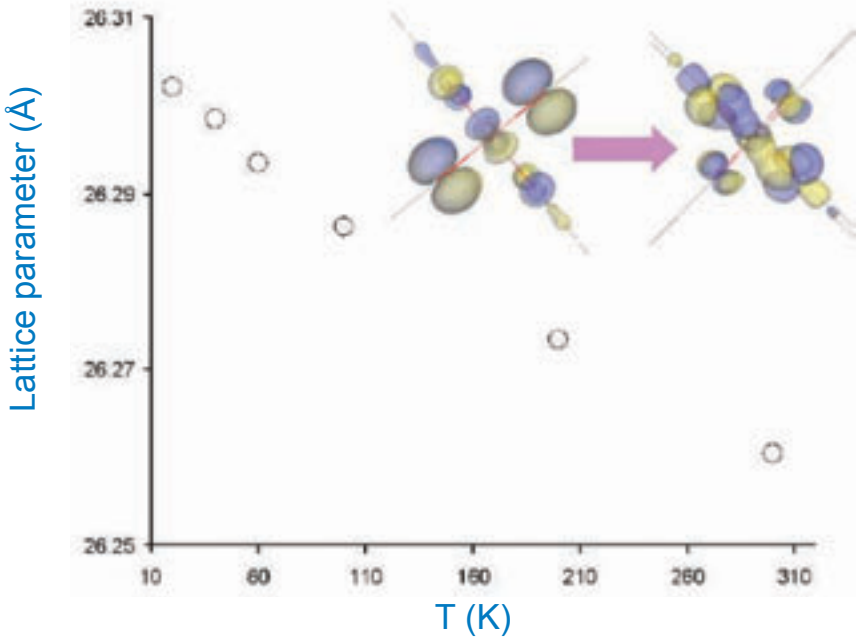

Figure 2 - Temperature dependence of the $Cu_3(btc)_2$ lattice parameter. Inset shows the dynamic paddlewheel distortion (undistorted = left, distorted = right) which results in NTE and the associated changes in bonding which makes the distortion low energy.

Next steps

Having elucidated the NTE mechanism we are now investigating methods by which the distortion (twisting) of the paddlewheel can be reduced further in energy, through chemical modification that delocalises further the bonding in the unit. This is achievable through coordination of a wide range of molecular units to the coordinatively unsaturated copper atoms of the paddlewheel.

Our previous characterisation of the vibrational modes that arise from motions of the paddlewheel is crucial in now determining how these change through chemical modification. Consequently, we can use neutron spectroscopy and molecular modelling to correlate the mechanism of NTE with the structure and degree of NTE as determined using neutron and X-ray diffraction.

References

[1] V K. Peterson, G J. Kearley, Y Wu, A J Ramirez-Cuesta, E Kemner, C J. Kepert "Local Vibrational Mechanism for Negative Thermal Expansion: A Combined Neutron Scattering and First-Principles Study" *Angewandte Chemie International Edition 49* (3) 2010, 585-588.

[2] Y. Wu, A. Kobay, V.K. Peterson, G. J. Halder, K. W. Chapman, N. Lock, P.D. Southon, C. J. Kepert, "Negative Thermal Expansion in the Metal-Organic Framework Material Cu3(btc)2 (btc = 1,3,5-benzenetricarboxylate)" *Angewandte Chemie International Edition 2008*, 47, 8929 –8932.

[3] Hao Y. M., Gao Y., Wang B.W., Qu J. P., Li Y. X., Hu J. F., Deng J. C., *Applied Physics Letters*, 78, (2001) 3277; Salvador J. R., Gu F., Hogan T., Kanatzidis M. G., *Nature*, 425, (2003) 702; Arvanitidis J., Papagelis K., Margadonna S., Prassides K., Fitch A. N., *Nature*, 425, (2003) 599; Takenaka K., Takagi H., *Applied Physics Letters,* 87, (2005) 261902.

[4] Sleight A.W., *Annual Review of Materials Science*, 28, (1998) 29; Evans J. S. O., *Journal of the Chemical Society Dalton Transactions*, (1999), 3317; Kepert C. J., *Chemical Communications*, (2006), 695.

[5] Korthuis V., Khosrovani N., Sleight A.W., Roberts N., Dupree R., Warren W.W., *Chemistry of Materials*, 7, (1995) 412; Mary T. A., Evans J. S. O., Vogt T., Sleight A.W., *Science*, 272, (1996) 90; Evans J. S. O., Hu Z., Jorgensen J. D., Argyriou D. N., Short S., Sleight A.W., *Science*, 275, (1997) 61; Lind C., Wilkinson A. P., Hu Z. B., Short S., Jorgensen J. D., *Chemistry of Materials,* 10, (1998) 2335; Evans J. S. O., David W. I. F., Sleight A.W., *Acta Crystallographica Section B*, 55, (1999) 333; Lightfoot P., Woodcock D. A., Maple M. J., Villaescusa L. A., Wright P. A., *Journal of Materials Chemistry*, 11, (2001) 212.

[6] Phillips A. E., Goodwin A. L., Halder G. J., Southon P. D., Kepert C. J., *Angewandte Chemie,* 120, (2008) 1418; *Angewandte Chemie International Edition,* 47, (2008) 1396.; Goodwin A. L., Calleja M., Conterio M. J., Dove M. T., Evans J. S. O., Keen D. A., Peters L.,. Tucker M. G, *Science,* 319, (2008) 794.; Chapman K.W., Chupas P. J., Kepert C. J., *Journal of the American Chemical Society*, 128, (2006) 7009; Goodwin A. L., Chapman K. W., Kepert C. J., *Journal of the American Chemical Society*, 2005, 127, 17980; Chapman K. W., Chupas P. J., Kepert C. J., *Journal of the American Chemical Society*, 127, (2005) 11232; Margadonna S., Prassides K., Fitch A. N, *Journal of the American Chemical Society*, 126, (2004) 15390.; Goodwin A. L., Kepert C. J., Physical Review B, 71, (2005) 140301; Goodwin A. L., Physical Review B, 74, (2006) 134302; Pretsch T., Chapman K.W., Halder G. J., Kepert C. Journal of the Chemical Society - Chemical Communications, (2006), 1857; Chapman K. W., Chupas P. J., Kepert C. J., Journal of the American Chemical Society, 127, (2005) 15630.

[7] Pryde A. K. A., Hammonds K. D., Dove M. T., Heine V., Gale J. D., Warren M. C, *Journal of Physics: Condensed Matter*, 8, (1996) 10973.

[8] Chui S. S. Y., Lo S. M. F., Charmant J. P. H., Orpen A. G., Williams I. D., *Science*, 283, (1999) 1148.


SHUT

Understanding piezoelectric materials

Jacob L. Jones[1], Abhijit Pramanick[1] and Andrew Studer[2]
[1]University of Florida, USA and [2]ANSTO

Studying the mechanisms of piezoelectric materials requires instrumentation that can provide short real-time measurements. Wombat, the high-intensity powder diffractometer at the OPAL reactor, is capable of performing high-speed stroboscopic measurements down to the sub-millisecond time scale. This capability has been used to measure the real-time response of piezoelectric materials to cyclic electric fields.

Piezoelectric materials

Piezoelectrics are materials whose electrical and mechanical properties are deeply intertwined. Putting an electric field across a piezoelectric causes it to change shape, which makes it useful as an actuator material. Conversely, the materials are also used as mechanical sensors: putting the material under strain causes it to generate an electric field. They have a wide range of uses in society - from pacemakers to hydrophones.

Ideally, in order to study the piezoelectric response in realistic conditions, the material structure should be measured in real time as it is subjected to a cyclic electrical load. What is required is an instrument that can measure rapid, real-time structural change in materials. The OPAL reactor has such an instrument: the Wombat high-speed neutron diffractometer. Wombat's speed comes from a combination of the high neutron flux from the OPAL reactor and guide system and the rapid data-acquisition capabilities of the instrument [1].

Despite their ubiquity, there is a lot still to be learned about piezoelectrics and the precise nature of the electromechanical coupling. The overarching scientific question is: what are the details of the structural changes happening to the material as an electric field is applied, and how does that relate to performance? Understanding this dynamic behaviour is important for developing applications and for understanding the subtleties in the physics of their behaviour.

The sample under investigation

Measurements were performed on a particular commercial PZT material called EC-65 (ITT Corporation). Commercial piezoelectrics such as PZTs are polycrystalline materials; on a microscopic scale they consist of a myriad of tiny crystals or domains, oriented in different directions. When an electric field is placed across the material, the individual grains are "stretched" by the field. This strain is the piezoelectric effect that is the basis of the material's usefulness.

The grains are stretched by different amounts depending on their orientations. As a result, this causes a build-up of internal strain between the grains within the material and atoms will "switch" between different domains to relieve that strain (Figure 1). However, as time goes on and the material is cycled, the domains become more fixed. This loss of mobility is a key cause of fatigue damage in these materials.

The Experiment

Wombat measures the piezoelectric response using a stroboscopic technique. The instrument can measure an individual event down to the microsecond level, but even on Wombat, for a rapidly oscillating system there may not be enough neutrons measured within one cycle to obtain meaningful information. By synchronising the detector to the electrical cycling equipment, we can measure over multiple cycles and combine them to obtain statistically useful results (Figure 2). This process is rapid, and a full measurement can usually be performed in minutes.

In a Wombat experiment, a beam of neutrons is directed at the sample, and some of the beam is diffracted at a number of different angles which relate to the spacing between different atomic planes in the materials. If a piezoelectric material is deformed by an electric field, the change in position of the atoms can cause shifts in the diffraction peaks or changes in their intensity. Different peaks are sensitive to the strain and domain switching components by different amounts. Wombat's large 120° area detector, measuring multiple diffraction peaks, can observe both of these characteristics simultaneously.

We performed two types of measurements on the samples: firstly, the response of the sample to a static electric field; then time-resolved stroboscopic measurements over a range of frequencies and electric fields.

Results and Future Work

Our measurements, performed with electric fields cycling over a range of field strengths and frequencies between 1 and 500 Hz, one of which is shown in Figure 3. This measurement was performed at 100 Hz for a field of +/-0.4 kV/mm. An important detail here is that the field is sub-coercive, less than the 0.5kV/mm threshold required to induce irreversible changes in the sample. This use of real-time neutron diffraction to measure sub-coercive domain switching was pioneered at ANSTO [2].

There is a strong dependence of domain switching with field strength, however there is no variation in the domain switching with frequency. This was unexpected by the investigators because their property measurements indicate both field-amplitude and frequency dependence. Further experiments are underway to determine the cause of this discrepancy. In particular, the diffraction measurements show that the domain switching is fast; there is no evidence of relaxation behaviour down to the ~10μs resolution of Wombat.

This work was the first post-commissioning user experiment using the stroboscopic technique to be performed on Wombat and is also the first to be published [3]. It is the first step in an ongoing programme which will continue to correlate the structure response (measured with Wombat) with other property measurements such as permittivity. In the future, the work will be expanded to look explicitly at fatiguing effects and also at characterising new classes of lead-free piezoelectric materials.

References

[1] Studer A. J, Hagen M. E and Noakes T. J, "Wombat: The High Intensity Powder Diffractometer at the OPAL Reactor", *Physica* B 385-386 (2006) 1013-1015.

[2]] J. L. Jones, M. Hoffman, J. E. Daniels, and A. J. Studer, "Direct measurement of the domain switching contribution to the dynamic piezoelectric response in ferroelectric ceramics", *Appl. Phys. Lett.* 89 (2006) 092901.

[3] Pramanick A., Prewitt A. D, Cottrell M. A., Lee W., Studer A. J., An K., Hubbard C. R., and Jones J. L., "In situ neutron diffraction studies of a commercial, soft lead zirconate titanate ceramic: Response to electric fields and mechanical stress", *Applied Physics A: Materials Science & Processing* 99 (3) 557-564.

FIGURE 1

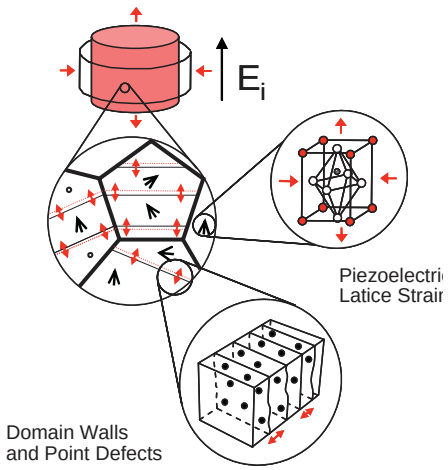

Figure 1 - Applying an electric field to a piezoelectric material causes it to respond on the atomic scale (atomic positions are shifted and the unit cell is strained) and the nano scale (clusters of atoms, or domains, change shape or orientation).

FIGURE 2

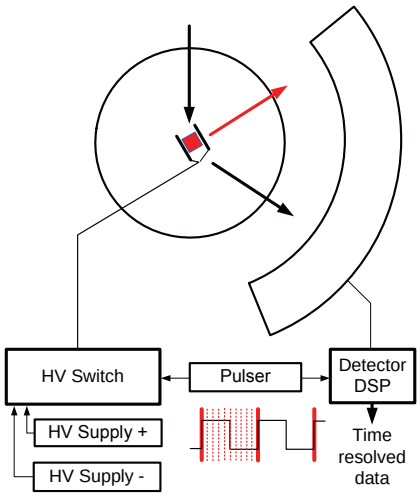

Figure 2 - Schematic of the experiment. An electric field (red arrow) is applied to the sample. Incoming neutrons are diffracted in to the detector (represented by the 120° arc). The detector is synchronised to the pulser applying the electric field.

FIGURE 3

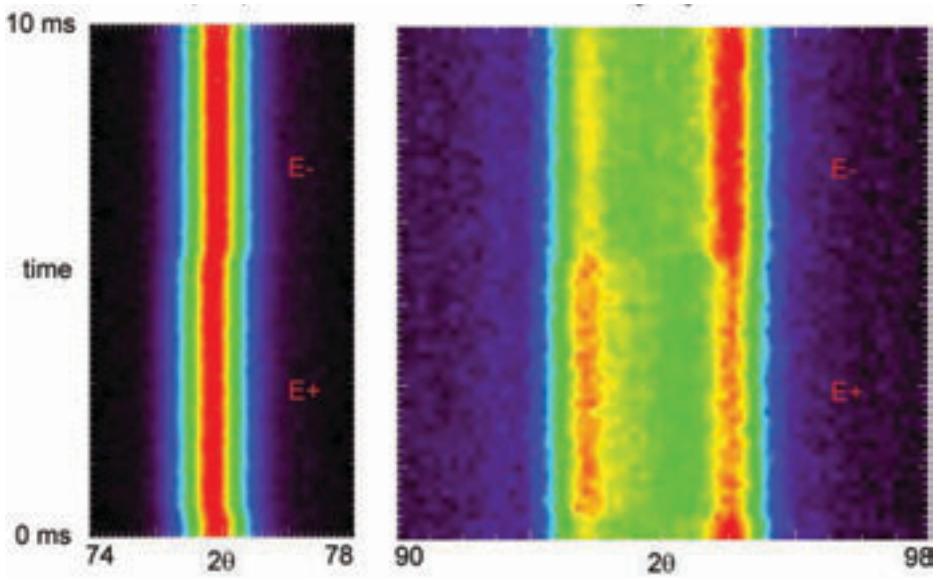

Figure 3 - The time-resolved response of commercial piezoelectric ceramic EC-65 to a bipolar, square wave electric field of amplitude 0.4 kV/mm. The positive and negative portions of the waveforms are indicated. The shift of the (111) peak (left) shows the induced strain and the shift in intensities between the two {200} peaks (right) shows the domain switching.

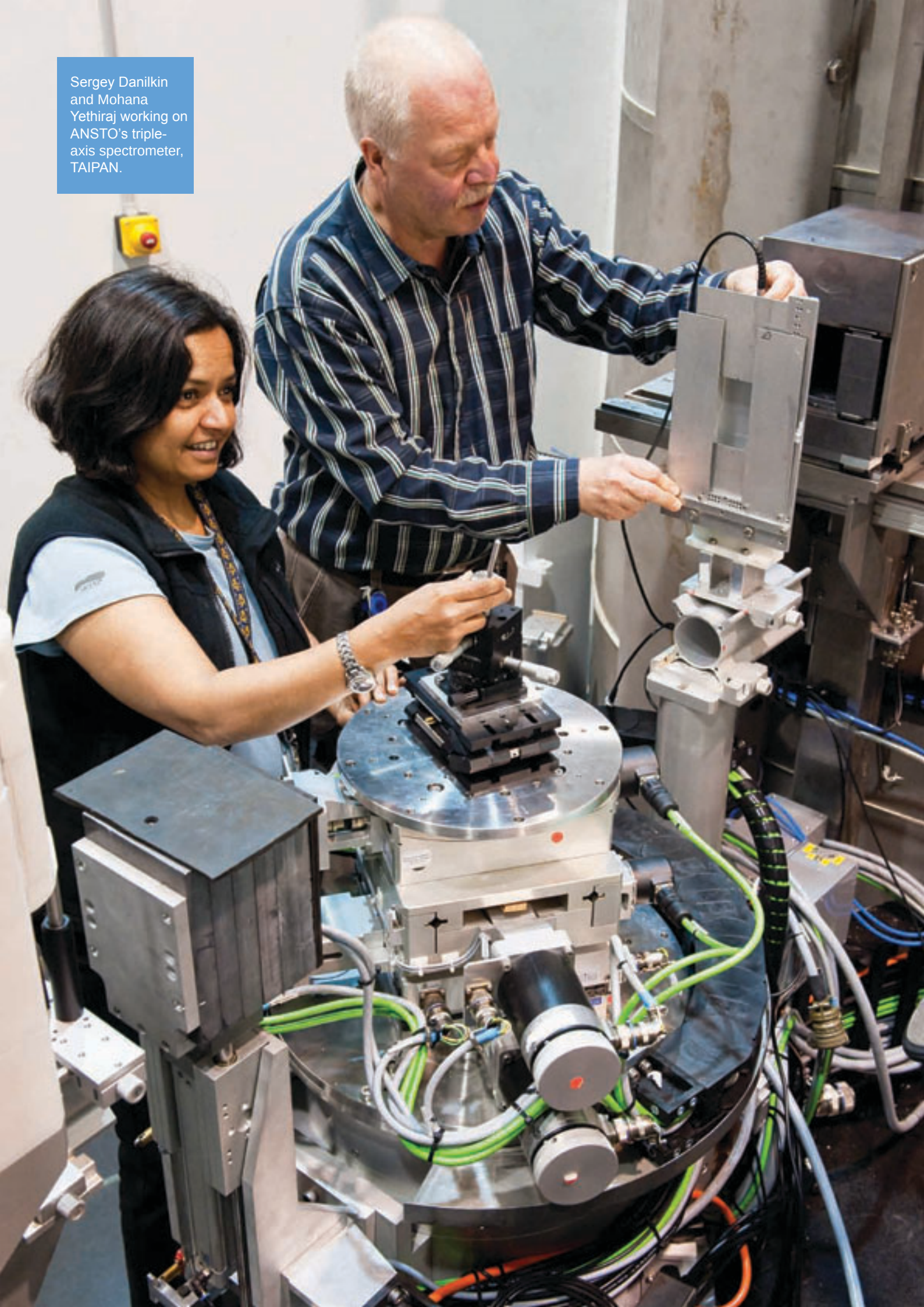

Sergey Danilkin and Mohana Yethiraj working on ANSTO's triple-axis spectrometer, TAIPAN.

Observation of soft phonon modes in superionic copper selenide

Sergey A. Danilkin, Mohana Yethiraj and Gordon J. Kearley
ANSTO

In the first experimental data obtained with the new triple-axis spectrometer TAIPAN at the OPAL reactor, we measured a superionic conductor. Superionic conductors are superior in conductivity and therefore sought after in a number of technological applications. Our measurements on copper selenide contribute to the understanding of the structure and mechanism of superionic conductors.

Superionic conductors, particularly copper selenide

Superionic conductors are materials that exhibit very high conductivity. Because of this, they have a wide range of technological applications such as solid-state capacitors (which can have 2-3 orders of magnitude higher capacitance than a conventional equivalent at the same working voltage), fuel cells, batteries and more. Their high power density or ability to store and release large amounts of energy in a short time has already led to their consideration in regenerative braking applications for hybrid vehicles, for instance. However, they are not completely understood and display very interesting physics.

Copper selenide is a mixed ionic-electronic conductor which received attention specifically due to its high ionic conductivity. In $Cu_{2-\delta}Se$, at room temperature the superionic α-phase exists in the concentration range δ = 0.15 to 0.25 [1]. The characteristic features of copper selenide are the ordering of Cu atoms in the low-temperature phase and a random distribution of Cu over interstitial sites in the high-temperature superionic phase. Lattice dynamics of $Cu_{2-\delta}Se$ are similar to other Cu and Ag fast ionic conductors showing the presence of low-energy excitations. The importance of low-lying modes that make most of the contribution to thermal motion, due to high density of states and low activation energy, is widely recognised.

What measuring phonons tells us about the material

Phonons measure the characteristic way in which copper and selenium atoms move within the material - this determines, among other things, how stiff the material is and how fast sound travels in it. (Hint: stiffer materials have higher sound velocity.) Phonons were so named because they form the waves that propagate sound (from the Greek: phonos for sound). When a phonon "softens", it means that there is something along the arrangement of atoms in that particular direction that makes the crystal somewhat less stiff. Acoustic modes go through $E = \hbar\omega = 0$ at phonon wave vector $q = 0$, the slope is linear at low q. The slope of the dispersion curve at low-q (where it is linear) represents sound velocity for that mode of propagation.

Collectively, the property of the phonons is called "lattice dynamics" and describes how the lattice moves! The lattice sites of superionic conductors generally are not fully occupied, as is the case for copper sites in the material $Cu_{2-\delta}Se$; the vacancies form conduits for ionic hopping behaviour, which makes the superionic characteristics possible. The structure although solid, has liquid-like characteristics where the diffusion is considered. Hence, studies of the lattice dynamics and the phonon dispersion relations in these materials should give a wealth of information about the mechanism related to superionic behaviour.

The measured data and interpretation using models

Measurements of phonon dispersion curves were performed on a single-crystal sample of $Cu_{1.8}Se$ which has the structure of the superionic α-phase at room temperature. The inelastic neutron scattering data were obtained with the TAIPAN thermal triple-axis spectrometer [2]. For phonon wave-vectors $q/q_m \approx 0.5$, all measured phonon branches had a pronounced broadening. These data cover a wider q-range and were measured with higher accuracy, and we found that the transverse acoustic phonons TA_1 [110], TA [100] and TA [111] demonstrate a decrease in frequency at $q/q_m \geq 0.5$ rather than the flattening seen previously [3]. The transverse acoustic [111] branch shows a considerably greater decrease for $q/q_m \geq 0.25$ than the other TA phonon branches (Figure 1). In contrast, the q-dependence of frequency of TA_2 [110] phonons and longitudinal modes shows almost linear behaviour (Figure 2).

Much of the time, it is difficult to interpret the phonon measurements directly. Hence, it is useful to calculate some models and see whether the model fits the data reasonably well. Naturally, the "best" model resembles the data the most and then can be used to make a meaningful interpretation of the observations.

Experimental phonon dispersion curves were compared with calculations performed in the frame of density-functional theoretical approach [4]. The most remarkable features of calculated acoustic modes are the low frequencies and the instability over a large area of reciprocal space. In agreement with experiment TA [111] phonon mode show instability and go to negative values at $q/q_m \geq 0.3 - 0.4$ (Figure 1). Similar behaviour demonstrate calculated acoustic TA [100], TA_1 [110] and LA [110] modes. This indicates that the stoichiometric compound is dynamically unstable and antifluorite structure is not the true low-temperature one. The instability of acoustic modes is directly related to the order–disorder transformations observed in copper-selenide followed by α-phase transition at a lower temperature [1].

Previously, in neutron-diffraction experiments, we observed the superstructure reflections in non-stoichiometric $Cu_{1.8}Se$ single crystal at ambient temperature [5]. The intensity of the superstructural reflection is quite large in [111] direction (saturated area at $\hbar\omega = 0$, $q/q_m = 0.5$ in Figure 1) and comparable with the (222) Bragg peak at $\hbar\omega = 0$, $q/q_m = 0$. The appearance of strong reflections at the edge of the Brillouin zone (BZ) can cause effects similar to the folding of the BZ. Indeed, TA phonon branch in [111] direction has clear tendency to soften (Figure 1) and the boundary of BZ can be considered as a new BZ centre, although phonon intensities at "new" (2.5 2.5 1.5) BZ center are weak. Wakamura suggested that the low-energy mode in β-AgI originates from the zone-edge acoustic phonons in γ-AgI because of folding of BZ [6]. However, the important difference in the case of the $Cu_{1.8}Se$ compound is that the ordering process and folding of the BZ are driven by a soft mode.

Next experiments

In the next experiments at TAIPAN we will investigate the almost stoichiometric compound $Cu_{1.98}Se$ just below and above their superionic phase transition. We already know that quasielastic broadening changes dramatically during the phase transitions reflecting enhancement of Cu diffusion in the superionic phase. Dispersion curves should tell us more about the interatomic correlation and the mechanism of ionic transport.

Acknowledgement

These experimental data are amongst the first to be recorded with the new instrument TAIPAN and we would like to take this opportunity to thank all those who have been involved with the building of this instrument. The authors would like to thank N.N. Bickulova from Sterlitamak University for synthesising the crystal studied in this work.

References

[1] N.H. Abrikosov, V.F. Bankina, M.A. Korzhuev, G.K. Demenski and O.A. Teplov, Sov. Phys. - *Solid State 25* (1983) 1678.

[2] S. Danilkin, G. Horton, R. Moore, G. Braoudakis and M. Hagen, *J. Neutron Res. 15* (2007) 55.

[3] S.A. Danilkin, A.N. Skomorokhov, A. Hoser, H. Fuess, V. Rajevac and N.N. Bickulova, *J. Alloys Compd. 361* (2003) 57.

[4] G. Kresse and J. Furthmüller, *Software VASP*, Vienna (1999).

[5] S.A. Danilkin, *Solid State Ionics 180* (2009) 483.

[6] K. Wakamura, *Phys. Rev. B. 59* (1999) 3560.

FIGURE 1

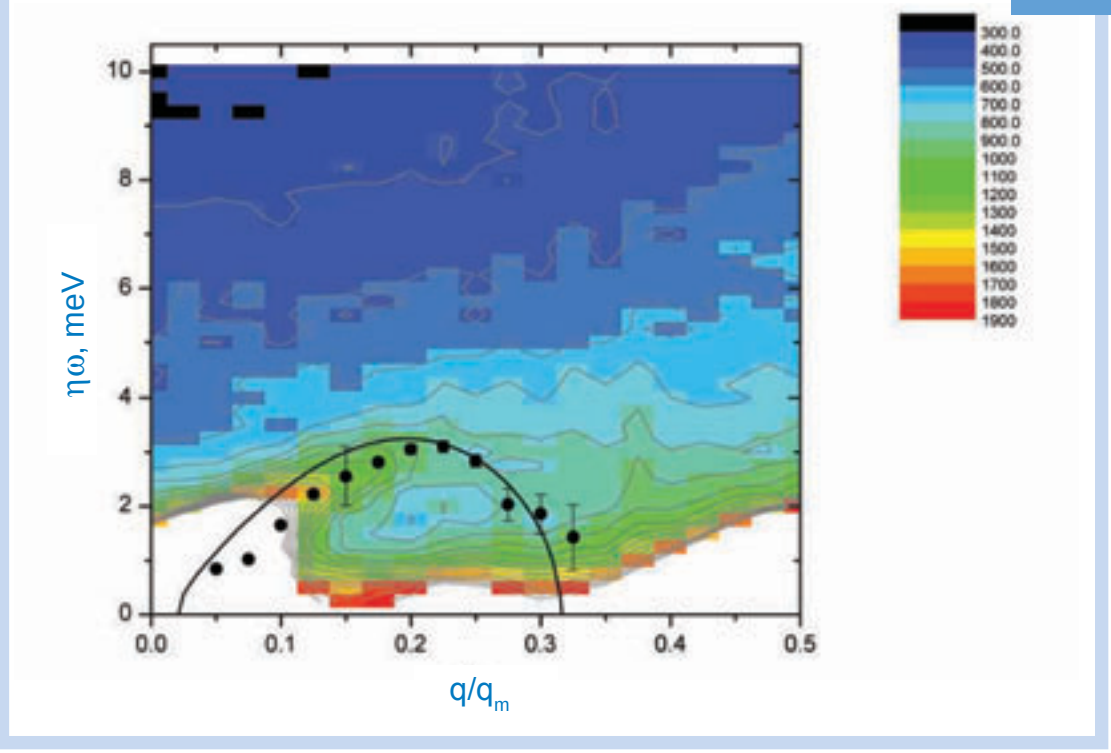

Figure 1 - Transverse acoustic [111] phonons. Surface plot of inelastic scattering intensity in $Cu_{1.8}Se$ determined from a series of constant–Q scans along direction [2+q, 2+q, 2-q]. Dots correspond to fitted positions on phonon peaks in individual scans. Line shows calculated dispersion curve.

FIGURE 2

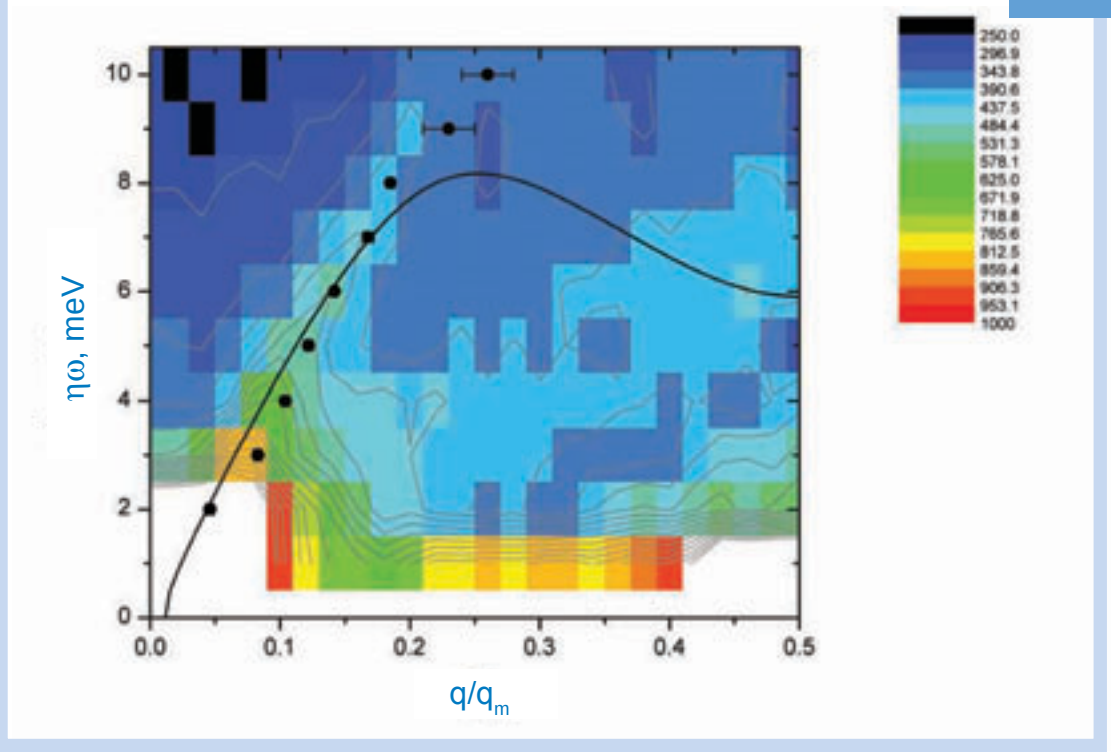

Figure 2 - Longitudinal acoustic [111] phonons. Surface plot of inelastic scattering intensity in $Cu_{1.8}Se$ determined from a series of constant–E scans along direction [1+*q*, 1+*q*, 1+*q*].

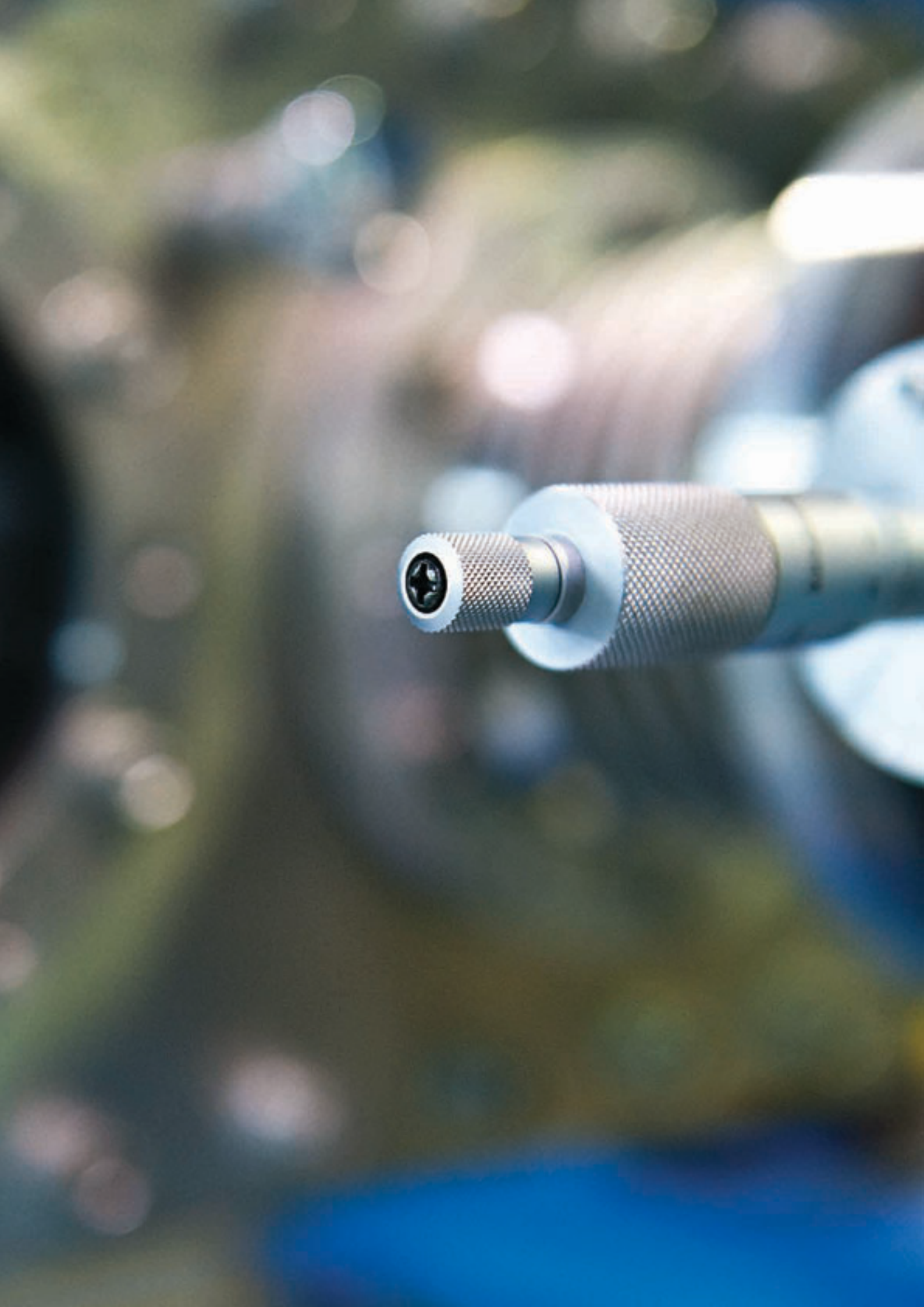

Analysis of neutron-scattering data using atomistic modelling methods

Gordon J. Kearley and Maxim Avdeev
ANSTO

In many cases the scientific value of neutron-scattering data can be increased considerably by using atomistic or molecular modelling methods as an aid to understanding the experimental data. We give examples of how modelling helps to choose between ambiguous analyses, provide starting models for analytical methods and give understanding of how the structure and dynamics of a material relate to its function.

Experimental data collected at major facilities such as ANSTO are raw material that is used to build scientific understanding. The bridge between the data and understanding may be simply a case of fitting the various pieces of information together, but modern materials are complex and, in the same way that the picture helps solve a jig-saw puzzle, modelling can help enormously in putting the pieces together correctly. Therefore scientists and computers link the output of neutron-scattering experiments to real models that allow "where atoms are and how they move" to be visualised. Computing clusters with robust software offer the opportunity to not only treat the data, but also to calculate the atomistic model of the structure (or dynamics) and compare it with the experimental data. For neutron scattering, the critical part is linking these atomistic-modelling packages with the calculation of the corresponding neutron-scattering signal.

Over the past couple of years we have been developing the expertise and resources that are needed to analyse experimental neutron-scattering data by use of atomistic modelling. Comparison of experimental data with results from modelling can now be a required part of the analysis. A significant part of neutron-scattering data collected at OPAL has been and continues to be analysed using our modelling facilities.

A complete list of modelling capability is given at the end of this report and some recent examples showing modelling of "where atoms are and how they move" are given below.

Modelling for neutron diffraction - "where atoms are"

For example, fast-ion conductors that are used in fuel cells require that atoms are in a regular grid, but with spaces, or vacancies that allow the atoms to move. This is analogous to the game where letters are moved around in a square grid to make words – which would be impossible if there were no space. The problem in more complex systems is to find where the spaces are so that we can understand the conduction process. Clearly, there is a huge number of possibilities but which is right? Our measured data can give us some important clues in this, but it's like the jig-saw without the picture – too hard to solve when it gets beyond a certain complexity. Modelling helps here because the real answer is the arrangement with the lowest energy (mountains crumble to the sea). We can calculate the energy of all possible arrangements, but in a complex system there may be many arrangements with similar energy. Think of these arrangements as the pictures and the best answer is obviously where the picture that makes sense with the pieces so that the jig-saw puzzle can be solved.

A good example of an essential role atomistic modelling can play in understanding structure and behaviour of materials is a study of $Ba_4Nb_2O_9$ which we recently carried out using OPAL, ISIS (UK), FRM-II (Germany) facilities and the ANSTO computing cluster. The composition with such a deceptively simple chemical formula was first prepared in the early 1970s. However, its crystal structure and hence the physical properties were never fully understood despite a substantial effort of several groups over the years. We initially used a variety of experimental techniques to study the material (X-ray and neutron powder and single crystal diffraction, thermal analysis, ionic conductivity measurements) gradually helped us realise that the material contains significant amount of hydrogen and is in fact a hydrate better described by a formula $Ba_6Nb_3O_{13.5}$*nH_2O.

While the basic blocks of the crystal structure (Nb_2O_9 dimers) were quickly revealed from the diffraction data the details of arrangement of extra oxygen atoms and protons were still difficult to determine, as the material proved to be both oxygen and proton conducting having highly disordered and mobile oxygen/proton sublattices. Semi-empirical modelling of the crystal structure using force-fields did not produce any meaningful results as the structure apparently contains both covalent and ionic bonds that is a difficult task for the classical force-field approach. Finally, structure optimisation using DFT (density-functional theory) framework (Vienna Ab-Initio Simulation Package, VASP code at ANSTO) revealed that protons exist in the structure as hydroxyl OH groups (Fig. 1). Furthermore, the following *ab initio* molecular dynamics study suggested the mechanism of proton conductivity when proton is transferred by hopping between pairs of cooperatively rotating tetrahedra [1].

FIGURE 1

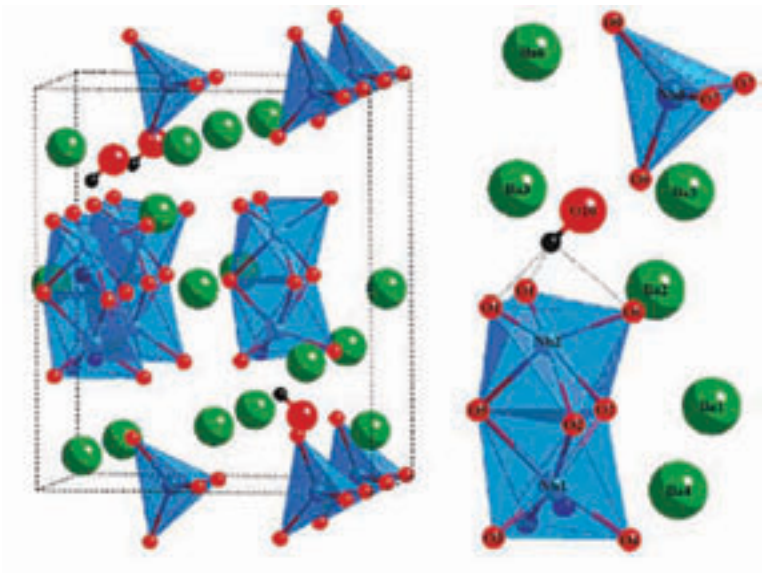

Figure 1 - Crystal structure of $Ba_6Nb_3O_{13.5}$*1/3H_2O from DFT optimisation assisted diffraction analysis. Black spheres represent protons in hydroxyl groups. High proton conductivity is mediated by dynamically disordered [NbO_4] tetrahedra.

Modelling for neutron spectroscopy- "how atoms move"

We also use modelling to understand why a material performs well or badly in its desired application so that we can improve it. This usually involves understanding not only where the atoms are, but also how they move due to the effects of temperature. The way in which neutrons are scattered by atomic nuclei is extremely well characterised, which makes it straightforward to calculate the expected neutron spectrum for any dynamical model, providing a very convenient link between atomistic models and experimental neutron-scattering data. Other articles in this report [2-5] show how this modelling (VASP) allows the observed spectral peaks to be assigned to particular atomic motions which then allow us to understand the origin of properties such as negative thermal expansion [2] and super-ionic conductivity [3]. Molecular dynamics of organic photovoltaic materials have an important effect on charge transport and have previously been studied by neutron scattering [4].

In these systems light excites one of the molecules as shown in Figure 2 which allows an electron to be separated from the molecules, passed along the column and then extracted at an electrode to provide electrical energy. One of the difficulties is that thermal motion causes the molecules (discs) to move around which hinders passing the electron up the column. Neutron experiments and modelling have characterised the motions of the disks [4] and we are now working with the Technical University of Delft, The Netherlands, and the Institute Laue-Langevin, France, to understand how these motions affect the transfer of charge. The disc-like molecules must have radial-branches, or tails attached to them which were always thought to play a purely structural role, causing the discs to stick together in columns. Modelling has recently shown not only the importance of disc-dynamics, but also that a significant part of the charge is actually passed via the tails [5].

FIGURE 2

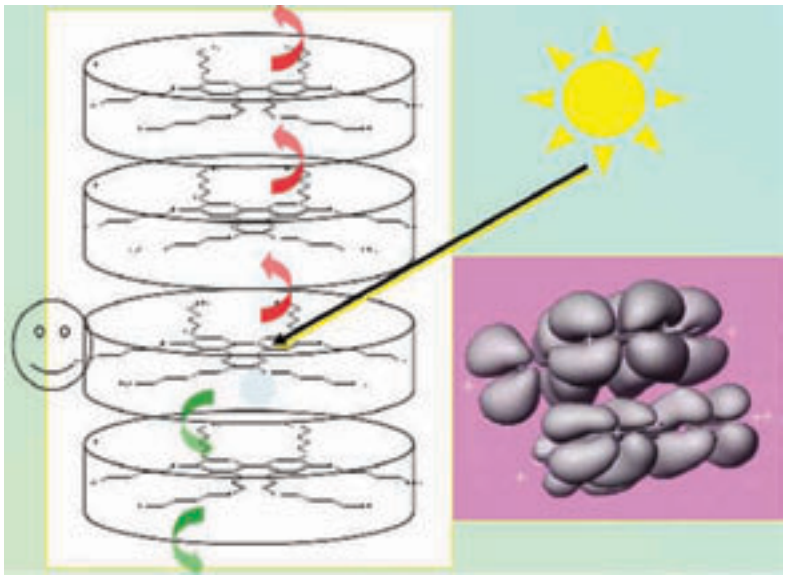

Figure 2 - Light excites a molecule within the column which allows positive and negative charges to form and separate. These then travel along the column passing between the molecular orbitals (shown only for the disc cores). Thermal motion (previously measured by neutron scattering) disturbs the overlap of orbitals on different disc hindering transport of charge.

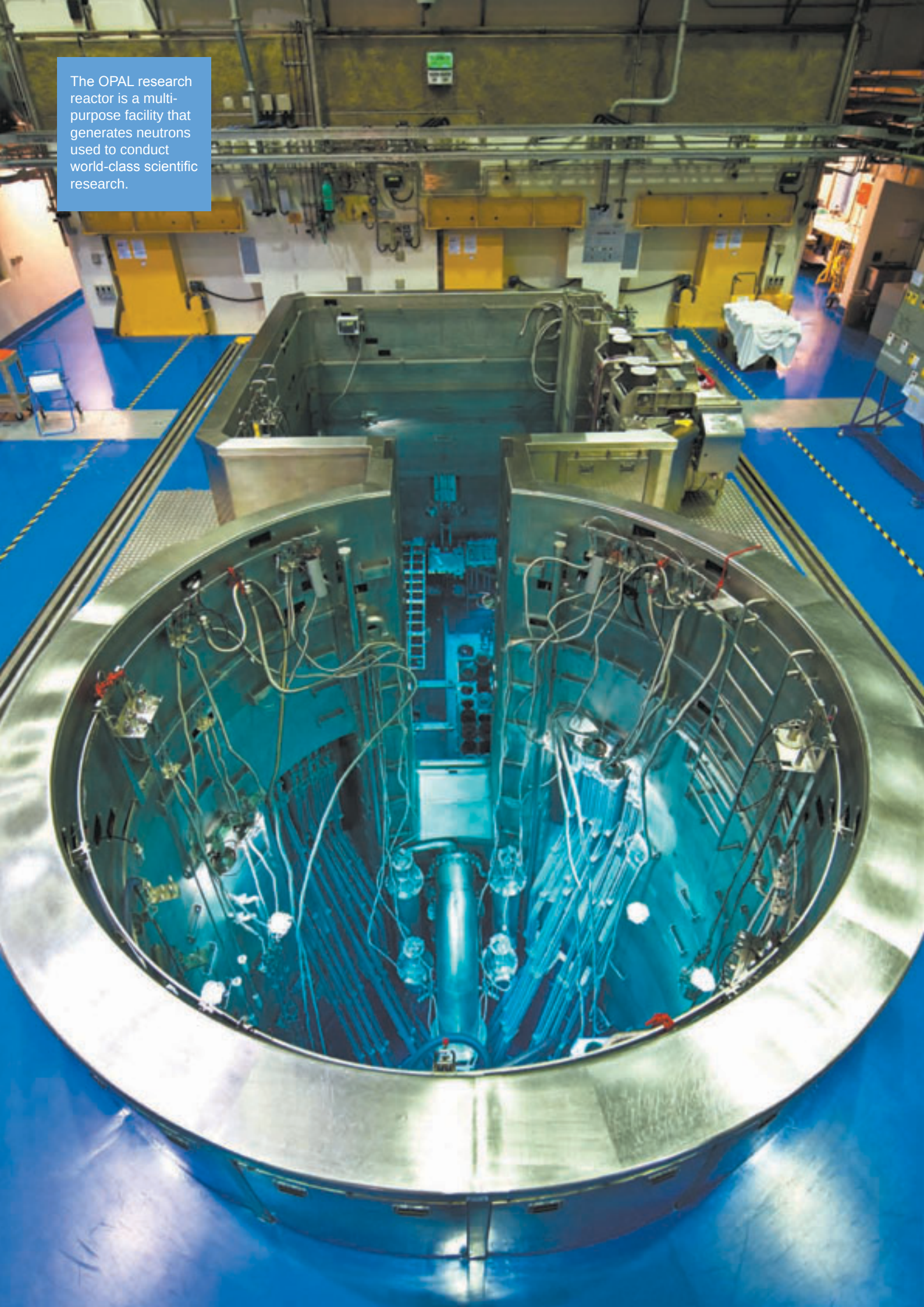

The OPAL research reactor is a multi-purpose facility that generates neutrons used to conduct world-class scientific research.

Current modelling capability for neutron scattering analysis and physical property prediction.

The following is a fairly complete list of the modelling expertise that we now have available for neutron scattering analysis:

1. Verifying crystal structures again first-principles energy calculations.
2. Deriving and energetically reasonable starting models for structure refinement.
3. Choosing between different disordered structures.
4. Structure of glasses and amorphous systems.
5. Spin-density distributions.
6. Electron density distribution.
7. Lattice dynamics for temperature factors and inelastic scattering.
8. Molecular dynamics for temperature factors, thermal expansion and inelastic scattering.
9. Band structure and density of states.
10. Elastic, dielectric and piezoelectric constants.
11. Optical properties (UV spectra, polarisability, reflectivity and refractive index).

Acknowledgement

The work presented here has been done in close collaboration with colleagues from the University of Sydney, University of Aveiro (Portugal), Institut Laue Langevin (France) and the Technical University of Delft (The Netherlands).

References

[1] C. D Ling, M. Avdeev, R. Kutteh, V.V. Kharton, A.A. Yaremchenko, S. Fialkova, N. Sharma, R.B. Macquart, M. Hoelzel and M. Gutmann, *Chemistry of Materials 21*, 3853-3864 (2009).

[2] V. K. Peterson, G. J. Kearley, Y. Wu, C. J. Kepert, A. J. Ramirez-Cuesta and E. Kemner, *Angew. Chem. Int. Ed. 49* (3), 585-588 (2010).

[3] S. A. Danilkin, M. Yethiraj and G. J. Kearley, *J. Phys. Soc. Japan, 79* (Supplement A), 25-28. (2010).

[4] Mulder, F. M.; Stride, J.; Picken, S. J.; Kouwer, P. H. J.; de Haas, M. P.; Siebbeles, L. D. A.; Kearley, G.J., *J Am. Chem. Soc.*, 2003; 125(13) 3860.

[5] Mohamed Zbiri, Mark R. Johnson, Gordon J. Kearley and Fokko M. Mulder, *Theor. Chem. Acc. 125(3-6)*, 445-451 (2010).

Karl Whittle's research is being incorporated into models showing how materials recover from radiation damage.

Radiation damage and disorder of materials

Karl Whittle, Mark Blackford, Zhaoming Zhang, Gordon Thorogood, Jeff Ferenczy, Meng Jun Qin, Eugenia Kuo, Robert Aughterson and Joel Davis
ANSTO

The study of radiation damage is not only essential for the development of new materials used in reactor design, but also for designing new waste forms. In the following, we highlight our study of titanium dioxide, a model system with different polymorphs at room temperature. This allows the change in structure with no change in composition, to be studied and better understood, and then used to understand the effects on structure on radiation.

Why we study radiation damage

The effects of radiation damage on materials are vital factors in both designing new waste forms, and new materials for use in future reactor designs, e.g. GenIV (Generation IV reactor designs incorporate advanced materials for cladding and structural components) and fusion. For any material to be used in future design, its ability to withstand high levels of radiation must be understood, and if possible predictable. As part of this process we study damage in materials using both experimental and molecular-dynamics simulation techniques, enhancing predictive capabilities. As models they can be applied to future waste forms and reactor materials, thus increasing the usability of a material over long periods of time.

Three Polymorphs of TiO_2

In this study we focused on anatase, rutile and brookite, the three commonly found structures of TiO_2. Polymorphs are formed under different conditions and have different structure, but they do not change chemically. Rutile is more stable than anatase, whereas brookite is difficult to assess as it is formed under high pressure and temperature in nature. Due to its simplicity, TiO_2 is a model compound that allows the change in structure, without a change in composition to be investigated, and linked with recovery from radiation damage. The samples were irradiated, using the *in situ* ion irradiation facility at the Argonne National Laboratory (IVEM-TANDEM), at different temperatures providing a means by which the recovery from damage can be correlated with temperature and the kinetics for recovery determined, see Figure 1. The results can then be used to calculate the activation energy for recovery that can be used in predictive studies.

When any material is irradiated the fluence required to amorphise the material is defined as the critical fluence (Fc). When irradiated at increasing temperatures, a temperature is reached whereby it is not possible to amorphise the material, i.e. the recovery process is quicker than the damaging process. This is called the critical temperature (Tc) and is obtained by analysis of the critical fluences at different temperatures. The lower the critical temperature the more rapid the recrystallisation is and thus the more stable to damage, a high Tc indicates a material which is easily amorphisable, and therefore unlikely to be used in reactors.

Our findings after irradiation

The studies showed that each of the structures behaves differently, for example synthetic rutile at 50 K was impossible to amorphise (indicating a Tc lower than 50 K), while a natural rutile (with impurities) was amorphisable with difficulty, whereas anatase and brookite were significantly easier. The structures of rutile, anatase and brookite are based on TiO_6 octahedra, in different arrangements, e.g. rutile has 2-shared edges between octahedra, while brookite and anatase have 3 and 4. The octahedra themselves have differing degrees of asymmetry with rutile being the most symmetric and anatase the least. The damage/recovery at 50 K can be directly contributed to the TiO_6 octahedral connectivity, octahedral distortion, and the volume expansion from crystalline to amorphous. The tolerance was found to change anatase < brookite < rutile with the decrease in octahedral-edge sharing, and a subsequent increase in volume expansion between crystalline and amorphous forms. Applying molecular-dynamics based simulations a similar trend was found agreeing with the experimental results [1], shown in Figure 2 for anatase and rutile. Molecular-dynamics simulations took an amorphous region within a crystalline phase, and raised the temperature to recrystallise the structure back.

After the samples were irradiated and analysed (shown in Figure 3), there was a difference from the results obtained at 50 K. At 50 K synthetic rutile was found to be the most tolerant, while anatase was the least tolerant, with brookite inbetween. Using Tc as a measure for damage resistance brookite was most tolerant (discounting the previously unamorphisable synthetic rutile), and anatase the least, with rutile inbetween [2]. These differences are complex, but can be linked to the changes in

structure, and how the polyhedra interconnect. In general, rutile is more stable than anatase when the structure is considered, while brookite is difficult to assess as it is formed under high pressure and temperature in nature. Rutile, which is more resistant to damage than anatase, has the largest crystalline to amorphous volume change, and the most symmetrical TiO_6 octahedral co-ordination, while anatase has the smallest volume change and the most asymmetric TiO_6 octahedral co-ordination. Such structural information can now be added to predictive models being developed for materials in high radiation fields, and shows that structure directly impacts on the tolerance of materials.

Outlook

The results from this work are being incorporated into models describing how materials recover from radiation damage. The models are being used in predicting the effects of radiation on Y-Ti-O oxides, which are used as additives in ODS materials (Oxide Dispersion Strengthened materials have oxides added to help improve the performance), which have been proposed for use in future reactor technologies.

FIGURE 1

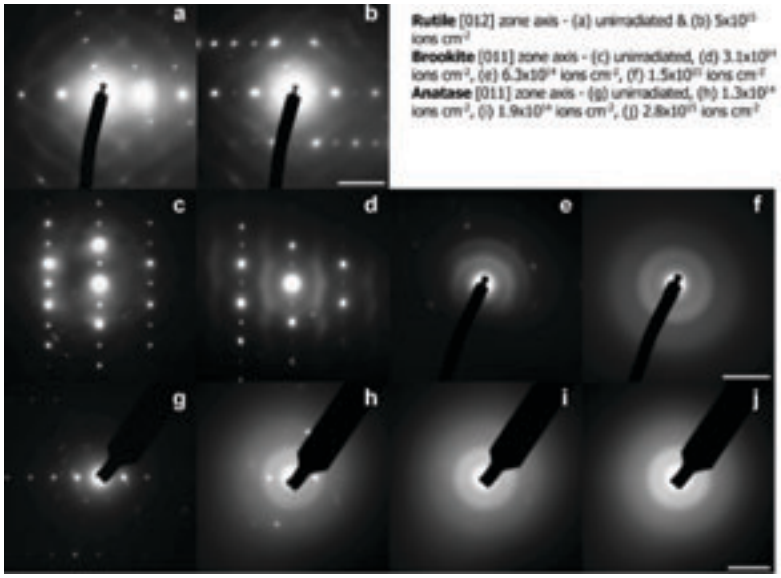

Figure 1 - Effects of increasing radiation damage on samples observed using Transmission Electron Microscopy (TEM). The numbers refer to how many ions have impacted upon the sample within the microscope.

FIGURE 2

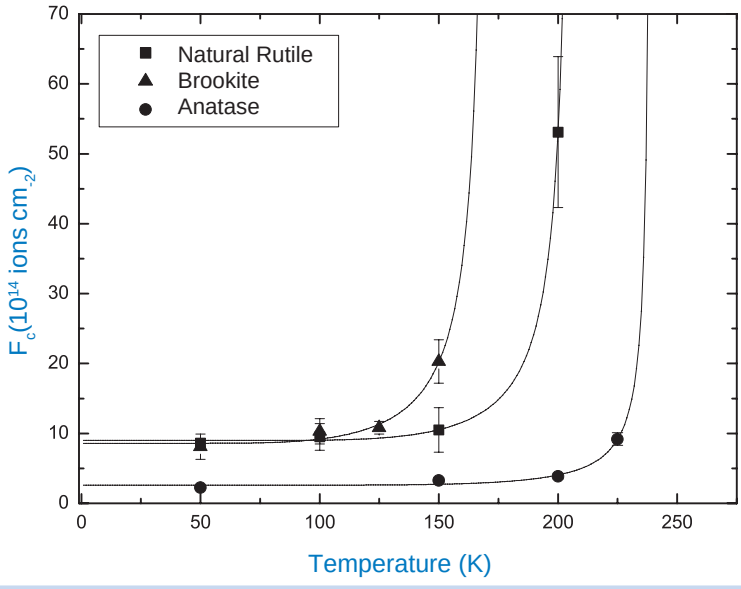

Figure 2 - A plot of fluences required to amorphise rutile, anatase and brookite at different temperatures.

FIGURE 3

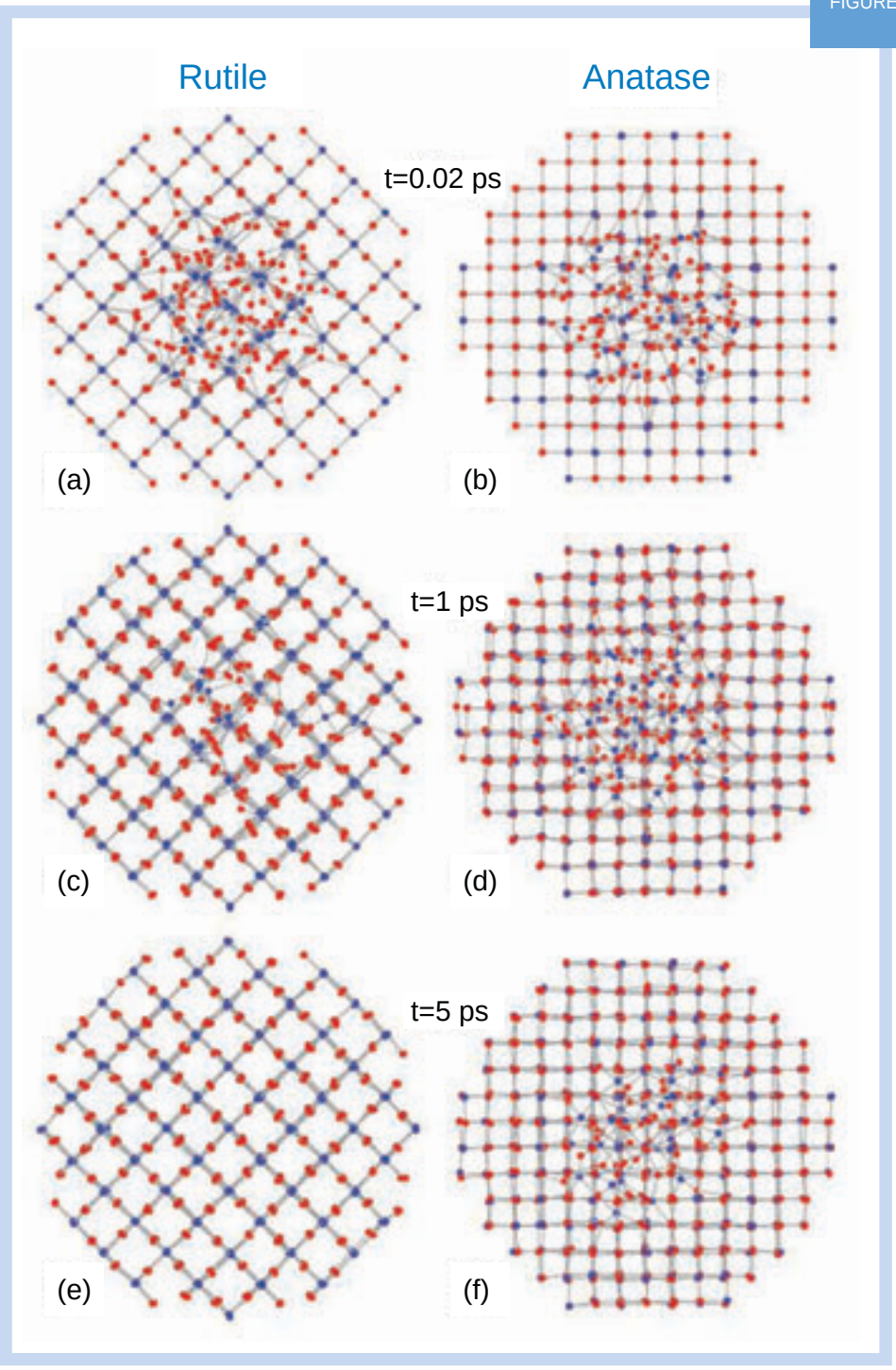

Figure 3 - The results from the molecular-dynamics simulation of rutile and anatase (brookite has been omitted for clarity). The results show that rutile (a), (c), and (e), the most symmetric, recovers more rapidly than anatase (b), (d), and (f) the most asymmetric.

References

[1] Lumpkin G. R.; Smith K. L.; Blackford M. G.; Thomas B. S.; Whittle K. R; Marks N. A.; Zaluzec N. J., *Physical Review* B, 77, (2008), 212401.

[2] Lumpkin G. R.; Blackford M. G.; Smith K. L.; Whittle K. R.; Zaluzec N. J., Ryan E. A.; Baldo P., *American Mineralogist, 95,* (2010), 192-195.

Klaus-Dieter Liss' studies of plastic deformation of materials shows not only the beginning and end conditions of the materials but the full evolution of the microstructure.

From crystal grains to texture

Kun Yan [1,2], Klaus-Dieter Liss [1], Ulf Garbe [1], John Daniels [3], Oliver Kirstein [1], Huijun Li [1,2] and Rian Dippenaar [2]
[1]ANSTO, [2] University of Wollongong, Wollongong, Australia and [3] European Synchrotron Radiation Facility, Grenoble, France

Plastic deformation of metals is inherently linked to the microstructure of materials, defining their mechanical properties and thermal behaviour. For the first time we have continuously followed the *in situ* evolution of embedded bulk grains of copper during the plastic deformation process of cold uniaxial compression. Initially, coarse grains break up into subgrains and, depending on their initial alignment, rotate into their preferred orientation merging finally into a continuous texture. In contrast to previous investigations, the study shows not only the starting and final conditions but the full evolution of the microstructure.

Better materials through microstructure engineering

One challenge in materials science and engineering is the ever more detailed understanding of materials for modelling and lifetime prediction as well as the design of novel materials, which are lighter, stronger and longer lasting under extreme conditions. Many of the structural materials, such as metals, ceramics and their composites are made out of little crystallites each of which has a more or less perfect crystal structure. They can be of different phase-composition, shape and inter-penetration. This so-called microstructure is responsible for the majority of mechanical properties of the final product; and the art to design novel materials is to find particular arrangements which make them harder, more shock absorbing, heat resistant or self-recovering upon damage and aging. It is important to start with simple materials that can be modelled and then be used to understand more complex systems. At present, our study focuses on copper and its grain and textural behaviour.

Making synchrotron X-ray movies

Here we present *in situ* data of cold plastic deformation in coarse grained copper which gives detailed insight into the real-time evolution of the microstructure [1]. High-energy X-ray diffraction at the beamline ID15B of the European Synchrotron Radiation Facility was used to probe the bulk of the material. The morphology of the Debye-Scherrer rings (Fig. 1a and 1b) is evaluated to obtain information about the grain statistics, crystallite perfection and grain orientation. For each time step, the Debye-Scherrer ring of a selected reflection (Fig. 1a and 1b) was cut at the 9 o'clock position and straightened into one line of Fig. 1c, the vertical axis is in the dimension 'time'.

Texture measurements at OPAL

The full sample texture has been measured after the compression process using neutrons on the Kowari instrument at the OPAL reactor at the Australian Nuclear Science and Technology Organisation. The 111 pole figure is shown in Fig. 1d, which is not yet totally axial symmetric but close to the asymptotic limit of the compression texture. Schematically, the final intensity distribution in Fig. 1c corresponds to the solid-dotted circle on the surface of Fig. 1d.

How texture forms

It is interesting to follow how differently oriented grains merge into the final texture. If grains are arbitrarily oriented, for example with the (111) normal in the 70°-80° and 100°-110° regions of in Fig. 1c, they rotate away from the longitudinal direction into the preferred orientation of 56°. A similar process appears to form the second texture maximum in the T direction at 0° and 180°. Grains which were already oriented close to those directions do not rotate much, however they develop subgrains due to deformation. In particular, strong mosaic spread evolves in the T±56° direction, where slip planes and deformation bands are highly activated. Grains oriented with the normal of (111) along the longitudinal stress direction L (90° and 270°) are in an unstable equilibrium in which the slip system of that plane is not activated. Therefore, these grains do not rotate. Subgrains, however, are formed through the deformation systems of the other {111} planes which creates symmetric mosaic spread of several 10°. Finally, the subgrains take over the role of individual grains and merge into the preferred orientation maxima at T±56°.

A revolution for materials design

The presented mechanism and method allows one to track the evolution of embedded grains in detail giving valuable input for further theoretical modelling and the understanding of plastic deformation. Validated on the well understood system of Cu, we have recently applied this model to twinning induced plasticity steel [2]: a novel, high strength and ductile material being developed for the transportation and defence industries. There are fundamentally different deformation mechanisms existent at high temperatures, like dynamic recrystallisation and dynamic recovery which compete with each other. We observed this for the first time *in situ* and in real time on a Zr alloy, a material relevant for the nuclear power industry [3]. In addition, we studied a Ti-Al based light metal alloy (at 1300°C with presented technique) that is being designed for aero-space applications. Here, the different deformation mechanisms simultaneously occurring in the two coexisting phases could be visualised and separated revealing the origin of the good formability aimed during near-conventional forging [4].

The new method gives immediate feedback on what is happening in the material, which is considerably more efficient than the conventional processing, quenching, preparation and characterization techniques. Therefore, thermo-mechanic simulation shall routinely be done in a synchrotron or neutron beam in order to receive instantaneous feedback from the process.

FIGURE 1

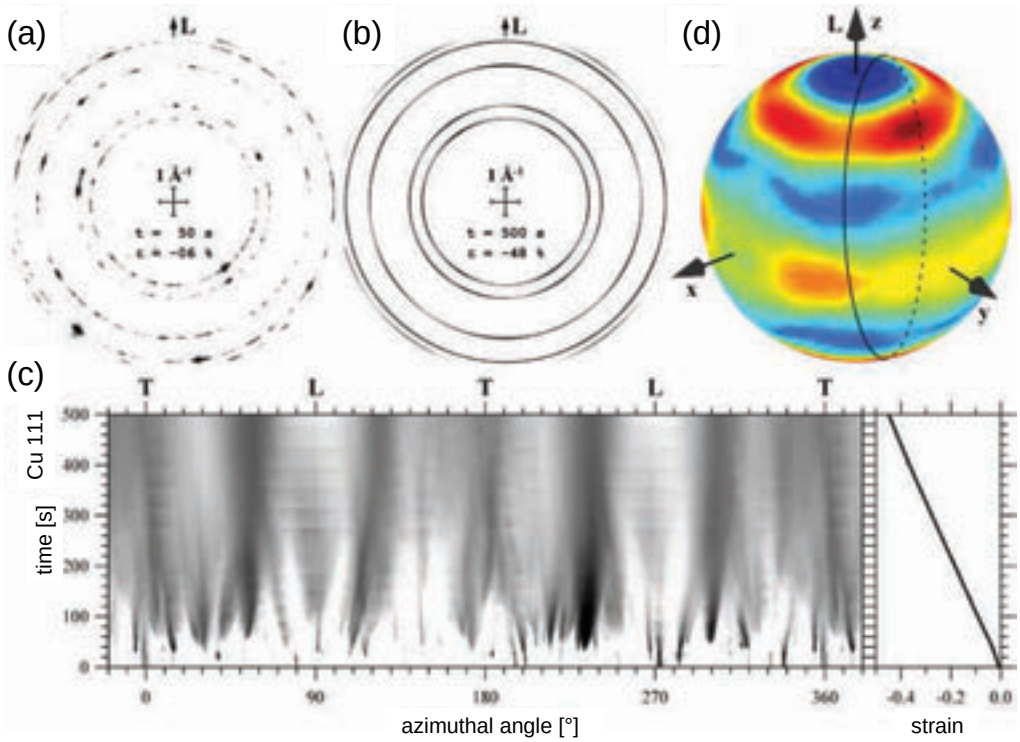

Figure 1 - Two-dimensional X-ray diffraction patterns (dark is high intensity) showing initially spotty Debye-Scherrer rings from a small number of crystallites (a) evolving upon plastic deformation into continuous, but textured rings (b). The intensities of the Cu-111 ring are plotted in dependence of azimuthal angle and time in (c) with longitudinal L and transverse direction T marked. A reconstructed 111 pole figure from a full texture measurement is given in (d) indicating schematically a line of measurement obtained from one Debye-Scherrer ring.

References

[1] Yan K., Liss K.-D., Garbe U., Daniels J., Kirstein O., Li H., Dippenaar R., "*From single grains to texture", Advanced Engineering Materials*, 11/10 (2009), p. 771-773. doi:10.1002/adem.200900163.

[2] Yan K., Carr D.G., Callaghan M.D., Liss K-D., Li H, *"Deformation mechanisms of twinning induced plasticity steels: In situ synchrotron characterization and modeling", Scripta Materialia* (2009), doi: 10.1016/j.scriptamat.2009.11.008.

[3] Liss K.-D., Garbe U., Li H., Schambron T., Almer J. D., Yan K, *"In situ observation of dynamic recrystallization in the bulk of zirconium alloy", Advanced Engineering Materials,* 11/8 (2009), p. 637-640. doi:10.1002/adem.200900094.

[4] Liss K.-D., Schmoelzer T., Yan K., Reid M., Peel M., Dippenaar R., Clemens H., *"In situ study of dynamic recrystallization and hot deformation behavior of a multi-phase titanium aluminide alloy"*, Journal of Applied Physics, 106, (2009), p. 113526/1-6 doi:10.1063/1.3266177.

Engineering

Engineering

ANSTO's engineering research is very closely linked and often overlaps with our materials research.

The organisation's engineering studies look at the effects of high-velocity impacts on materials including the localised deformations that often occur that cannot be predicted using conventional analysis techniques.

ANSTO also studies metal welds. Welds are an essential part of most engineering projects however residual stresses induced by welding can accelerate failure.

ANSTO has studied metal welds of different metal compositions, which is a frequent joining method in the construction of nuclear power facilities, to determine the behaviour of the welds and used neutron diffraction to measure residual stresses in welds of a new connection to a major gas pipeline.

Michael Saleh's research into the modelling and simulation of material responses to high strain-rate and high temperature phenomena will help develop new analysis techniques.

Characterisation of ductile material response to dynamic loading

Michael Saleh and Lyndon Edwards
ANSTO

ANSTO's Structural Integrity and Material Research Unit is actively engaged with the modelling and simulation of material responses to high strain-rate and high temperature phenomena. Analysis of high velocity impacts has shown that material behaviour demonstrates sensitivity to both strain rate and the adiabatic heating of the material. This often leads to localised deformations which cannot be predicted using conventional analysis techniques. e.g. shear banding, adiabatic thermal softening and pressure induced phase transformations amongst others. Therefore we are now developing this high strain-rate method for use in a wide variety of fields including the defence sector.

Material Response to Large Dynamic loads

The analysis of the material response is reliant on a firm understanding of the complexities of dynamic loading and the associated physical responses that govern the material's deformation. Examples of high strain rate/high temperature events are seen in metal stamping and tooling in the manufacturing industry, collision evaluation in the automotive industry, bird strike in the aerospace industry and ballistic and blast protection in the defence sector. These highly transient events occur in tens or hundreds of microseconds and require the use of non-linear continuum mechanics. New Finite Element Analysis codes were commissioned for this work, namely LS-DYNA [1] which is the fastest explicit Finite Element solver available. The new analysis procedure developed has built capabilities within ANSTO and for its partners that were previously unavailable. The solution was made possible through new material models, contact algorithms, new element formulation (SPH, Smoothed Particle Hydrodynamics and ALE, Arbitrary Lagrangian- Eulerian). Further work is envisioned in the area of meshless simulations which negates the effect of element distortion in Lagrangian based analysis.

Having amassed a great degree of nuclear expertise in the areas of material identification, testing and the development of material modelling techniques, ANSTO is an important core participant of the Defence Materials Technology Centre (DMTC). Established in 2008, the centre is a collaborative engagement of industry, universities, defence organisations and other national research facilities. Here, we report about the research project with the DMTC, including partnerships with the University of Wollongong and the University of Melbourne.

Preparing tests

Our research has built capabilities in the area of high strain-rate analysis, using both phenomenological and mechanistic approaches to describe material behaviour. This will be used in the future as we will bridge the gap between atomistic and macroscopic modelling. High strain-rate research is being carried out by a number of manufacturing, automotive and defence institutions around the globe. The DMTC has also deemed this research essential for the development of indigenous armoured structures. High strain-rate testing will be carried out in conjunction with our project partners in the first quarter of 2010. A concerted effort has been made to identify the required material tests to accurately define the necessary constitutive models. The testing will likely include Split-Hopkinson pressure bar tests, high and low-strain rate furnace tensile tests to account for adiabatic heating and pressure testing for calibration of the model. Transmission electron microscope and scanning electron microscope analysis techniques will likely be used in the mechanistic constitutive model derivation. Amongst the most widely used constitutive models are those by Johnson-Cook [2] and Zerilli-Armstrong [3]. The research may also lead to new user defined material models for inclusion in the Finite Element Analysis.

Validating data for models

Figure 1 shows one step in the 3D axis-symmetric Lagrangian mesh simulation of a 7.62 mm armour piercing round impacting two 6 mm Armox560T plates. Armox560T is manufactured by Swedish steel maker SSAB and is claimed to be the "world's toughest protection plate" [4]. It is a low alloy quenched and tempered steel with a yield stress of 1300 MPa and a reported tensile strength of 1600-1900 MPa. This steel has been evaluated by the Norwegian defence force and published literature [5] provided the necessary data and results to benchmark our numerical result. Some of the metrics used in the evaluation of these models include depth of penetration, residual bullet velocity, hole diameters, and other components.

The ANSTO model uses the Johnson-Cook plasticity [2] relation and the Cockcroft-Latham [6] fracture model. A penalty based element contact algorithm with an erosion criteria that deletes highly distorted elements is utilised, thus alleviating premature termination of the simulation due to floating point errors or stress singularities. This models is better in predicting the projectile response than the published simulations [5] on which it is based. The brass bullet jacket has been stripped and the tip of the steel core has been eroded. The residual velocity, (V_r) of this simulation was 198 m/s compared to the measured V_r of 200 m/s and the original papers [5] simulation of 286 m/s. The physical features of the model are validated against published results [5]. Figure 2 combines a high-speed photograph of the ballistic experiment together with a post-experiment metallographic cross-section of the impact area. The rotation of the bullet, the erosion on the bullet tip and the cratering of the entry hole all provide good validation data for the models produced.

FIGURE 1

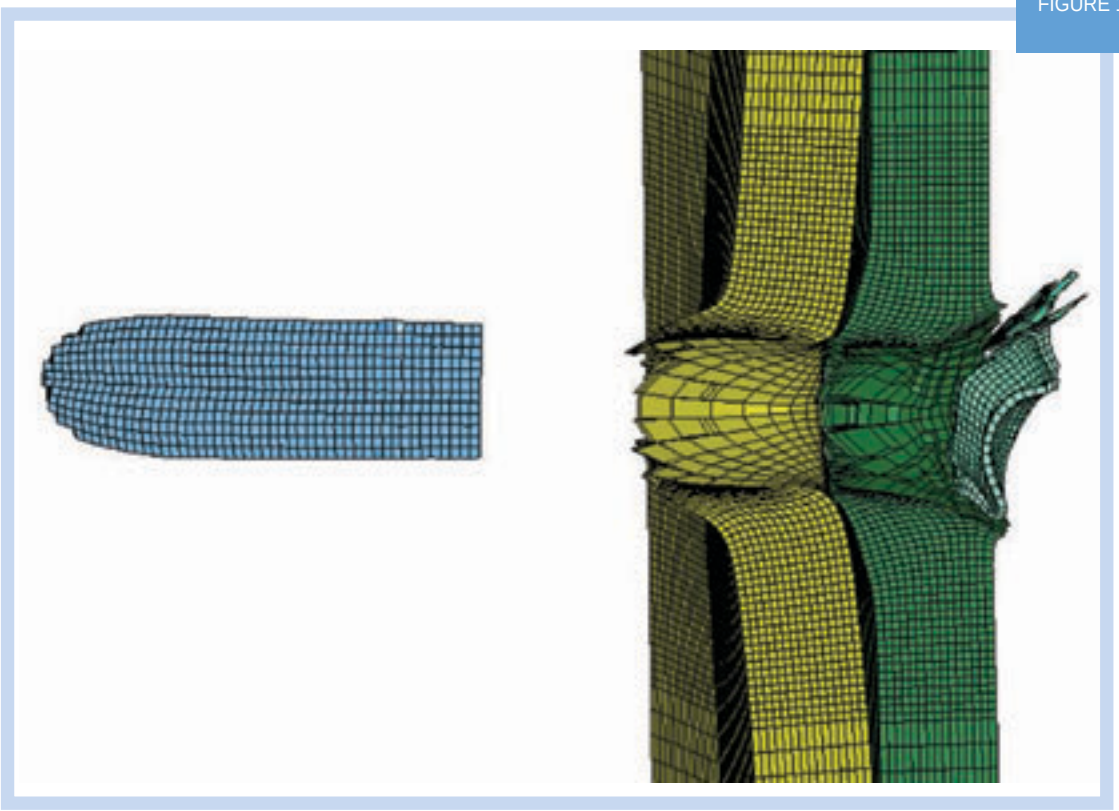

Figure 1 - Simulating a 7.62 mm Armour piercing round impacting two 6 mm Armox560T plates.

FIGURE 2

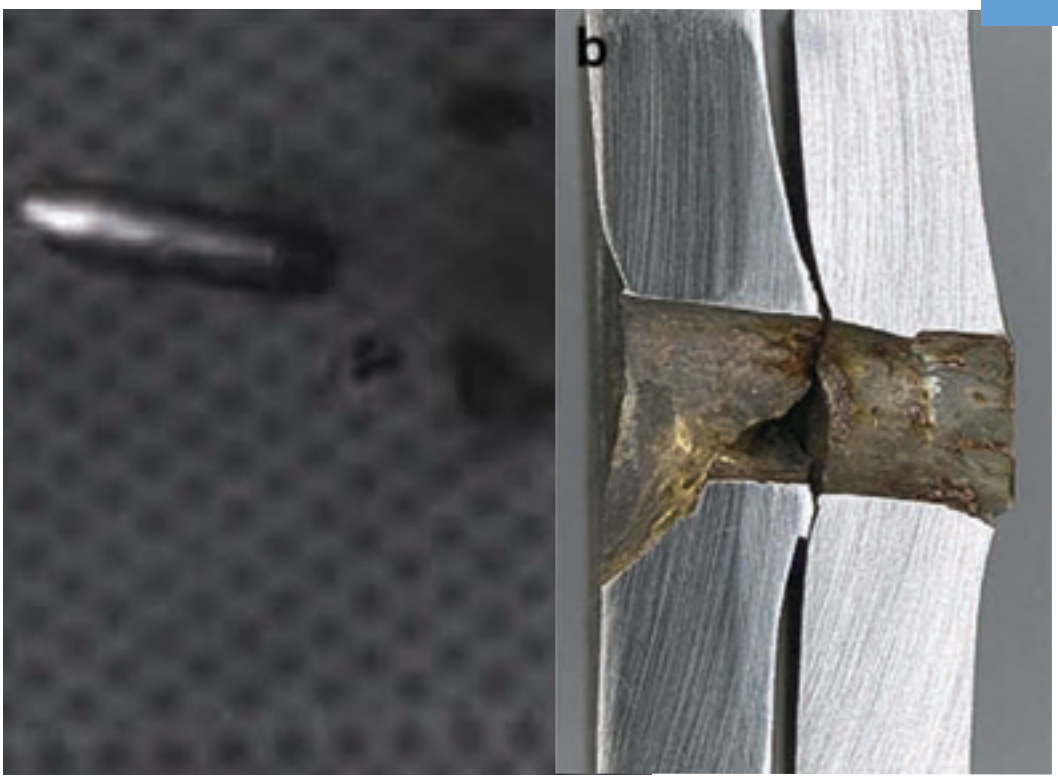

Figure 2 - Ballistic test of a 7.62 mm Armour piercing round impacting two 6 mm Armox560T plates. [6]

The development of these models is essential in harnessing scientific techniques for the engineering design process. The capabilities developed have, for the first time, allowed the industry partner to anticipate material failure in a virtual environment with minimal need for expensive and often complicated ballistic tests. The development of the next generation armour will employ these models in lieu of the current ad hoc design strategies.

Another development in our modelling capability is the evaluation of Fluid Structure Interaction (FSI) models which couple the fluid motion to the mechanical response of the material. These have seen use in sloshing analysis of fluid containers, fluid motion analysis and the development of airborne blast models.

Figure 3 shows the results of a coupled FSI simulation of a 6 kg mine blast on a 590 kg steel plate. The expanding gas cloud moves through a static mesh (Euler mesh) where material transfer between elements occurs. Momentum transport formulation is used in this simulation. This simplified model is significant as it accounts for the concentrating effects of soil craters and the inclusion of an equation of state characterises the fluid behaviour of the blast gases and the surrounding air. This model was built after two previous iterations using the CONWEP [7] blast method and this formed part of our continuing contribution to the DMTC's collaborative effort.

The next iteration of the blast model will include a soil formulation to capture the large effects entrapment have on the imparted kinetic energy. This has been identified as an urgent analysis tool to combat the increased use of improvised explosive devices against Australian Defence Force (ADF) personnel. ANSTO's effort in both the ballistic and blast simulation provides measurable benefits to the ADF and secondly to Australian Industry. Our work has also been publicised through the International Symposium on Ballistics [8] with the aim of furthering our knowledge and demonstrating our capabilities.

The materials research conducted by ANSTO is being used in a wide range of fields including the defence sector.

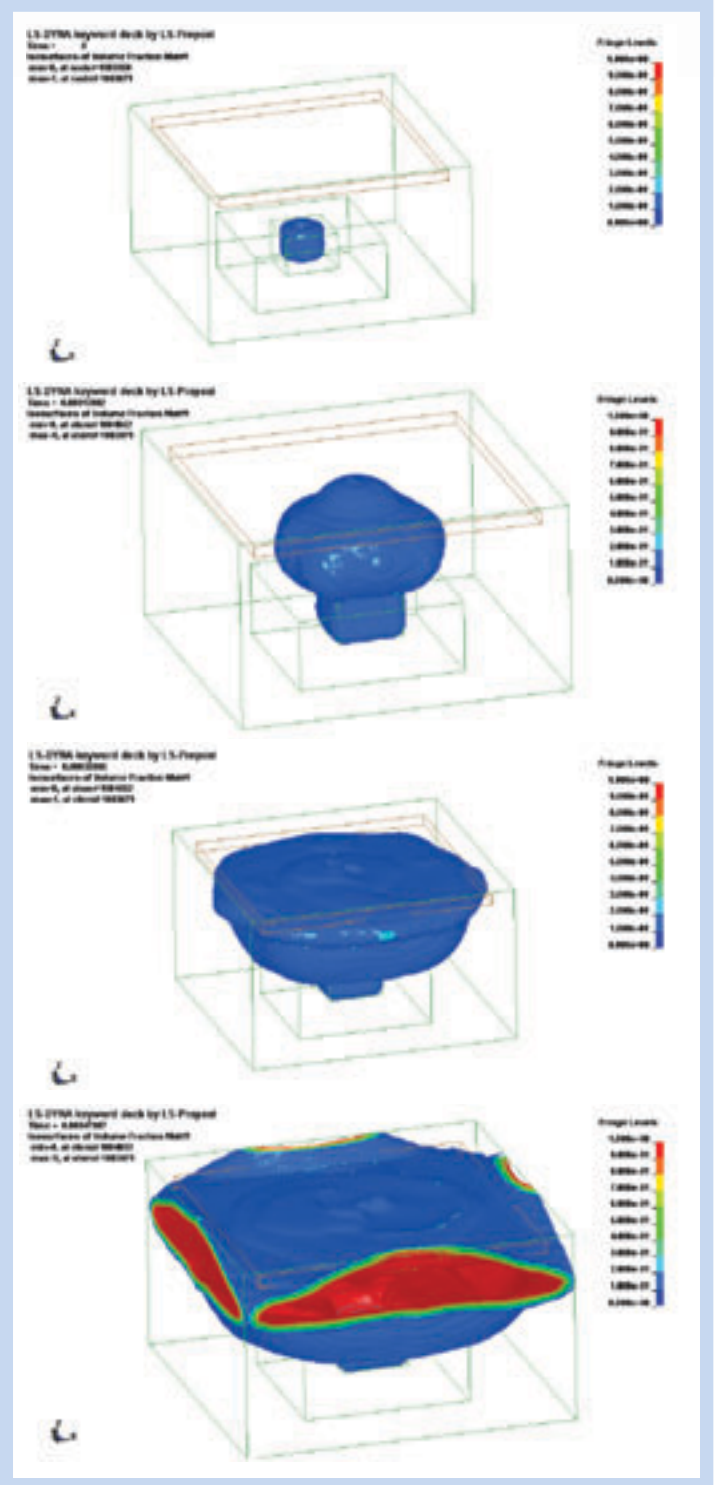

Figure 3 - SEQ Figure * ARABIC 3. Coupled Fluid Structure Interaction simulation of a 6 kg mine blast on a 590 kg steel plate.

References

[1] Hallquist, J.O "LS-DYNA Keyword User's Manual, version 971, Volumes 1 and 2, (2007) Livermore Software Technology Corporation, Livermore, CA.

[2] Johnson, G R; Cook, W, H, *Proceedings from the 7th International Symposium on Ballistics, The Netherlands,* (1983) pp. 541–547.

[3] Zerilli, F.J; Armstrong, R.W, *Journal of Applied Mechanics* Vol.61 Issue 5 (1987) pp1816-1825.

[4] HYPERLINK "http://www.ssab.com/en/Products-and-solutions/Armox/" http://www.ssab.com/en/Products-and-solutions/Armox/

[5] Børvik, T; Dey, S; Clausen, A.H, *International Journal of Impact Engineering,* Vol 36 (2009) pp948-964.

[6] Cockcroft, M.G; Latham D.J., J. *Inst. Metals* 96 (1968), pp. 33–39.

[7] TM5-855-1, "Fundamentals of Protective Design for Conventional Weapons" U.S. Department of the Army, Washington DC, 1986.

[8] Saleh, M; Edwards, L "Evaluation of a hydrocode in modelling NATO threats against steel armour" *Proceedings of the 25th International Symposium on Ballistics. 2010.*

ANSTO's materials research is looking for ways to improve weld procedures.

Simulation of a weld procedure used in nuclear power facilities for residual stress determination

Ondrej Muransky[1], Philip Bendeich[1], Lyndon Edwards[1] and Mike Smith[2]
[1]ANSTO and [2]British Energy – Electricite De France

Metal welds of different metal compositions are a frequent joining method of two sections in the construction of nuclear power facilities. Here we report on our computer simulation of one of these "dissimilar" metal welds in a pressuriser safety relief line. The weld has a complex manufacturing history, including for example transition layers to the intended weld, heat treatment, and machining, before attachment of an extension pipe. The results of the analyses have been used to help interpret the behaviour of the nozzle welds on the plant.

Description of weld

Our finite-element computer simulation of a pressurising safety relief line for a dissimilar metal weld procedure has been performed in collaboration with British Energy (BE) - Electricité De France (EDF)[1] . BE-EDF has contracted an external constructor to manufacture mock-ups of welds in one of their power stations, Figure 1, as part of a project to assess the risk of primary water stress corrosion cracking and to develop an appropriate mitigation strategy. The simulation work was carried out partly to gain experience in this form of analysis prior to participation in an upcoming international Nuclear Regulatory Commission (NRC) round robin, and partly to address perceived deficiencies in existing simulations performed by other contractors. The weld has a complex manufacturing history: it comprises over 90 buttering passes to provide a transition layer from one material to the intended weld material; after application of the buttering layer intermediate heat treatment followed to relax stresses. This treatment led to machining of the butter layer in order to provide a new welding surface. Using 46 transition layers, so-called "passes", the main dissimilar metal weld could be applied, and finally the extension pipe could be attached via a standard metal weld of the same metal composition. The large number of weld passes proved a challenge to model efficiently with many software tools being developed to augment the existing packages (Abaqus [1] and FEAT weld modelling tool [2]) used for this type of analysis. The results of the analyses have been used to help interpret the behaviour of the nozzle welds on the actual plant.

In order to perform this simulation with a degree of confidence a considerable amount of background work has been carried out in conjunction with BE-EDF and the European Network on Neutron Techniques (NeT). NeT has organised several round robins for simplified welding simulations and measurements whose sole purpose was to identify the key elements to accurate welding simulations and verify the results using advanced measurement techniques [3]. The key elements identified in successful welding simulations are: i) an accurate heat-source model utilising an appropriate heat-flux energy distribution; and ii) detailed temperature-dependant material properties, both thermal and mechanical.

[1] The ANSTO/ BE-EDF collaboration has been partially supported by a grant from the UK Royal Academy of Engineering.

Simulation Procedure and Results

In the current work as much detail of the welding procedure as possible has been incorporated in the model. For simplicity, several sequential axi-symmetric (2-dimensional) models were developed. Each model was used in turn to provide the stress/strain field for the next step in the welding process which included surface machining to remove excess material.

In overview the nozzle/extension, Figure 2, undergoes several steps in its construction: 1) application of an Inconel 82/182 buttering layer to the SA508 ferritic steel nozzle, 2) machining of the transition layer, i.e. buttering layer to provide a good welding surface, and 3) 46 pass welds for attachment of the nozzle/buttering layer to the stainless steel 316L extension.

Traditionally, buttering layers and weld passes might be applied in a single lumped step in order to simplify computational effort with the assumption that this did not significantly affect the final results. In this work, all 93 passes of the buttering layer and 43 passes of the extension weld attachment were individually applied. At the end of each step, the results were mapped to a new model where the outer layers could be removed to simulate the machining of the weld surface.

As thermocouple records were taken during the mock-up construction each pass was allowed to cool until the “actual” interpass temperature had been achieved, at which point the current step was automatically terminated and the next pass commenced. This is a level of detail that is rarely possible and did provide a noticeable variation in the resulting residual stress field, Figure 3.

A full cyclic strain hardening law (tensile/compressive) was applied for all three materials used in the construction of the dissimilar weld. Once again, this level of detail is rarely utilised in welding simulations primarily due to the lack of accurate test data and the necessary experience in applying the properties to a numerical material model. A further level of material complexity was applied with the use of two-stage annealing for both strain relief then strain hardening. This final step was shown to have only a limited influence on the resulting residual stress field.

The lessons learnt will enable more accurate solutions for a wide range of welding situations with a better insight on what is important to consider and what can be omitted to accelerate the process in what is a very time consuming analysis. With the knowledge and experience gained from the current study we have pushed the boundaries of accurate welding simulations for residual stress determination. Considering that welds are the most common joining method in high temperature plants the applications will be many and varied. Further work will include combining our complimentary knowledge on creep/fatigue analysis and applying this to estimate the life exhaustion of the material resulting from the welding process alone.

FIGURE 1

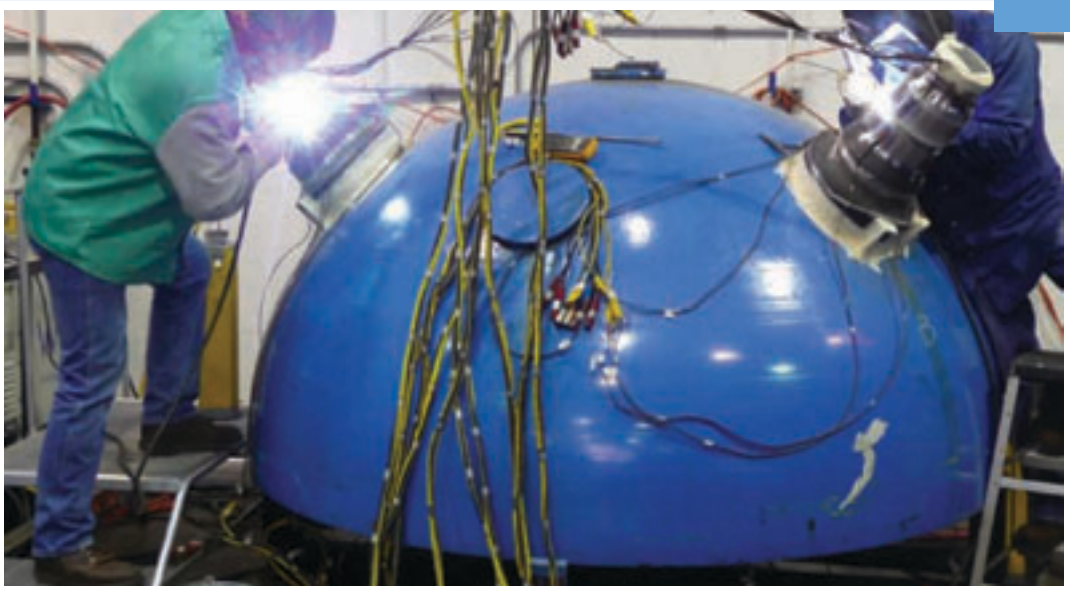

Figure 1 - Mock-up construction of nozzle and safe-end extension on pressure vessel end cap. Nozzles are constructed under identical welding conditions either side.

FIGURE 2

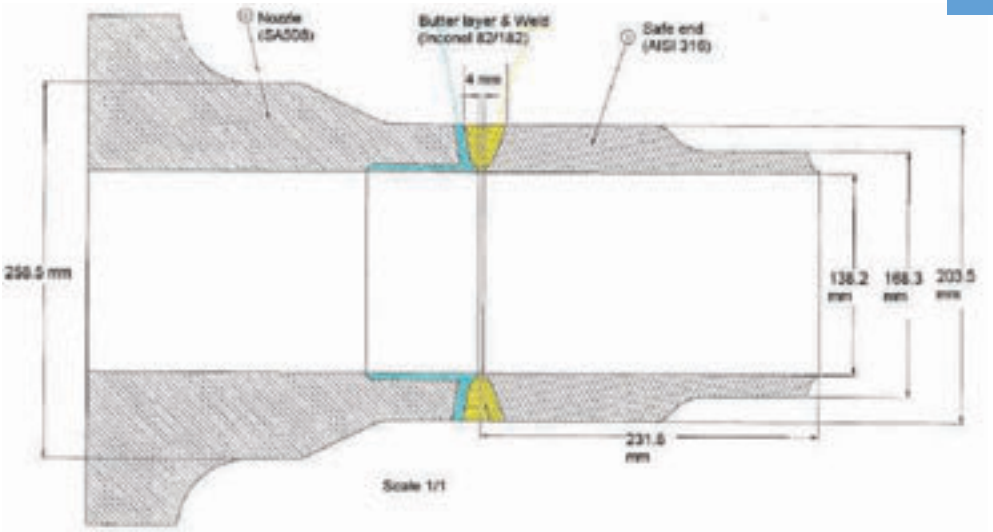

Figure 2 - Section view of dissimilar weld. Nozzle attached to pressure vessel end-cap.

FIGURE 3

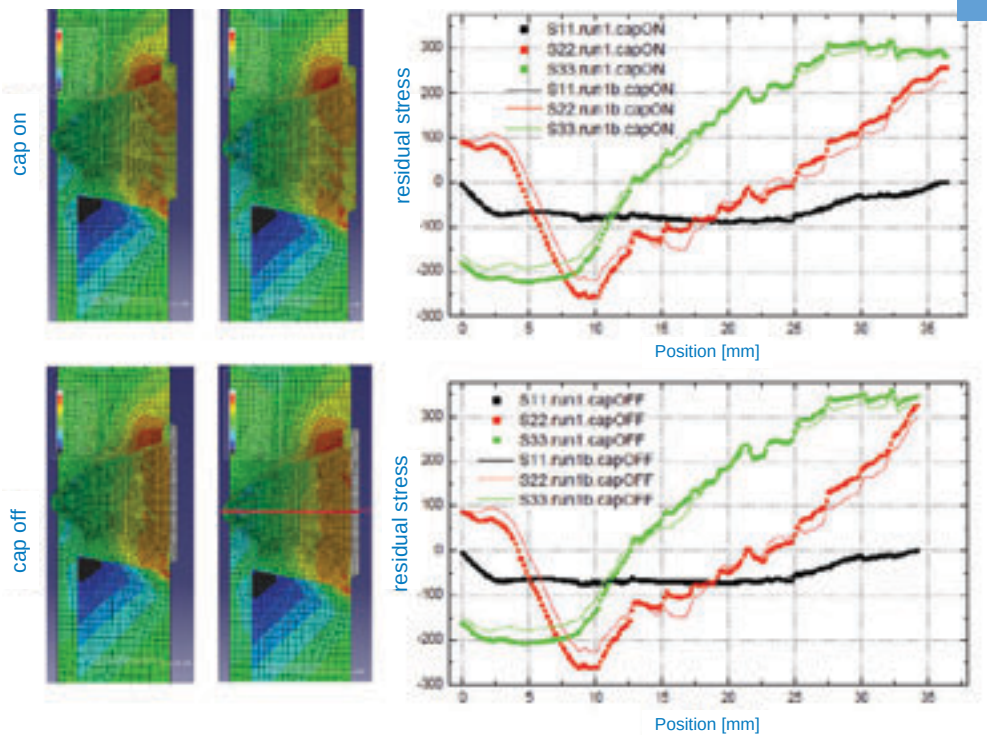

Figure 3 - Through thickness hoop stress profiles (left) with bead cap on (top) and removed (bottom). Implied interpass temperature control (left and dotted), accurate T/C interpass temperature control (right and solid line). Directions: S11-through wall; S22 -transverse to weld path; S33 –hoop.

References

[1] SIMULIA. ABAQUS/Standard. Dassault Systems, 2008.

[2] Smith RM. FEAT-WMT: Weld-Modelling Tool 1.0.9 User Guide. 2008.

[3] Smith MC, Smith AC. NeT bead-on-plate round robin: Comparison of residual stress predictions and measurements. *International Journal of Pressure Vessels and Piping; 86* (1): (2009) 79-95.

[4] Chaboche JL. *A review of some plasticity and viscoplasticity constitutive theories. International Journal of Plasticity;* 24(10) (2008) 1642-1693.

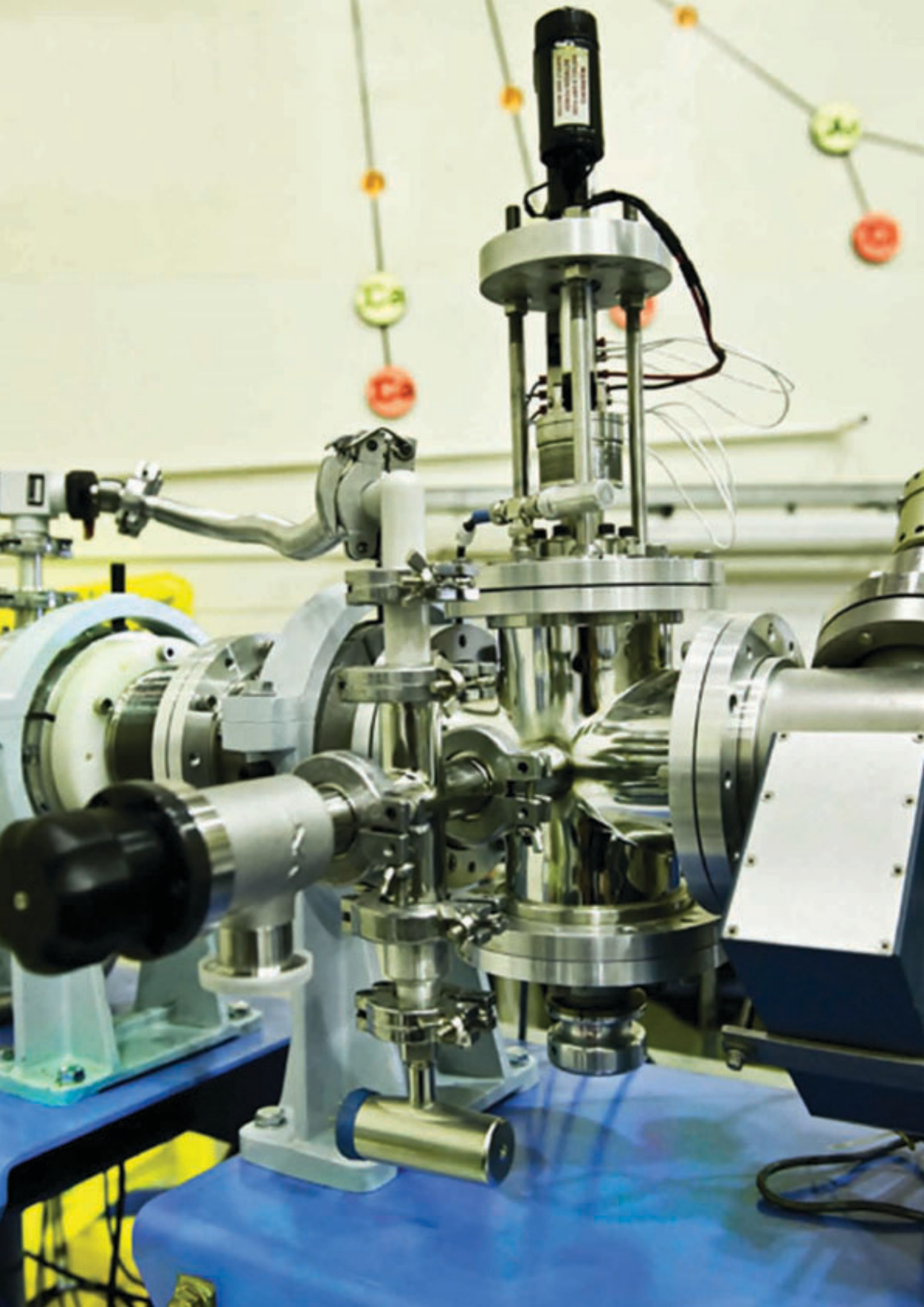

Residual stress and integrity of a gas pipeline connection measured by neutron diffraction

Michael Law, Oliver Kirstein and Vladimir Luzin
ANSTO

Welds are an essential part of most engineering projects, however, residual stresses induced by welding can cause or accelerate failure by several mechanisms. Residual stresses are difficult to measure and there is little information on residual stresses in welds. The integrity assessment of components is often based on residual stress estimates from assessment codes.

Neutron diffraction is an ideal tool for measuring residual stresses as it provides accurate values through the entire component thickness. We measured the residual stresses in welds of a new connection to a major gas pipeline. The critical crack size was evaluated from the measured stress and compared to that estimated from integrity assessment codes. Some code estimates dangerously overestimated the critical crack size. Neutron diffraction provides a more accurate assessment of component integrity than estimates from assessment codes. With neutron diffraction we could compare and validate assessments codes following our measurements.

Many gas pipelines require connections to allow a branch to feed new facilities, especially gas-fired power stations. Frequently, this requires welding on 'live' pipeline connections, i.e. they are welded directly onto a pressurised pipeline with a special welding procedure. A valve is put on the new branch pipe and a cutter removes the remaining wall between the 2 pipes. The welds in this connection cannot be post-weld heat treated as the pipeline product carries away heat; this causes significant residual stresses to remain in the welds. As these residual stresses may contribute to premature failure by fatigue; stress corrosion cracking; hydrogen assisted cold cracking; or fracture; it is important to investigate these welds for further understanding of stresses induced by this method.

FIGURE 1

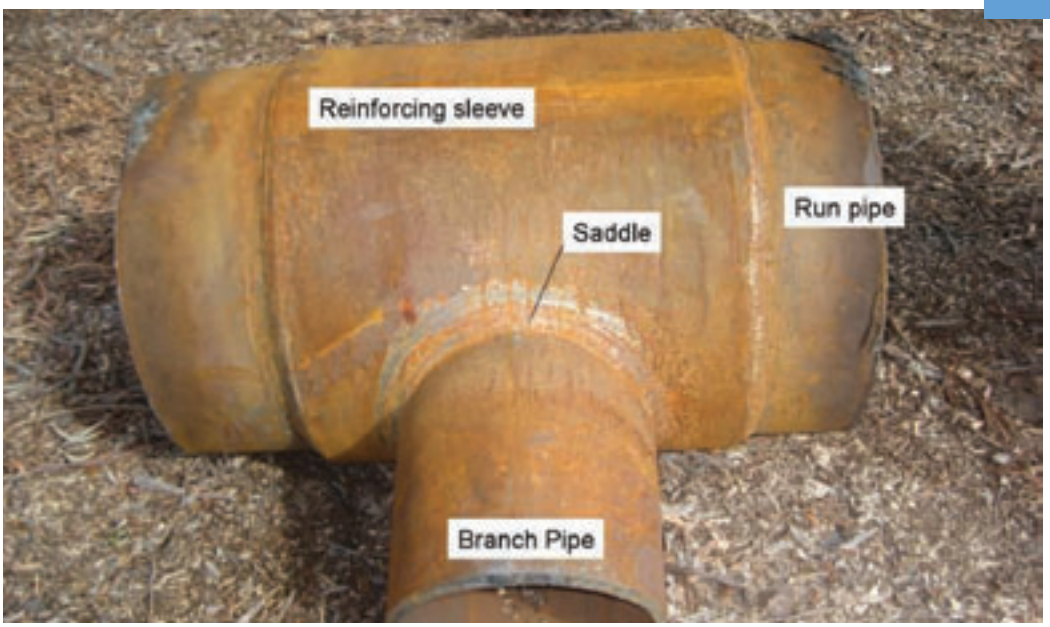

Figure 1 - Samples for measurement were cut from the saddle of the branch connection made during welding qualification.

Using Kowari

The residual stresses were measured on the Kowari strain scanner. Measurement points were chosen in the weld, heat affected zone, and parent material. A monochromatic beam with λ = 1.666 Å diffracted from Si{400} planes of the monochromator was used in this analysis. This wavelength resulted in a scattering angle of 90° for the Fe(211) reflection used for the measurements using a nominal gauge volume of 3 x 3 x 3 mm^3.

FIGURE 2

Figure 2 - Positioning a section cut from the branch connection on Kowari.

FIGURE 3

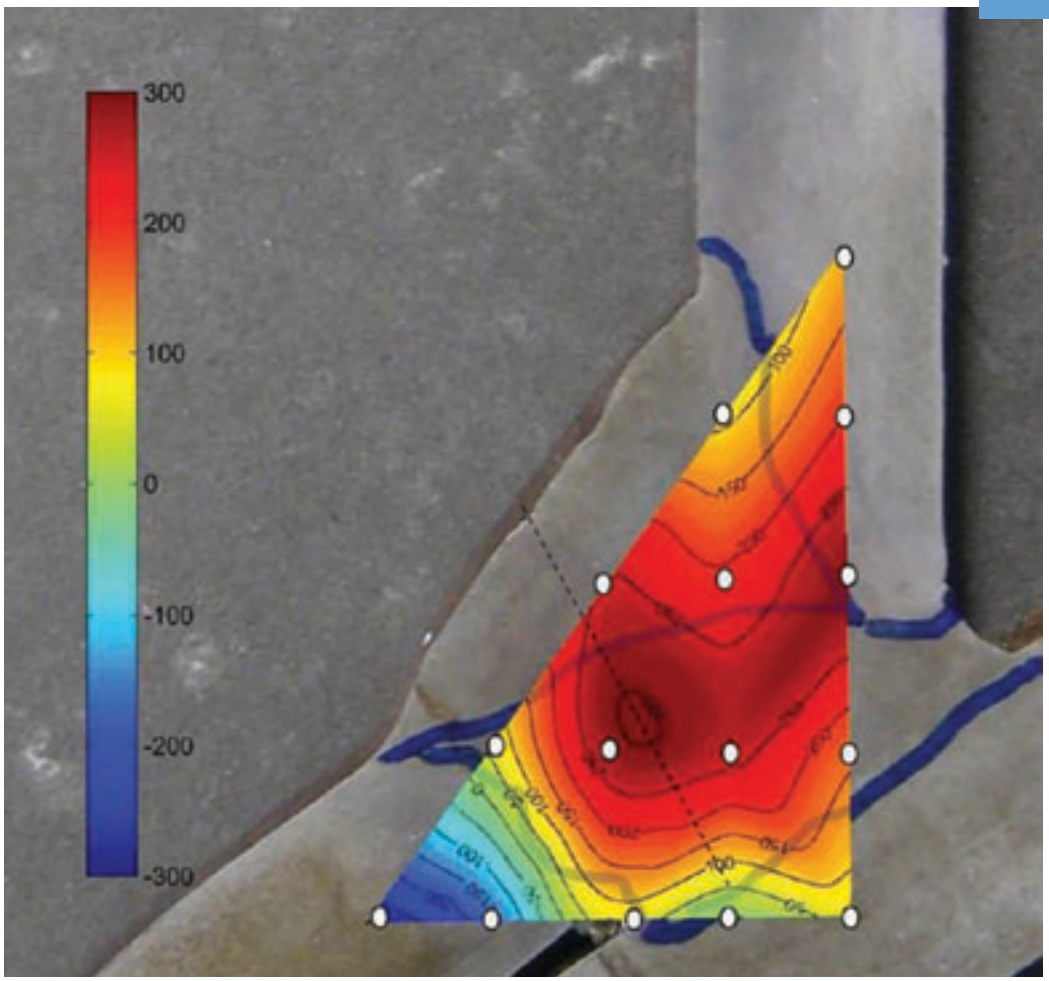

Figure 3 - Stresses in direction of weld (out of page) with a maximum error of 33 MPa. Measurement points are marked in white.

The residual stresses measured

Residual stresses were measured in the saddle, an area where transverse residual stresses are expected to be highest. The maximum stresses (290 MPa) were along the weld direction (figure 3) and may lead to cross weld cracking. Stresses in this direction are rarely significant for brittle fracture as crack growth slows or stops when cracks propagate into the parent material due to reduced imposed stresses, reduced residual stresses, and higher toughness.

Brittle fracture assessment

Stresses across the weld (Figure 4) are more significant for brittle fracture, causing cracking along the weld direction. Brittle fracture was analysed with an assumed surface breaking defect situated at the saddle subject to the maximum pressure the connection will experience of 20.7 MPa.

Brittle fracture is driven by both operational and residual stresses. Estimates of residual stress (Figure 4) were taken from two integrity assessment codes, API 579 [1] and BS 7910 [2]. The residual stress predictions in API 579 are based on modelling. The residual stress predictions in BS 7190 are either conservatively assumed to equal yield strength, or use an equation based on a compendium of measurements.

FIGURE 4

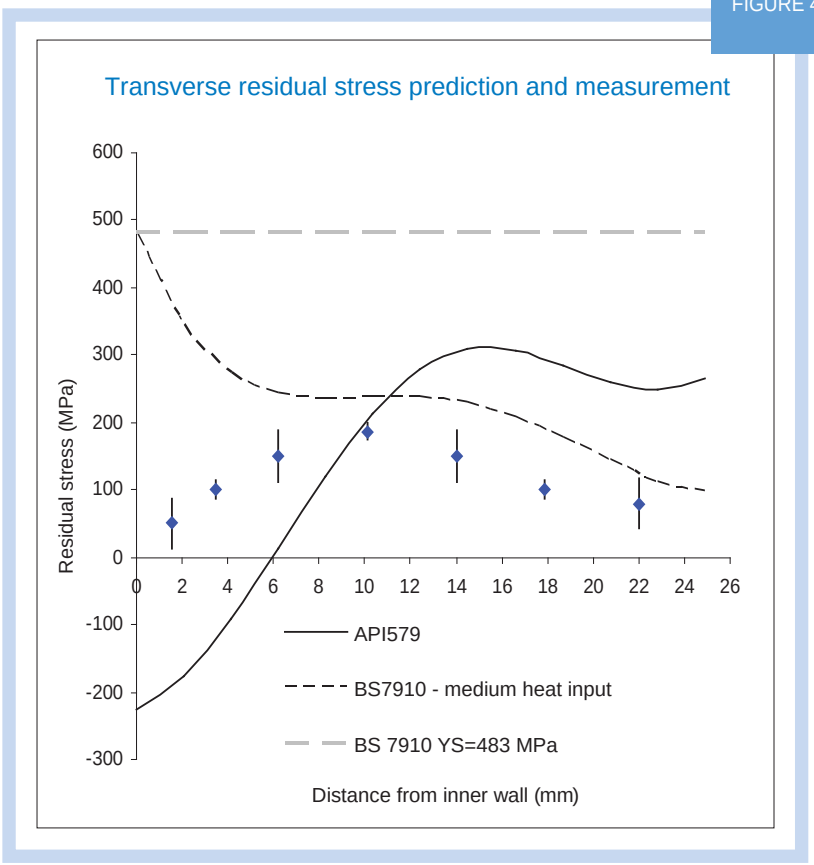

Figure 4 - Predicted and measured longitudinal and transverse residual stresses.

Four estimates of the transverse residual stress were used in the critical crack size analysis (Figure 4):

- The yield strength level residual stress prediction from BS 7910 (YS).
- The calculated residual stress prediction from BS 7910 (BS 7910).
- The actual variation through wall (measured).
- The residual stress prediction from API 579 (API 579).

The results of this analysis are shown in the table:
Table 1: Critical crack size (mm) for different residual stress states

Case	Depth	Length
YS	5.9	49.4
BS 7910	8.6	72
Measured	15	129
API 579	17	144

Critical crack sizes obtained

Residual stresses in a branch connection weld were measured by neutron diffraction on the Kowari strain scanner. The critical crack sizes calculated from code estimates of residual stress and measured residual stresses were compared. Critical crack sizes based on residual stress estimates from BS 7910 were conservative (shorter than) the critical crack size derived from measurements. An estimate of residual stress based on API 579 lead to a non-conservative critical crack size, a potentially dangerous situation. This work shows the importance of making project-specific measurements of residual stress. Neutron diffraction contributes significantly to our understanding of residual stresses in welds, as it provides accurate through-thickness measurements. As a result of these measurements we were able to compare and validate assessment codes, and therefore obtain a more accurate assessment of component integrity. This is vital for engineering projects.

Further residual stress measurements are planned which will create a compendium of results. This will be used to generate more accurate estimates for assessment codes in the future.

References

[1] API 579/ASME FFS-1, *American Petroleum Institute*, 2nd edition 2007.

[2] BS 7910:2005 - Guide to methods for assessing the acceptability of flaws in metallic structures.

ANSTO Facts and Figures

Financial Statement for Calendar Year 2009

The total expenditure by ANSTO for the calendar year 2009 was AUD 216.1 million. Of this AUD 59.3 million or 27.5% was utilised in scientific research. Federal government (block) funding represented 86% of this research funding and 14% came from third parties. These third parties include significant private industry investment (72%) while the rest came through grants from Government, Universities and Co-operative Research Centres (CRCs).

FINANCIAL STATEMENT (AUD'000)				
	2009 Research		2009 Total ANSTO	
Expenditure				
Operations	40,646	68%	165,752	77%
Investments	18,697	32%	50,306	23%
Total	59,343	100%	216,058	100%
Exp according to source of income				
Federal Govt. funding	50,934	86%	158,622	76%
Third Party	8,409	14%	57,436	27%
Third Party revenue				
Private Industry	6,025	72%	54,759	95%
Grants #1	2,384	28%	2,677	5%
Total	8,409	100%	57,436	100%
#1 Incls grants from Govt, Universities and CRCs				

ANSTO Employees

At the end of 2009, ANSTO had 985 full time equivalent employees of which 27.8% were women. The chart below shows ANSTO's reliance on a growing group of Technical and Engineering Staff (52.1%) for a successful user based research facility.

Our next biggest group is the research ranks of which 29 were PhD students and 29 were Post-doctoral Research Fellows.

ANSTO Employment Categories

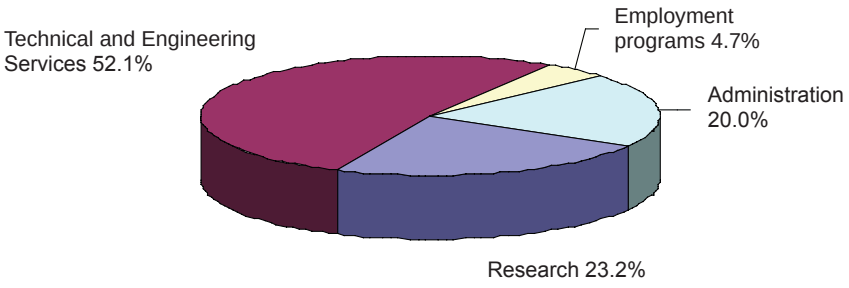

At the end of 2009, ANSTO had 985 full time employees.

Education

As part of its commitment to education, ANSTO runs an Annual Neutron School. This school is run over a week and provides PhD students and Post Doctoral Fellows with an opportunity to learn about and perform experiments using ANSTO's beam line instruments. 40 scientists attended this school in 2009.

Our commitment to further education also extends to secondary teachers. A total of 62 teachers attended the 5 individual professional development days for secondary teachers that were hosted this year at ANSTO. These one day courses provided an overview of all areas of the science curriculum including Chemistry, Physics, Biology as well as Earth and Environmental Science that are covered (at a High School Certificate level) as part of the tours at ANSTO. As well as helping to encourage more students and teachers to visit our facility, it is also designed to help encourage the teaching of the nuclear science elective in the HSC school syllabus.

We also wish to report that, in 2009 ANSTO had 15 scientists lecturing at Universities and higher education establishments across New South Wales and Australia.

User Services

During 2009 the OPAL reactor and its associated beam lines along with our two accelerators (ANTARES and STAR) attracted over 370 users with more than 1,300 visits. These came from 60 different institutions in over 20 countries.
In 2009, ANSTO received an allocation of special Federal Government funding of $62M for the building of additional neutron-beam instruments for the OPAL research reactor and the establishment of a Centre for Accelerator Science.

Memberships

• Dr David Cohen has been invited to sit on the Editorial Board for the International Journal X-Spectrometry as Executive Director for the Australian region by the journal's Editor in Chief, Professor Rene Van Grieken, Head of Department of Chemistry, University of Antwerp, Belgium.

• Professor John Dodson was made a member Quaternary Science Reviews, Quaternary Research, The Holocene.

Invention Disclosures

In 2009, there were 6 'invention disclosures' to the patent office for the purposes of securing provisional patents at ANSTO:

Invention disclosures

1.	Method for hermetically sealing metal ceramic feed through
2.	AUS4-Maritime Container Test Standard
3.	Ceramic Internal Combustion Linear Alternator
4.	Automatic Mesh Generator
5.	Automated Electrical Circuit Calculations
6.	Ga-68 Generator

Awards

• Dr Andrew Whitten - NHMRC Australian Biomedical Fellowship on "How SNARE proteins regulate glucose transport" at University of Queensland.

• Dr Ron Cameron, Dr David Cohen and Dr Adi Paterson - elected to the Australian Academy of Technological Sciences and Engineering (ATSE).

• Dr Quan Hua - Invited Academy Fellowship to Japan: FY 2009 Japan Society for the Promotion of Science (JSPS) Invitation Fellowship Program for Research in Japan (16 Feb – 16 Apr 2009).

• Dr Henk Heijnis - Honorary Fellow of the Australian Institute for Nuclear Science and Engineering, as well as a Visiting Professorship 'Grant' from the Royal Netherlands Academy of Arts and Sciences.

• Dr Tim Payne – Fellow of the Royal Australian Chemical Institute.

• Best Technical Paper Award - International Association of Hydrogeologists Sydney Basin Symposium (Waring C.L.*, Stepanyants Y.A., Hankin S.I., Airey P.L., Peterson M.A).

• The Bragg Institute - Poster Prize at IEEE School on Magnetics.

Grants in which ANSTO collaborates

ARC Discovery Grants

• "Materials science and superconductivity in the new Fe-based high-temperature superconductors" (University of Wollongong).

• The Late Pleistocene Peopling of East Asia and Associated Climate-Environment History, (UNSW, Sydney, ANSTO, Griffiths, Witwatersrand (SA) and Yunnan (China)); and (UNSW).

• Untangling the links between El Niño and the Changing global climate, Dr McGregor (Univ. of Wollongong, Univ. of Glasgow and ANSTO), (UoW) and (UNSW).

• Thresholds and hysteresis: how do abrupt changes in the Asian monsoon affect ecosystems and environmental processes? (Univ. Sydney).

• Industries of Angkor: Material Production and the Decline of the Khmer Empire (11th to 15th centuries CE). (Univ. Sydney).

ARC Linkage Infrastructure, Equipment and Facilities (LIEF) Grants

• New single-crystal X-ray diffractometer at Sydney University.

• Sample-characterisation equipment at UNSW.

• Sample-characterisation equipment at Univ. of Wollongong.

• A high performance stable-isotope micro-analytical facility for the earth, palaeo-environmental, and climate change sciences. (ANU).

• The future of palaeo-climate and archaeological research in Australia: next generation instrumentation for chronology and environmental reconstruction. (Univ. Queensland) and (Univ. Melbourne).

Marsden Fund of Royal Society of New Zealand

• "Probing the effects of oxidative stress on cellular membranes", - University of Auckland

Department of Education, Science and Training Grant

• Australia-China International Linkage Scheme. 2007-2010. Evolution of palaeo-lake systems on the Tibetan plateau and formation of terraces along Yangtze River using cosmogenic exposure dating. (ANSTO, China Academy of Sciences and Institute for Geophysics, Beijing, China).

ANSTO - University of Melbourne Collaborative Research Support Scheme

• How do coral atolls evolve over time - can laser ablation U-Th "range–finding" ages provide an answer?

• Quantifying the response of Australian landscapes to climatic and tectonic forcing using cosmogenic isotope analysis.

Large NERC Grant

• “A calibrated climate record from Gibraltar speleothem: the instrumental era, the Holocene and the last interglacial” RHUL, Birmingham.

National Geographic NGS Grant

• Industries of Angkor Project: Production and decline of the Khmer Empire (11th to 15th centuries CE). Univ. Sydney.

National Science Foundation, USA, 05-514 Antarctic Research

• Understanding causes of atmospheric methane and carbon cycle variability in the Holocene: the roles of climate change and human perturbations, 2009-2012, University of Colorado, NIWA, CSIRO-Atmospheric Research.

Australian Antarctic Division, (ANARE)

• Concentration and isotopic measurements of radiatively important gases in the southern atmosphere , CSIRO Division of Atmospheric Research, ANSTO, University of Heidelberg, Princeton University.

• Air sampling and analysis from Antarctic fire and ice , CSIRO, ANSTO, NIWA (NZ), University of Colorado), Pennsylvania State University, University of East Anglia, University of Heidelberg.

Bureau of Meteorology

• Cape Grim BAPS Research Allocation to Dr David Fink.

Spanish Government I+D project

• L. Rosell and other 11 researchers from several European and non-European institutions. Diagenetic models in evaporitic basins and formations.

Partnerships

Co-operative Research Centres (CRCs) and their equivalents are an integral part of the scientific research landscape in Australia today. From their inception, ANSTO has been involved in these centres and our current involvements are described below.

CRC (OR SIMILAR)	PROJECT NAME/S
CRC for integrated engineering asset management (CIEAM)	Improved OPAL Monitoring and Management System
	Integrated Asset Health Manager
	Stratigic Work Design in Asset Management
	Multi Criteria Asset Decision Report Tool
Nuclear Structural Integrity Modelling	Defence Materials Technology Centre (DMTC) - Non CRC Partnership
CRC for Polymers III	3.1 Functional Polymers for Photovoltaic devices
	3.3 Degradable Polymer films
CRC for Biomedical Imaging and Development	Protein Biosynthetic Pathway Targeting
	Neuroreceptor Ligand Targeting
	Development of Novel Receptor Based Radio-Pharma
	Apoptotic Pathway Targeting
	Development of Synthesis Mods for Tracer Product
	General
	CRC Revenue and Contributions
	Evaluation and Characterisation of Detector Materials
CRC for Sustainable Resource Processing	4b – Geo-polymers

Workshops and Reviews

• 26 and 27 March 2009 – *Bragg Institute Advisory Committee Meeting*

This group makes recommendations to ANSTO regarding prioritisation and balance in the Bragg Institute user program, following external peer review of neutron beam time proposals.

• 12-14 August 2009 – *IAEA Consultants Meeting – at the Bragg Institute*

Strategic Planning and Regional Networking for Sustainability: 'Concerted Actions on Neutron Scattering in the Asian-Pacific Region'.

• 16 to 21 August 2009 – *Neutron School – at the Bragg Institute*

The Asia-Oceania Neutron Scattering Association's (AONSA) Neutron School for PhD and Post Doctoral students.

• 27-28 August 2009 – *Workshop on New Guides, Instruments and Sample-Environment Apparatus – at the Bragg Institute*

• October 2009 – *Accelerator Advisory Committee – at Institute of Environmental Research*

Committee commissioned to advise and recommend on future Accelerator work hosted at ANSTO.

• 9 November – 4 December 2009 – *OPAL and Bragg Instrument Design Workshop*

NIST Center for Neutron Research, hosted a Conceptual Design Workshop in Washington DC, USA.

ANSTO Top Management Team

In 2009, the ANSTO Top Management Team, comprising representatives from each of ANSTO's research and administrative areas, met regularly to discuss and disseminate information relating to 'whole of ANSTO' issues.

Dr Adi Paterson – Chief Executive Officer

Dr Ron Cameron – Executive General Manager, Strategy, Government and International Relations

Mr Doug Cubbin – Chief Financial Officer, Executive General Manager, Business and Enterprise

Mr Con Lyras – General Manager, Engineering and Technical Services

Dr Rob Robinson – Head, The Bragg Institute

Dr Greg Storr – General Manager, Reactor Operations

Professor John Dodson – Head, Institute of Environmental Research

Mr Ian Turner – General Manager, ARI

Professor Lyndon Edwards – Head, Institute Materials Engineering

Ms Stephanie Cole – Legal Counsel

Dr Ron Weiner – Head, Radiopharmaceutical Research Institute

Dr Bob Ring – General Manager, ANSTO Minerals

Mr Andrew Humpherson – General Manager, Government and Public Affairs

Mr Michael Beckett – Chief Information Officer, Information Management Systems

Mr Hefin Griffiths – Manager, Quality Safety Environment and Radiation Protection

Dr Paul Di Pietro – Manager, Campus Services

Ms Margaret Fittler – Manager, Human Resource

Ms Tanya Karma – Manager, Silicon Irradiation

ANSTO Publications 2009

Referred Journal Publications 2009

Anderson, P. S., Guerin, S., Hayden, B. E., Han, Y., Pasha, M., Whittle, K. R., et al. (2009). Optimization of synthesis of the solid solution, pb(zr1-xtix)o-3 on a single substrate using a high-throughput modified molecular-beam epitaxy technique. *Journal of Materials Research,* 24(1), 164-172.

Anokhin, I., Zinets, O., Rosenfeld, R., Lerch, M., Yudelev, M., Perevertaylo, V., et al. (2009). Studies of the characterisation of a silicon neutron sensor. *IEEE Transactions on Nucear Science,* 56(4), 2290-2293.

Anovitz, L. M., Lynn, G. W., Cole, D. R., Rother, G., Allard, L. F., Hamilton, W. A., et al. (2009). A new approach to quantification of metamorphism using ultra-small and small angle neutron scattering. *Geochimica Et Cosmochimica Acta,* 73(24), 7303-7324.

Arrachart, G., Carcel, C., Trens, P., Moreau, J. J. E., and Man, M. W. C. (2009). Silylated melamine and cyanuric acid as precursors for imprinted and hybrid silica materials with molecular recognition properties. *Chemistry-a European Journal,* 15(25), 6279-6288.

Arrachart, G., Cassidy, D. J., Karatchevtseva, I., and Triani, G. (2009). Nanostructural evolution of titania-based materials using modified titanium precursors. *Journal of the American Ceramic Society,* 92(9), 2109-2115.

Arrachart, G., Creff, G., Wadepohl, H., Blanc, C., Bonhomme, C., Babonneau, F., et al. (2009). Nanostructuring of hybrid silicas through a self-recognition process. *Chemistry-a European Journal,* 15(20), 5002-5005.

Atuchin, V. V., Grivel, J. C., and Zhang, Z. M. (2009). Core level photoemission spectroscopy and chemical bonding in sr2ta2o7. *Chemical Physics,* 360(1-3), 74-78.

Baikie, T., Ng, G. M. H., Madhavi, S., Pramana, S. S., Blake, K., Elcombe, M., et al. (2009). The crystal chemistry of the alkaline-earth apatites A(10)(PO4)(6)CuxOy(H)(z) (A = Ca, Sr and Ba). *Dalton Transactions*(34), 6722-6726.

Benson, S. J., Lennard, C. J., Maynard, P., Hill, D. M., Andrew, A. S., and Roux, C. (2009). Forensic analysis of explosives using isotope ratio mass spectrometry (irms) - discrimination of ammonium nitrate sources. *Science and Justice,* 49(2), 73-80.

Benson, S. J., Lennard, C. J., Maynard, P., Hill, D. M., Andrew, A. S., and Roux, C. (2009). Forensic analysis of explosives using isotope ratio mass spectrometry (irms) - preliminary study on tatp and petn. *Science and Justice,* 49(2), 81-86.

Bhaskaran, M., Sriram, S., Perova, T. S., Ermakov, V., Thorogood, G. J., Short, K. T., et al. (2009). In situ micro-raman analysis and x-ray diffraction of nickel silicide thin films on silicon. *Micron,* 40(1), 89-93.

Bignell, L. J., and Lewis, R. A. (2009). Reflectance studies of candidate thz emitters. *Journal of Materials Science-Materials in Electronics,* 20, 326-331.

Blazek, J., and Copeland, L. (2009). Effect of monopalmitin on pasting properties of wheat starches with varying arnylose content. *Carbohydrate Polymers,* 78(1), 131-136.

Blazek, J., Salman, H., Rubio, A. L., Gilbert, E., Hanley, T., and Copeland, L. (2009). Structural characterization of wheat starch granules differing in amylose content and functional characteristics. *Carbohydrate Polymers,* 75(4), 705-711.

Bleuel, M., Carpenter, J. M., Micklich, B. J., Geltenbort, P., Mishima, K., Shimizu, H. M., et al. (2009). A small angle neutron scattering (SANS) experiment using very cold neutrons (VCN). *Physica B-Condensed Matter,* 404(17), 2629-2632.

Bourke, S., Zoppi, U., Meadows, J., Hua, Q., and Gibbins, S. (2009). The beginning of the early bronze age in the north Jordan valley: New c-14 determinations from Pella in Jordan. *Radiocarbon,* 51(3), 905-913.

Brew, D. R. M., de Beer, F. C., Radebe, M. J., Nshimirimana, R., McGlinn, P. J., Aldridge, L. P., et al. (2009). Water transport through cement-based barriers-a preliminary study using neutron radiography and tomography. *Nuclear Instruments and Methods in Physics Research Section a-Accelerators Spectrometers Detectors and Associated Equipment,* 605(1-2), 163-166.

Brown, C. M., Liu, Y., Yildirim, T., Peterson, V. K., and Kepert, C. J. (2009). Hydrogen adsorption in HKUST-1: a combined inelastic neutron scattering and first-principles study. *Nanotechnology,* 20(20), 11.

Burn, L. J., Rosman, K. J. R., Candelone, J. P., Vallelonga, P., Burton, G. R., Smith, A. M., et al. (2009). An ultra-clean technique for accurately analysing pb isotopes and heavy metals at high spatial resolution in ice cores with sub-pg g(-1) pb concentrations. *Analytica Chimica Acta,* 634(2), 228-236.

Burton, E. D., Bush, R. T., Sullivan, L. A., Hocking, R. K., Mitchell, D. R. G., Johnston, S. G., et al. (2009). Iron-monosulfide oxidation in natural sediments: Resolving microbially mediated s transformations using xanes, electron microscopy, and selective extractions. *Environmental Science and Technology,* 43(9), 3128-3134.

Carter, M. L., Gillen, A. L., Olufson, K., and Vance, E. R. (2009). Hiped tailored hollandite waste forms for the immobilization of radioactive cs and sr. *Journal of the American Ceramic Society,* 92(5), 1112-1117.

Carter, M. L., Li, H., Zhang, Y., Vance, E. R., and Mitchell, D. R. G. (2009). Titanate ceramics for immobilisation of uranium-rich radioactive wastes arising from mo-99 production. *Journal of Nuclear Materials,* 384(3), 322-326.

Cavaye, H., Smith, A. R. G., James, M., Nelson, A., Burn, P. L., Gentle, I. R., et al. (2009). Solid-state dendrimer sensors: probing the diffusion of an explosive analogue using neutron reflectometry. *Langmuir,* 25(21), 12800-12805.

Chambers, S., Zahorowski, W., Matsumoto, K., and Uematsu, M. (2009). Seasonal variability of radon-derived fetch regions for Sado Island, Japan, based on 3 years of observations: 2002-2004. *Atmospheric Environment,* 43(2), 271-279.

Chilcott, T. C., Wong, E. L. S., Coster, H. G. L., Coster, A. C. F., and James, M. (2009). Ionic double layer of atomically flat gold formed on mica templates. *Electrochimica Acta,* 54(14), 3766-3774.

Choucair, M., Thordarson, P., and Stride, J. A. (2009). Gram-scale production of graphene based on solvothermal synthesis and sonication. *Nature Nanotechnology,* 4(1), 30-33.

Ciampi, S., Eggers, P. K., Le Saux, G., James, M., Harper, J. B., and Gooding, J. J. (2009). Silicon (100) electrodes resistant to oxidation in aqueous solutions: an unexpected benefit of surface acetylene moieties. *Langmuir,* 25(4), 2530-2539.

Claridge, J. K., Headey, S. J., Chow, J. Y. H., Schwalbe, M., Edwards, P. J., Jeffries, C. M., et al. (2009). A picornaviral loop-to-loop replication complex. *Journal of Structural Biology,* 166(3), 251-262.

Colella, M., Parkinson, A., Evans, T., Lennard, C., and Roux, C. (2009). The recovery of latent fingermarks from evidence exposed to ionizing radiation. *Journal of Forensic Sciences,* 54(3), 583-590.

Copeland, L., Blazek, J., Salman, H., and Tang, M. C. M. (2009). Form and functionality of starch. *Food Hydrocolloids,* 23(6), 1527-1534.

Crawford, J., Zahorowski, W., and Cohen, D. D. (2009). A new metric space incorporating radon-222 for generation of back trajectory clusters in atmospheric pollution studies. *Atmospheric Environment,* 43(2), 371-381.

Crompton, K. E., Forsythe, J. S., Horne, M. K., Finkelstein, D. I., and Knott, R. B. (2009). Molecular level and microstructural characterisation of thermally sensitive chitosan hydrogels. *Soft Matter,* 5(23), 4704-4711.

Dalton, V. S., Wang, H. Q., and Zavitsanou, K. (2009). Hu210-induced downregulation in cannabinoid cb1 receptor binding strongly correlates with body weight loss in the adult rat. *Neurochemical Research,* 34(7), 1343-1353.

Danilkin, S. A. (2009). An investigation of the structural dynamics in the fast ionic conductor Cu2-delta Se using neutron scattering. *Journal of Alloys and Compounds,* 467(1-2), 509-513.

Danilkin, S. A. (2009). Diffuse scattering and lattice dynamics of superionic copper chalcogenides. *Solid State Ionics,* 180(6-8), 483-487.

Dedeurwaerdere, S., Gregoire, M. C., Vivash, L., Roselt, P., Binns, D., Fookes, C., et al. (2009). In-vivo imaging characteristics of two fluorinated flumazenil radiotracers in the rat. *European Journal of Nuclear Medicine and Molecular Imaging,* 36(6), 958-965.

Deslandes, A., Jasieniak, M., Ionescu, M., Shapter, J. G., Fairman, C., Gooding, J. J., et al. (2009). Tof-sims characterisation of methane- and hydrogen-plasma-modified graphite using principal component analysis. *Surface and Interface Analysis,* 41(3), 216-224.

Di Bartolo, N., Smith, S. V., Hetherington, E., and Sargeson, A. (2009). An investigation into the potential of sarar for use in cu-64 radioimmunotherapy. *Australian Journal of Chemistry,* 62(10), 1261-1270.

Dodson, J., Li, X. Q., Ji, M., Zhao, K. L., Zhou, X. Y., and Levchenko, V. (2009). Early bronze in two Holocene archaeological sites in Gansu, NW China. *Quaternary Research,* 72(3), 309-314.

Dolbin, A. V., Vinnikov, N. A., Gavrilko, V. G., Esel'son, V. B., Manzhelii, V. G., Gadd, G. E., et al. (2009). Thermal expansion of solutions of deuteromethane in fullerite c-60 at low temperatures. Isotopic effect. *Low Temperature Physics,* 35(3), 226-231.

Drabarek, E., McLeod, T. I., Hanna, J. V., Griffith, C. S., and Luca, V. (2009). Tungstate-based glass-ceramics for the immobilization of radio cesium. *Journal of Nuclear Materials,* 384(2), 119-129.

Drisko, G. L., Luca, V., Sizgek, E., Scales, N., and Caruso, R. A. (2009). Template synthesis and adsorption properties of hierarchically porous zirconium titanium oxides. *Langmuir,* 25(9), 5286-5293.

Druker, A. V., Sobrero, C., Malarria, J., Garbe, U., Brokmeier, H. G., and Bolmaro, R. E. (2009). Effect of texture heterogeneities on the shape memory properties of rolled Fe-Mn-Si SMA. *Zeitschrift Fur Kristallographie,* Suppl. 30, 297-302.

Fabian, C. P., Ridd, M. J., Sheehan, M. E., and Mandin, P. (2009). Modeling the charge-transfer resistance to determine the role of guar and activated polyacrylamide in copper electrodeposition. *Journal of the Electrochemical Society,* 156(10), D400-D407.

Finnie, K. S., Waller, D. J., Perret, F. L., Krause-Heuer, A. M., Lin, H. Q., Hanna, J. V., et al. (2009). Biodegradability of sol-gel silica microparticles for drug delivery. *Journal of Sol-Gel Science and Technology,* 49(1), 12-18.

Fong, W. K., Hanley, T., and Boyd, B. J. (2009). Stimuli responsive liquid crystals provide 'on-demand' drug delivery *in vitro* and *in vivo*. *Journal of Controlled Release,* 135(3), 218-226.

Fontaine-Vive, F., Merzel, F., Johnson, M. R., and Kearley, G. J. (2009). Collagen and component polypeptides: Low frequency and amide vibrations. *Chemical Physics,* 355(2-3), 141-148.

Garbe, U. (2009). New pole figure calculation software: 2DiffCalc. *Journal of Applied Crystallography,* 42, 730-733.

Ghahghaei, A., Rekas, A., Carver, J. A., and Augusteyn, R. C. (2009). Structure/function studies of dogfish alpha-crystallin, comparison with bovine alpha-crystallin. *Molecular Vision,* 15(256-59), 2411-2420.

Gillespie, R., Fink, D., and Petchey, G. (2009). Murray-darling basin freshwater shells: Riverine reservoir effect. *Archaeology in Oceania,* 44, 107-111.

Giulian, R., Araujo, L. L., Kluth, P., Sprouster, D. J., Schnohr, C. S., Foran, G. J., et al. (2009). Temperature-dependent EXAFS analysis of embedded Pt nanocrystals. *Journal of Physics-Condensed Matter,* 21(15), 6.

Giulian, R., Araujo, L. L., Kluth, P., Sprouster, D. J., Schnohr, C. S., Johannessen, B., et al. (2009). The influence of annealing conditions on the growth and structure of embedded Pt nanocrystals. *Journal of Applied Physics,* 105(4), 8.

Golab, A. N., Peterson, M. A., and Indraratna, B. (2009). Selection of permeable reactive barrier materials for treating acidic groundwater in acid sulphate soil terrains based on laboratory column tests. *Environmental Earth Sciences,* 59(1), 241-254.

Goossens, D. J., Beasley, A. G., Welberry, T. R., Gutmann, M. J., and Piltz, R. O. (2009). Neutron diffuse scattering in deuterated para-terphenyl, C18D14. *Journal of Physics-Condensed Matter,* 21(12), 10.

Greguric, I., Taylor, S. R., Denoyer, D., Ballantyne, P., Berghofer, P., Roselt, P., et al. (2009). Discovery of [f-18]n-(2-(diethylamino)ethyl)-6-fluoronicotinamide: A melanoma positron emission tomography imaging radiotracer with high tumor to body contrast ratio and rapid renal clearance. *Journal of Medicinal Chemistry,* 52(17), 5299-5302.

Grice, K., Lu, H., Atahan, P., Asif, M., Hallmann, C., Greenwood, P., et al. (2009). New insights into the origin of perylene in geological samples. *Geochimica Et Cosmochimica Acta,* 73(21), 6531-6543.

Griffith, C. S., Luca, V., Hanna, J. V., Pike, K. J., Smith, M. E., and Thorogood, G. S. (2009). Microcrystalline hexagonal tungsten bronze. 1. Basis of ion exchange selectivity for cesium and strontium. *Inorganic Chemistry,* 48(13), 5648-5662.

Griffith, D. W. T., Parkes, S. D., Haverd, V., Paton-Walsh, C., and Wilson, S. R. (2009). Absolute calibration of the intramolecular site preference of n-15 fractionation in tropospheric n2o by ft-ir spectroscopy. *Analytical Chemistry,* 81(6), 2227-2234.

Griffiths, M. L., Drysdale, R. N., Gagan, M. K., Zhao, J. X., Ayliffe, L. K., Hellstrom, J. C., et al. (2009). Increasing Australian-Indonesian monsoon rainfall linked to early Holocene sea-level rise. *Nature Geoscience,* 2(9), 636-639.

Guralnik, B., Matmon, A., Avni, Y., and Fink, D. (2009). 10be exposure ages of ancient desert pavements reveal quaternary evolution of the Dead Sea drainage basin and rift margin tilting. *Earth and Planetary Science Letters,* 290(1-2), 132-141.

Hanley, H. J. M., and Payne, T. E. (2009). Adsorption of a jet fuel on a model organic-clay soil: Application of small angle neutron scattering. *Canadian Journal of Civil Engineering,* 36(3), 559-563.

Hargreaves, S., Bignell, L. J., Lewis, R. A., Sigmund, J., and Hartnagel, H. L. (2009). New modes of thz generation by low-temperature-grown gaassb. *Solid-State Electronics,* 53(2), 160-165.

Heimsath, A. M., Fink, D., and Hancock, G. R. (2009). The 'humped' soil production function: Eroding Arnhem Land, Australia. *Earth Surface Processes and Landforms,* 34(12), 1674-1684.

Hollins, S. E., Heron, S. F., and Ridd, P. V. (2009). Methods for monitoring tidal flushing in large animal burrows in tropical mangrove swamps. *Estuarine Coastal and Shelf Science,* 82(4), 615-620.

Holmes, R. L., Campbell, J. A., Burford, R. P., and Karatchevtseva, I. (2009). Pyrolysis behaviour of titanium dioxide-poly(vinyl pyrrolidone) composite materials. *Polymer Degradation and Stability,* 94(10), 1882-1889.

Htoon, A., Shrestha, A. K., Flanagan, B. M., Lopez-Rubio, A., Bird, A. R., Gilbert, E. P., et al. (2009). Effects of processing high amylose maize starches under controlled conditions on structural organisation and amylase digestibility. *Carbohydrate Polymers,* 75(2), 236-245.

Hua, Q. (2009). Radiocarbon: A chronological tool for the recent past. *Quaternary Geochronology,* 4(5), 378-390.

Hua, Q., Barbetti, M., Fink, D., Kaiser, K. F., Friedrich, M., Kromer, B., et al. (2009). Atmospheric c-14 variations derived from tree rings during the early younger dryas. *Quaternary Science Reviews,* 28(25-26), 2982-2990.

Hudspeth, J. M., Goossens, D. J., Studer, A. J., Withers, R. L., and Noren, L. (2009). The crystal and magnetic structures of LaCa2Fe3O8 and NdCa2Fe3O8. *Journal of Physics-Condensed Matter,* 21(12), 8.

Jacques, D. A., Streamer, M., Rowland, S. L., King, G. F., Guss, J. M., Trewhella, J., et al. (2009). Structure of the sporulation histidine kinase inhibitor Sda from Bacillus subtilis and insights into its solution state. *Acta Crystallographica Section D-Biological Crystallography,* 65, 574-581.

Ju, P. C., Pages, G., Riek, R. P., Chen, P. C., Torres, A. M., Bansal, P. S., et al. (2009). The pore domain outer helix contributes to both activation and inactivation of the hERG K+ channel. *Journal of Biological Chemistry,* 284(2), 1000-1008.

Kachenko, A. G., Bhatia, N. P., Siegele, R., Walsh, K. B., and Singh, B. (2009). Nickel, zn and cd localisation in seeds of metal hyperaccumulators using mu-pixe spectroscopy. *Nuclear Instruments and Methods in Physics Research Section B-Beam Interactions with Materials and Atoms,* 267(12-13), 2176-2180.

Kamarulzaman, N., Yusoff, R., Kamarudin, N., Shaari, N. H., Aziz, N. A. A., Bustam, M. A., et al. (2009). Investigation of cell parameters, microstructures and electrochemical behaviour of limn2o4 normal and nano powders. *Journal of Power Sources,* 188(1), 274-280.

Kas, A., Bottlaender, M., Gallezot, J. D., Vidailhet, M., Villafane, G., Gregoire, M. C., et al. (2009). Decrease of nicotinic receptors in the nigrostriatal system in parkinson's disease. *Journal of Cerebral Blood Flow and Metabolism,* 29(9), 1601-1608.

Keiser, D. D., Robinson, A. B., Jue, J. F., Medvedev, P., Wachs, D. M., and Finlay, M. R. (2009). Microstructural development in irradiated u-7mo/6061 al alloy matrix dispersion fuel. *Journal of Nuclear Materials,* 393(2), 311-320.

Kennedy, B. J., Ting, J., Zhou, Q. D., Zhang, Z. M., Matsuda, M., and Miyake, M. (2009). Structural characterisation of the perovskite series sr0.9-xcaxce0.1mno3: Influence of the jahn-teller effect. *Journal of Solid State Chemistry,* 182(4), 954-959.

Kent, B., Garvey, C. J., Cookson, D., and Bryant, G. (2009). The inverse hexagonal - inverse ribbon - lamellar gel phase transition sequence in low hydration DOPC:DOPE phospholipid mixtures. *Chemistry and Physics of Lipids,* 157(1), 56-60.

Khan, M. K., Fitzpatrick, M. E., Hainsworth, S. V., and Edwards, L. (2009). Effect of tool profile and fatigue loading on the local hardness around scratches in clad and unclad aluminium alloy 2024. *Materials Science and Engineering a-Structural Materials Properties Microstructure and Processing,* 527(1-2), 297-304.

Khan, M. K., Hainsworth, S. V., Fitzpatrick, M. E., and Edwards, L. (2009). Application of the work of indentation approach for the characterization of aluminium 2024-t351 and al cladding by nanoindentation. *Journal of Materials Science,* 44(4), 1006-1015.

Kiernan, K., Gore, D. B., Fink, D., White, D. A., McConnell, A., and Sigurdsson, I. A. (2009). Deglaciation and weathering of Larsemann Hills, east Antarctica. *Antarctic Science,* 21(4), 373-382.

Kirstein, O., Prager, M., and Schneider, G. J. (2009). Rotational dynamics and coupling of methyl group rotations in methyl fluoride studied by high resolution inelastic neutron scattering. *Journal of Chemical Physics,* 130(21), 5.

Koh, J. M. S., Bansal, P. S., Torres, A. M., and Kuchel, P. W. (2009). Platypus venom: source of novel compounds. *Australian Journal of Zoology,* 57(3-4), 203-210.

Kong, P., Fink, D., Na, C. G., and Huang, F. X. (2009). Late quaternary glaciation of the Tianshan, central Asia, using cosmogenic be-10 surface exposure dating. *Quaternary Research,* 72(2), 229-233.

Kong, P., Na, C. G., Fink, D., Zhao, X. T., and Xiao, W. (2009). Moraine dam related to late quaternary glaciation in the Yulong Mountains, southwest China, and impacts on the Jinsha River. *Quaternary Science Reviews,* 28(27-28), 3224-3235.

Kosnik, M. A., Hua, Q., Kaufman, D. S., and Wust, R. A. (2009). Taphonomic bias and time-averaging in tropical molluscan death assemblages: Differential shell half-lives in Great Barrier Reef sediment. *Paleobiology,* 35(4), 565-586.

Ladd, B., Bonser, S. P., Peri, P. L., Larsen, J. R., Laffan, S. W., Pepper, D. A., et al. (2009). Towards a physical description of habitat: Quantifying environmental adversity (abiotic stress) in temperate forest and woodland ecosystems. *Journal of Ecology,* 97(5), 964-971.

Lai, N. S., Lim, W. H., Ziebell, A. L., Reinhard, M. I., Rosenfeld, A. B., and Dzurak, A. S. (2009). Development and fabrication of cylindrical silicon-on-insulator microdosimeter arrays. *IEEE Transactions on Nuclear Science,* 56(3), 1637-1641.

Lauw, Y., Horne, M. D., Rodopoulos, T., Webster, N. A. S., Minofar, B., and Nelson, A. (2009). X-Ray reflectometry studies on the effect of water on the surface structure of [C(4)mpyr][NTf2] ionic liquid. *Physical Chemistry Chemical Physics,* 11(48), 11507-11514.

Law, B. M., Brown, M. D., Marchand, L., Lurio, L. B., Hamilton, W. A., Kuzmenko, I., et al. (2009). Adsorption at liquid interfaces: a comparison of multiple experimental techniques. *European Physical Journal-Special Topics,* 167, 127-132.

Le, V. S., Howse, J., Zaw, M., Pellegrini, P., Katsifis, A., Greguric, I., et al. (2009). Alternative method for cu-64 radioisotope production. *Applied Radiation and Isotopes,* 67(7-8), 1324-1331.

Le Bail, A., Cranswick, L. M. D., Adil, K., Altomare, A., Avdeev, M., Cerny, R., et al. (2009). Third structure determination by powder diffractometry round robin (SDPDRR-3). *Powder Diffraction,* 24(3), 254-262.

Lee, C., Wacklin, H., and Bain, C. D. (2009). Changes in molecular composition and packing during lipid membrane reconstitution from phospholipid-surfactant micelles. *Soft Matter,* 5(3), 568-575.

Lee, K. W. Y., Nguyen, T. H., Hanley, T., and Boyd, B. J. (2009). Nanostructure of liquid crystalline matrix determines *in vitro* sustained release and *in vivo* oral absorption kinetics for hydrophilic model drugs. *International Journal of Pharmaceutics,* 365(1-2), 190-199.

Lenne, T., Garvey, C. J., Koster, K. L., and Bryant, G. (2009). Effects of sugars on lipid bilayers during dehydration - SAXS/WAXS measurements and quantitative model. *Journal of Physical Chemistry B,* 113(8), 2486-2491.

Leriche, L., Bjorklund, T., Breysse, N., Besret, L., Gregoire, M. C., Carlsson, T., et al. (2009). Positron emission tomography imaging demonstrates correlation between behavioral recovery and correction of dopamine neurotransmission after gene therapy. *Journal of Neuroscience,* 29(5), 1544-1553.

Leroy, C., Bragulat, V., Berlin, I., Gregoire, M. C., Bottlaender, M., Roumenov, D., et al. (2009). Cerebral monoamine oxidase a inhibition in tobacco smokers confirmed with pet and [c-11]befloxatone. *Journal of Clinical Psychopharmacology,* 29(1), 86-88.

Li, X. Q., Dodson, J., Zhou, J., and Zhou, X. Y. (2009). Increases of population and expansion of rice agriculture in Asia, and anthropogenic methane emissions since 5000 bp. *Quaternary International,* 202, 41-50.

Li, X. Q., Shang, X., Dodson, J., and Zhou, X. Y. (2009). Holocene agriculture in the Guanzhong Basin in NW China indicated by pollen and charcoal evidence. *Holocene,* 19(8), 1213-1220.

Liljedahl, C. D. M., Brouard, J., Zanellato, O., Lin, J., Tan, M. L., Ganguly, S., et al. (2009). Weld residual stress effects on fatigue crack growth behaviour of aluminium alloy 2024-t351. *International Journal of Fatigue,* 31(6), 1081-1088.

Liljedahl, C. D. M., Fitzpatrick, M. E., and Edwards, L. (2009). Evolution of residual stresses with fatigue crack growth in integral structures with crack retarders. *Materials Science and Engineering a-Structural Materials Properties Microstructure and Processing,* 523(1-2), 152-159.

Lim, W. H., Ziebell, A. L., Cornelius, I., Reinhard, M. I., Prokopovich, D. A., Dzurak, A. S., et al. (2009). Cylindrical silicon-on-insulator microdosimeter: Design, fabrication and tcad modeling. *IEEE Transactions on Nuclear Science,* 56(2), 424-428.

Lindsay, M. J., Skyllas-Kazacos, M., and Luca, V. (2009). Anodically synthesized titania films for lithium batteries: Effect of titanium substrate and surface treatment. *Electrochimica Acta,* 54(13), 3501-3509.

Ling, C. D., Avdeev, M., Kutteh, R., Kharton, V. V., Yaremchenko, A. A., Fialkova, S., et al. (2009). Structures, phase transitions, hydration, and ionic conductivity of Ba4Nb2O9. *Chemistry of Materials,* 21(16), 3853-3864.

Ling, C. D., Rowda, B., Avdeev, M., and Pullar, R. (2009). Structures, phase transitions and microwave dielectric properties of the 6H perovskites Ba3BSb2O9, B = Mg, Ca, Sr, Ba. *Journal of Solid State Chemistry,* 182(3), 479-483.

Liss, K. D., d'Almeida, T., Kaiser, M., Hock, R., Magerl, A., and Eloy, J. F. (2009). Time-resolved x-ray diffraction study of laser-induced shock and acoustic waves in single crystalline silicon. *Journal of Applied Physics,* 106(4), 6.

Liss, K. D., Garbe, U., Li, H. J., Schambron, T., Almer, J. D., and Yan, K. (2009). In situ observation of dynamic recrystallization in the bulk of zirconium alloy. *Advanced Engineering Materials,* 11(8), 637-640.

Liss, K. D., Schmoelzer, T., Yan, K., Reid, M., Peel, M., Dippenaar, R., et al. (2009). In situ study of dynamic recrystallization and hot deformation behavior of a multiphase titanium aluminide alloy. *Journal of Applied Physics,* 106(11), 6.

Liss, K. D., Whitfield, R. E., Xu, W., Buslaps, T., Yeoh, L. A., Wu, X. L., et al. (2009). In situ synchrotron high-energy X-ray diffraction analysis on phase transformations in Ti-Al alloys processed by equal-channel angular pressing. *Journal of Synchrotron Radiation,* 16, 825-834.

Lopez-Rubio, A., Clarke, J. M., Scherer, B., Topping, D. L., and Gilbert, E. P. (2009). Structural modifications of granular starch upon acylation with short-chain fatty acids. *Food Hydrocolloids,* 23(7), 1940-1946.

Lopez-Rubio, A., and Gilbert, E. P. (2009). Neutron scattering: a natural tool for food science and technology research. *Trends in Food Science and Technology,* 20(11-12), 576-586.

Low, I. M., Somers, J., Kho, H. S., Davies, I. J., and Latella, B. A. (2009). Fabrication and properties of recycled cellulose fibre-reinforced epoxy composites. *Composite Interfaces,* 16(7-9), 659-669.

Lu, Z., Walock, M. J., LeClair, P. R., Mankey, G. J., Mani, P., Lott, D., et al. (2009). Structural and magnetic properties of epitaxial Fe25Pt75. *Journal of Vacuum Science and Technology A,* 27(4), 770-775.

Luca, V. (2009). Comparison of size-sependent structural and electronic properties of anatase and rutile nanoparticles. *Journal of Physical Chemistry C,* 113(16), 6367-6380.

Luca, V., Griffith, C. S., and Hanna, J. V. (2009). Microcrystalline hexagonal tungsten bronze. 2. Dehydration dynamics. *Inorganic Chemistry,* 48(13), 5663-5676.

Luca, V., Soler-Illia, G., Angelome, P. C., Steinberg, P. Y., Drabarek, E., and Hanley, T. L. (2009). Striving for order and compositional homogeneity in bulk mesoporous zirconium titanium mixed metal oxides from triblock copolymers and metal chlorides. *Microporous and Mesoporous Materials,* 118(1-3), 443-452.

Lumpkin, G. R., Smith, K. L., Blackford, M. G., Whittle, K. R., Harvey, E. J., Redfern, S. A. T., et al. (2009). Ion irradiation of ternary pyrochlore oxides. *Chemistry of Materials,* 21(13), 2746-2754.

Maddocks, A. R., Cassidy, D. J., Jones, A. S., and Harris, A. T. (2009). Synthesis of nanoporous silicon carbide via the preceramic polymer route. *Materials Chemistry and Physics,* 113(2-3), 861-867.

Matuchova, M., Zdansky, K., Zavadil, J., Danilewsky, A., Maixner, J., and Alexiev, D. (2009). Electrical, optical and structural properties of lead iodide. *Journal of Materials Science-Materials in Electronics,* 20(3), 289-294.

Matuchova, M., Zdansky, K., Zavadil, J., Danilewsky, A., Riesz, F., Hassan, M. A. S., et al. (2009). Study of the influence of the rare-earth elements on the properties of lead iodide. *Journal of Crystal Growth,* 311(14), 3557-3562.

Mazumder, D., Saintilan, N., and Williams, R. J. (2009). Zooplankton inputs and outputs in the saltmarsh at Towra Point, Australia. *Wetlands Ecology and Management,* 17(3), 225-230.

Meredith, K. T., Hollins, S. E., Hughes, C. E., Cendon, D. I., Hankin, S., and Stone, D. J. M. (2009). Temporal variation in stable isotopes (o-18 and h-2) and major ion concentrations within the Darling River between Bourke and Wilcannia due to variable flows, saline groundwater influx and evaporation. *Journal of Hydrology,* 378(3-4), 313-324.

Meure, L. A., Knott, R., Foster, N. R., and Dehghani, F. (2009). The depressurization of an expanded solution into aqueous media for the bulk production of liposomes. *Langmuir,* 25(1), 326-337.

Mills, R. D., Trewhella, J., Qiu, T. W., Welte, T., Ryan, T. M., Hanley, T., et al. (2009). Domain organization of the monomeric form of the Tom70 mitochondrial import receptor. *Journal of Molecular Biology,* 388(5), 1043-1058.

Milne, N. A., Skyllas-Kazacos, M., and Luca, V. (2009). Crystallite size dependence of lithium intercalation in nanocrystalline rutile. *Journal of Physical Chemistry C,* 113(30), 12983-12995.

Minakshi, M., Mitchell, D. R. G., Carter, M. L., Appadoo, D., and Nallathamby, K. (2009). Microstructural and spectroscopic investigations into the effect of ceo2 additions on the performance of a mno2 aqueous rechargeable battery. *Electrochimica Acta,* 54(12), 3244-3249.

Minakshi, M., Nallathamby, K., and Mitchell, D. R. G. (2009). Electrochemical characterization of an aqueous lithium rechargeable battery: The effect of ceo2 additions to the mno2 cathode. *Journal of Alloys and Compounds,* 479(1-2), 87-90.

Mulders, A. M., Lawrence, S. M., Staub, U., Garcia-Fernandez, M., Scagnoli, V., Mazzoli, C., et al. (2009). Direct observation of charge order and an orbital glass state in multiferroic LuFe2O4. *Physical Review Letters,* 103(7), 4.

Mulders, A. M., Loosvelt, H., Rodriguez, A. F., Popova, E., Konishi, T., Temst, K., et al. (2009). On the interface magnetism of thin oxidized Co films: orbital and spin moments. *Journal of Physics-Condensed Matter,* 21(12), 6.

Mulyana, Y., Nafady, A., Mukherjee, A., Bircher, R., Moubaraki, B., Murray, K. S., et al. (2009). New family of ferric spin clusters incorporating redox-active orthodioxolene ligands. *Inorganic Chemistry,* 48(16), 7765-7781.

Muransky, O., Carr, D. G., Sittner, P., and Oliver, E. C. (2009). In situ neutron diffraction investigation of deformation twinning and pseudoelastic-like behaviour of extruded az31 magnesium alloy. *International Journal of Plasticity,* 25(6), 1107-1127.

Murugaraj, P., Mainwaring, D., and Siegele, R. (2009). Electron transport properties of irradiated polyimide thin films in single track regime. *Applied Physics Letters,* 94(12), 3.

Neto, C., James, M., and Telford, A. M. (2009). On the composition of the top layer of microphase separated thin PS-PEO films. *Macromolecules,* 42(13), 4801-4808.

Ng, A., Ciampi, S., James, M., Harper, J. B., and Gooding, J. J. (2009). Comparing the reactivity of alkynes and alkenes on silicon (100) surfaces. *Langmuir,* 25(24), 13934-13941.

Ng, M. C. C., Craig, D. J., Harper, J. B., Van-Eijck, L., and Stride, J. A. (2009). The central atom size effect on the structure of group 14 tetratolyls. *Chemistry-a European Journal,* 15(27), 6569-6572.

Nguyen, C. L., Atanacio, A., Zhang, W., Prince, K. E., Hyland, M. M., and Metson, J. B. (2009). Phase-oriented surface segregation in an aluminium casting alloy. *Applied Surface Science,* 255(9), 4880-4885.

Noren, L., Withers, R. L., Goossens, D. J., Elcombe, M., and Kearley, G. J. (2009). Coupled Li1+/Nb5+ and O2-/F- ordering on the Na and Cl sites of the average NaCl structure of Li4NbO4F. *Journal of Solid State Chemistry,* 182(5), 1109-1114.

Pages, G., Torres, A. M., Ju, P. C., Bansal, P. S., Alewood, P. F., Kuchel, P. W., et al. (2009). Structure of the pore-helix of the hERG K+ channel. *European Biophysics Journal with Biophysics Letters,* 39(1), 111-120.

Paradowska, A. M., Price, J. W. H., Finlayson, T. R., Lienert, U., Walls, P., and Ibrahim, R. (2009). Residual stress distribution in steel butt welds measured using neutron and synchrotron diffraction. *Journal of Physics-Condensed Matter,* 21(12). 124213.

Payne, T. E., Itakura, T., Comarmond, M. J., and Harrison, J. J. (2009). Environmental mobility of cobalt-influence of solid phase characteristics and groundwater chemistry. *Applied Radiation and Isotopes,* 67(7-8), 1269-1276.

Peterson, V. K., and Whitten, A. E. (2009). Hydration processes in tricalcium silicate: application of the boundary nucleation model to quasielastic neutron scattering data. *Journal of Physical Chemistry C,* 113(6), 2347-2351.

Petrenko, V. V., Smith, A. M., Brook, E. J., Lowe, D., Riedel, K., Brailsford, G., et al. (2009). (ch4)-c-14 measurements in Greenland ice: Investigating last glacial termination ch4 sources. *Science,* 324(5926), 506-508.

Pooke, D. M., Chamritski, V., Fee, M., Gibson, S., King, B. T., Tallon, J. L., et al. (2009). HTS 5 Tesla Synchrotron and Neutron Beamline Magnets. *IEEE Transactions on Applied Superconductivity,* 19(3), 1372-1375.

Pratihar, S., Turski, M., Edwards, L., and Bouchard, P. J. (2009). Neutron diffraction residual stress measurements in a 316l stainless steel bead-on-plate weld specimen. *International Journal of Pressure Vessels and Piping,* 86(1), 13-19.

Pross, J., Kotthoff, U., Muller, U. C., Peyron, O., Dormoy, I., Schmiedl, G., et al. (2009). Massive perturbation in terrestrial ecosystems of the eastern Mediterranean region associated with the 8.2 kyr bp climatic event. *Geology,* 37(10), 887-890.

Radhi, M., Box, A., Box, G. P., Mitchell, R. M., Cohen, D. D., Stelcer, E., et al. (2009). Optical, physical and chemical characteristics of Australian desert dust aerosols: Results from a field experiment. *Atmospheric Chemistry and Physics Discussions,* 9, 25085-25125.

Rahlenbeck, M., Sun, G. L., Sun, D. L., Lin, C. T., Keimer, B., and Ulrich, C. (2009). Phonon anomalies in pure and underdoped R1-xKxFe2As2 (R=Ba, Sr) investigated by Raman light scattering. *Physical Review B*, 80(6), 5.

Ramli, M., Smith, S. V., and Lindoy, L. F. (2009). Investigation of novel bis- and tris-tetraazamacrocycles for use in the copper-64 (cu-64) radiolabeling of antibodies with potential to increase the therapeutic index for drug targeting. *Bioconjugate Chemistry,* 20(5), 868-876.

Rekas, A., Lo, V., Gadd, G. E., Cappai, R., and Yun, S. L. (2009). Pamam dendrimers as potential agents against fibrillation of alpha-synuclein, a parkinson's disease-related protein. *Macromolecular Bioscience,* 9(3), 230-238.

Reynolds, P. A., Gilbert, E. P., Henderson, M. J., and White, J. W. (2009). Structure of high internal phase aqueous-in-oil emulsions and related inverse micelle solutions. 3. variation of surfactant. *Journal of Physical Chemistry B,* 113(36), 12231-12242.

Reynolds, P. A., Gilbert, E. P., Henderson, M. J., and White, J. W. (2009). Structure of high internal phase aqueous-in-oil emulsions and related inverse micelle solutions. 4. surfactant mixtures. *Journal of Physical Chemistry B,* 113(36), 12243-12256.

Ridgway, M. C., Kluth, P., Giulian, R., Sprouster, D. J., Araujo, L. L., Schnohr, C. S., et al. (2009). Changes in metal nanoparticle shape and size induced by swift heavy-ion irradiation. *Nuclear Instruments and Methods in Physics Research Section B-Beam Interactions with Materials and Atoms,* 267(6), 931-935.

Rizwan, S. B., Hanley, T., Boyd, B. J., Rades, T., and Hook, S. (2009). Liquid crystalline systems of phytantriol and glyceryl monooleate containing a hydrophilic protein: characterisation, swelling and release kinetics. *Journal of Pharmaceutical Sciences,* 98(11), 4191-4204.

Sabri, Y. M., Ippolito, S. J., Tardio, J., Atanacio, A. J., Sood, D. K., and Bhargava, S. K. (2009). Mercury diffusion in gold and silver thin film electrodes on quartz crystal microbalance sensors. *Sensors and Actuators B-Chemical,* 137(1), 246-252.

Safavi-Naeini, M., Franklin, D. R., Lerch, M. L. F., Petasecca, M., Pignatel, G. U., Reinhard, M., et al. (2009). Evaluation of silicon detectors with integrated JFET for biomedical applications. *IEEE Transactions on Nuclear Science,* 56(3), 1051-1055.

Salman, H., Blazek, J., Lopez-Rubio, A., Gilbert, E. P., Hanley, T., and Copeland, L. (2009). Structure-function relationships in A and B granules from wheat starches of similar amylose content. *Carbohydrate Polymers,* 75(3), 420-427.

Schnohr, C. S., Kluth, P., Araujo, L. L., Sprouster, D. J., Byrne, A. P., Foran, G. J., et al. (2009). Anisotropic vibrations in crystalline and amorphous InP. *Physical Review B*, 79(19), 10.

Sharma, N., Macquart, R. B., Christensen, M., Avdeev, M., Chen, Y. S., and Ling, C. D. (2009). Structure and crystal chemistry of fluorite-related Bi38Mo7O78 from single crystal X-ray diffraction and ab initio calculations. *Journal of Solid State Chemistry,* 182(6), 1312-1318.

Sheppard, L. R., Atanacio, A. J., Bak, T., Nowotny, J., Nowotny, M. K., and Prince, K. E. (2009). Niobium diffusion in niobium-doped titanium dioxide. *Journal of Solid State Electrochemistry,* 13(7), 1115-1121.

Siddiqui, K. S., Parkin, D. M., Curmi, P. M. G., De Francisci, D., Poljak, A., Barrow, K., et al. (2009). A novel approach for enhancing the catalytic efficiency of a protease at low temperature: reduction in substrate inhibition by chemical modification. *Biotechnology and Bioengineering,* 103(4), 676-686.

Siegele, R., Kachenko, A. G., Ionescu, M., and Cohen, D. D. (2009). Improved resolution and sensitivity on the ansto microprobe and it's application to mu-pixe. *Nuclear Instruments and Methods in Physics Research Section B-Beam Interactions with Materials and Atoms,* 267(12-13), 2054-2059.

Sizgek, G. D., Griffith, C. S., Sizgek, E., and Luca, V. (2009). Mesoporous zirconium titanium oxides. Part 3. Synthesis and adsorption properties of unfunctionalized and phosphonate-functionalized hierarchical polyacrylonitrile-f-127-templated beads. *Langmuir,* 25(19), 11874-11882.

So, L., Nguyen, C. D., Pellegrini, P., and Bui, V. C. (2009). Polymeric titanium oxychloride sorbent for 188w/188re nuclide pair separation. *Separation Science and Technology,* 44(5), 1074-1098.

Sprouster, D. J., Giulian, R., Schnohr, C. S., Araujo, L. L., Kluth, P., Byrne, A. P., et al. (2009). fcc-hcp phase transformation in Co nanoparticles induced by swift heavy-ion irradiation. *Physical Review B,* 80(11), 5.

Sriprom, W., James, M., Perrier, S., and Neto, C. (2009). Ordered Microphase Separation in Thin Films of PMMA-PBA Synthesized by RAFT: Effect of Block Polydispersity. *Macromolecules,* 42(8), 3138-3146.

Sriram, S., Bhaskaran, M., Kostovski, G., Mitchell, D. R. G., Stoddart, P. R., Austin, M. W., et al. (2009). Synthesis of self-assembled island-structured complex oxide dielectric films. *Journal of Physical Chemistry C,* 113(38), 16610-16614.

Sriram, S., Bhaskaran, M., Mitchell, A., Mitchell, D. R. G., and Kostovski, G. (2009). Nanocolumnar preferentially oriented pszt thin films deposited on thermally grown silicon dioxide. *Nanoscale Research Letters,* 4(1), 29-33.

Sriram, S., Bhaskaran, M., Mitchell, D. R. G., Short, K. T., Holland, A. S., and Mitchell, A. (2009). Microstructural and compositional analysis of strontium-doped lead zirconate titanate thin films on gold-coated silicon substrates. *Microscopy and Microanalysis,* 15(1), 30-35.

Sun, Y. J., Qu, D. D., Huang, Y. J., Liss, K. D., Wei, X. S., Xing, D. W., et al. (2009). Zr-Cu-Ni-Al bulk metallic glasses with superhigh glass-forming ability. *Acta Materialia,* 57(4), 1290-1299.

Szekely, D., Yau, T. W., and Kuchel, P. W. (2009). Human erythrocyte flickering: temperature, ATP concentration, water transport, and cell aging, plus a computer simulation. *European Biophysics Journal with Biophysics Letters,* 38(7), 923-939.

Thackray, G. D., Shulmeister, J., and Fink, D. (2009). Evidence for expanded middle and late pleistocene glacier extent in northwest Nelson, New Zealand. *Geografiska Annaler Series a-Physical Geography,* 91A(4), 291-311.

Thorogood, G. J., Kennedy, B. J., Peterson, V. K., Elcombe, M. M., Kearley, G. J., Hanna, J. V., et al. (2009). Anomalous lattice parameter increase in alkali earth aluminium substituted tungsten defect pyrochlores. *Journal of Solid State Chemistry,* 182(3), 457-464.

Ting, J., Kennedy, B. J., Withers, R. L., and Avdeev, M. (2009). Synthesis and structural studies of lanthanide substituted bismuth-titanium pyrochlores. *Journal of Solid State Chemistry,* 182(4), 836-840.

Tsipis, E. V., Waerenborgh, J. C., Avdeev, M., and Kharton, V. V. (2009). Mossbauer spectroscopy analysis of Fe-57-doped YBaCo4O7+delta: Effects of oxygen intercalation. *Journal of Solid State Chemistry,* 182(3), 640-643.

Turski, M., and Edwards, L. (2009). Residual stress measurement of a 316l stainless steel bead-on-plate specimen utilising the contour method. International *Journal of Pressure Vessels and Piping,* 86(1), 126-131.

Turski, M., Smith, M. C., Bouchard, P. J., Edwards, L., and Withers, P. J. (2009). Spatially resolved materials property data from a uniaxial cross-weld tensile test. *Journal of Pressure Vessel Technology-Transactions of the Asme,* 131(6). 061496

van Eijck, L., Best, A. S., Long, S., Fernandez-Alonso, F., MacFarlane, D., Forsyth, M., et al. (2009). Localized relaxational dynamics of succinonitrile. *Journal of Physical Chemistry C,* 113(33), 15007-15013.

Vance, E. R., Perera, D. S., Imperia, P., Cassidy, D. J., Davis, J., and Gourley, J. T. (2009). Perlite waste as a precursor for geopolymer formation. *Journal of the Australian Ceramic Society,* 45, 44-49.

Varga, Z., Wallenius, M., Mayer, K., Keegan, E., and Millett, S. (2009). Application of lead and strontium isotope ratio measurements for the origin assessment of uranium ore concentrates. *Analytical Chemistry,* 81(20), 8327-8334.

Velleman, L., Triani, G., Evans, P. J., Shapter, J. G., and Losic, D. (2009). Structural and chemical modification of porous alumina membranes. *Microporous and Mesoporous Materials,* 126(1-2), 87-94.

Wacklin, H. P. (2009). Interfacial mechanism of phospholipase A(2): pH-dependent inhibition and Me-beta-cyclodextrin activation. *Biochemistry,* 48(25), 5874-5881.

Wang, J. L., Campbell, S. J., Studer, A. J., Avdeev, M., Zeng, R., and Dou, S. X. (2009). Magnetic phase transitions in pr(1-x)luxmn(2)ge(2) compounds. *Journal of Physics-Condensed Matter,* 21(12), 11.

Wang, J. L., Campbell, S. J., Zeng, R., Poh, C. K., Dou, S. X., and Kennedy, S. J. (2009). Re-entrant ferromagnet prmn2ge0.8si1.2: Magnetocaloric effect. *Journal of Applied Physics,* 105(7), 3.

Wang, Y. M., Wang, P., Kohls, D., Hamilton, W. A., and Schaefer, D. W. (2009). Water absorption and transport in bis-silane films. *Physical Chemistry Chemical Physics,* 11(1), 161-166.

Watson, I. J., Liss, K. D., Clemens, H., Wallgram, W., Schmoelzer, T., Hansen, T. C., et al. (2009). In situ characterization of a nb and mo containing gamma-tial based alloy using neutron diffraction and high-temperature microscopy. *Advanced Engineering Materials,* 11(11), 932-937.

Weber, W. J., Navrotsky, A., Stefanovsky, S., Vance, E. R., and Vernaz, E. (2009). Materials science of high-level nuclear waste immobilization. *Mrs Bulletin,* 34(1), 46-53.

Weisler, M. I., Hua, Q., and Zhao, J. X. (2009). Late Holocene c-14 marine reservoir corrections for Hawai'i derived from u-series dated archaeological coral. *Radiocarbon,* 51(3), 955-968.

White, C. E., Provis, J. L., Riley, D. P., Kearley, G. J., and van Deventer, J. S. J. (2009). What is the structure of kaolinite? Reconciling theory and experiment. *Journal of Physical Chemistry B,* 113(19), 6756-6765.

White, D. A., Bennike, O., Berg, S., Harley, S. L., Fink, D., Kiernan, K., et al. (2009). Geomorphology and glacial history of Rauer Group, east Antarctica. *Quaternary Research,* 72(1), 80-90.

Whitten, A. E., Smith, B. J., Menting, J. G., Margetts, M. B., McKern, N. M., Lovrecz, G. O., et al. (2009). Solution structure of ectodomains of the insulin receptor family: The ectodomain of the type 1 insulin-like growth factor receptor displays asymmetry of ligand binding accompanied by limited conformational change. *Journal of Molecular Biology,* 394(5), 878-892.

Whittle, K. R., Cranswick, L. M. D., Redfern, S. A. T., Swainson, I. P., and Lumpkin, G. R. (2009). Lanthanum pyrochlores and the effect of yttrium addition in the systems la2-xyxzr2o7 and la2-xyxhf2o7. *Journal of Solid State Chemistry,* 182(3), 442-450.

Williams, A. G., Chambers, S., Zahorowski, W., Crawford, J., Matsumoto, K., and Uematsu, M. (2009). Estimating the Asian radon flux density and its latitudinal gradient in winter using ground-based radon observations at Sado Island. *Tellus Series B-Chemical and Physical Meteorology,* 61(5), 732-746.

Yakovlev, S., Avdeev, M., and Mezouar, M. (2009). High-pressure structural behavior and equation of state of naznf3. *Journal of Solid State Chemistry,* 182(6), 1545-1549.

Yan, K., Liss, K. D., Garbe, U., Daniels, J., Kirstein, O., Li, H. J., et al. (2009). From single grains to texture. *Advanced Engineering Materials,* 11(10), 771-773.

Yu, D. H., Duriavig, J., Loh, N., Woodward, R., Lin, H. J., Chang, F. H., et al. (2009). Investigation of field-induced ferromagnetism in pd-ni-fe-p metallic glass by x-ray magnetic circular dichroism. *Applied Physics Letters,* 94(2), 3.

Yu, J., Yu, D. H., Chen, Y., Chen, H., Lin, M. Y., Cheng, B. M., et al. (2009). Narrowed bandgaps and stronger excitonic effects from small boron nitride nanotubes. *Chemical Physics Letters,* 476(4-6), 240-243.

Yver, C., Schmidt, M., Bousquet, P., Zahorowski, W., and Ramonet, M. (2009). Estimation of the molecular hydrogen soil uptake and traffic emissions at a suburban site near Paris through hydrogen, carbon monoxide, and radon-222 semicontinuous measurements. *Journal of Geophysical Research-Atmospheres,* 114, 12.

Zhang, Y., Stewart, M. W. A., Li, H., Carter, M. L., Vance, E. R., and Moricca, S. (2009). Zirconolite-rich titanate ceramics for immobilisation of actinides - waste form/hip can interactions and chemical durability. *Journal of Nuclear Materials,* 395(1-3), 69-74.

Zhang, Z. M., Howard, C. J., Kennedy, B. J., Matsuda, M., and Miyake, M. (2009). Crystal structures and phase transition in (sr0.8ce0.2)(mn(1-y)coy)o-3 (y=0 and 0.2): The influence of jahn-teller distortion. *Journal of Physics-Condensed Matter,* 21(12), 124218.

Zhou, Q. D., Kennedy, B. J., Avdeev, M., Giachini, L., and Kimpton, J. A. (2009). Structural studies of the phases in ba2lairo6-new light on an old problem. *Journal of Solid State Chemistry,* 182(11), 3195-3200.

Zhou, Q. D., Kennedy, B. J., Zhang, Z. M., Jang, L. Y., and Aitken, J. B. (2009). X-ray absorption near edge structure and crystallographic studies of the mixed valence oxides caru1-xmnxo3. *Chemistry of Materials,* 21(18), 4203-4209.

Book Chapters and Theses 2009

Book Chapters

Vance, E. R., and Perera, D. S. (2009). Geopolymers for nuclear waste immobilisation. In J. Provis and J. S. J. van Deventer (Eds.), Geopolymers: Structure, processing, properties and applications (pp. 401-420). Cambridge, UK: Woodhead Publishing.

Bourke, P., and Hua, Q. (2009). Examining late Holocene marine reservoir effect in archaeological fauna at Hope Inlet, Beagle Gulf, north Australia. In A. Fairbairn, S. O'Connor and B. Marwick (Eds.), Terra australis: New directions in archaeological science (Vol. 28, pp. 175-187). Canberra: ANU E Press.

Dodson, J., and Muhongo, S. M. (2009). International year of planet Earth: Science programme activity. In C. Ford, E. Derbyshire, V. Philpott, and Wicks, M (Eds.), International year of planet Earth (pp. 16-20). London: Boston Hannah International.

Mahowald, N. M., Engelstaedter, S., Luo, C., Sealy, A., Artaxo, P., Benitez-Nelson, C., et al. (2009). Atmospheric iron deposition: Global distribution, variability, and human perturbations. In Annual Review of Marine Science (Vol. 1, pp. 245-278). Palo Alto, California, USA: Annual Reviews.

Mazumder, D. (2009). Ecology of burrowing crabs in temperate saltmarsh of southeast Australia. In N. Saintilan (Ed.), Australian saltmarsh ecology (pp. 115-129). Collingwood, Victoria, Australia: CSIRO Publishing.

Theses

Luu, E. (2009). Hawkesbury sandstone aquifers of the Sydney basin, potential water-rock interactions on 14c groundwater dating (BSc Hons Thesis). University of NSW, Sydney, Australia.

Spencer, J. (2009). The surface and groundwaters of the Lawn Hill region, northwest Queensland (BSc Hons Thesis). University of NSW, Sydney, Australia.

Editing of Books and Special Journal Issues

Dodson, J. (Ed.). (2009). Quaternary International: The great arc of human dispersal (Vol. 202). Oxford, New York: Pergamon Press.

Twining, J. R. (Assoc. Ed.). (2009). Journal of Environmental Radioactivity. Barking: Elsevier Applied Science Publishers.

Buttner, H. G. (Ed). (2009). Neutron News, 20(1-4). Philadelphia, USA: Taylor and Francis Group.

Other

Larsen, J., Nanson, G., Cendon, D. I., and Jones, B. (2009). Billabongs (waterholes), unique geomorphology and hydrology in action in arid Australia. Vignettes: Key concepts in geomorphology. Retrieved Sept 3, 2010, from http://serc.carleton.edu/vignettes/collection/35395.html

Published Conference Proceedings 2009

Abbey, E., Webster, J., Jacobsen, G., Thomas, A., Henderson, G., Reimer, P., et al. (2009). Morphological variation, composition and age of submerged reefs of the Great Barrier Reef. IODP New Ventures in Exploring Scientific Targets (INVEST), 23rd – 25th September 2009. Bremen, Germany: University of Bremen Campus. Retrieved Sept 3, 2010, from http://www.deepreef.org/images/stories/publications/conference-proceedings/MorphologySubmergedReefs_IODP2009.pdf

Bendeich, P. J., Smith, M. C., Carr, D. G., and Edwards, L. (2009). Sensitivity of predicted weld residual stresses in the net task group 1 single bead on plate benchmark problem to finite element mesh design and heat source characteristics. 2009 ASME Pressure Vessels and Piping Division Conference, 26th – 30th July 2009. Prague, Czech Republic: The Hilton Prague. In *2009 Proceedings of the ASME Pressure Vessels and Piping Conference* (CD-ROM). New York, America: American Society of Mechanical Engineers.

Bignell, L. J., Mo, L., Alexiev, D., and Hashemi-Nezhad, S. R. (2009). Sensitivity and uncertainty analysis of the simulation of 123i and 54mn gamma and x-ray emissions in a liquid scintillation vial. International Committee on Radionuclide Metrology (ICRM) 2009 Conference, 7th – 11th September 2009. Bratislava, Slovak Republic: Slovak Institute of Metrology. In *Applied Radiation and Isotopes*, 68 (7-8), 1495-1502.

Carter, M. L., Li, H., Zhang, Y., Gillen, A. L., and Vance, E. R. (2009). HIPed tailored pyrochlore-rich glass-ceramic waste forms for the immobilization of nuclear waste. Materials Research Society 2008 Fall Meeting (Symposium Q), 1st – 5th December 2008. Boston, Massachusetts: Hynes Convention Center. In N. C. Hyatt, D. A. Pickett and R. B. Rebak (Eds.). Scientific Basis for Nuclear Waste Management XXXII: *MRS Proceedings* (Vol. 1124, Paper #1124-Q04-01). Pennsylvania, America: Materials Research Society.

Fink, D., Klein, J., Middleton, R., Albrecht, A., Ma, P., Herzog, G. F., et al. (2009). Cosmogenic samarium-150 and calcium-41 in Norton Country. 40th Lunar and Planetary Science Conference, 23rd – 27th March 2009. The Woodlands, Texas: The Woodlands Waterway Marriott Hotel and Convention Center. Retrieved Sept 3, 2010, from http://www.lpi.usra.edu/meetings/lpsc2010/pdf/1354.pdf

Fischer, M. J. (2009). Water isotope modelling in the Murray Darling Basin. Water and Energy Cycle of the Murray-Darling Basin Workshop 2009, 6th – 7th April 2009. Sydney, Australia: University of New South Wales. Retrieved Sept 3, 2010, from http://web.maths.unsw.edu.au/~jasone/mdb_rhp/workshop09/presentations/fischer.pdf

Keiser, D. D., Robinson, A. B., Jue, J. F., Medvedev, P., and Finlay, R. (2009). Characterization of the microstructure of irradiated U-MO dispersion fuel with a matrix that contains SI. Research Reactor Fuel Management 2009 (RRFM2009), 22nd – 25th March 2009. Vienna, Austria: Vienna International Centre (VIC). In *RRFM 2009 Transactions* (2009). Retrieved Sept 3, 2010, from http://www.euronuclear.org/meetings/rrfm2009/transactions/rrfm09-transactions-session-2.pdf

Knott, R. (2009). Liposome structure using small angle X-ray and neutron scattering (SAXS and SANS). International Conference on Neutron and X-Ray Scattering 2009 (ICNX 2009), 29th June – 1st July 2009. Kuala Lumpur, Malaysia: Putra World Trade Centre. In Abdul Aziz, B. M. (Ed.). *AIP Conference Proceedings: Neutron and X-Ray Scattering in Advancing Materials Research* (Vol. 1202). College Park, Maryland: American Institute of Physics.

Lumpkin, G. R., Smith, K. L., Blackford, M. G., Thomas, B. S., Whittle, K. R., Attard, D. J., et al. (2009). Experimental and atomistic modelling study of ion irradiation damage in thin crystals of the Ti02 polymorphs. Materials Research Society 2008 Fall Meeting (Symposium Q), 1st – 5th December 2008. Boston, Massachusetts: Hynes Convention Center. In N. C. Hyatt, D. A. Pickett and R. B. Rebak (Eds.). Scientific Basis for Nuclear Waste Management XXXII: *MRS Proceedings* (Vol. 1124, Paper #1124-Q04-09). Pennsylvania, America: Materials Research Society.

Lumpkin, G. R., Whittle, K. R., Smith, K. L., Blackford, M. G., and Zaluzec, N. J. (2009). Electron scattering and the order-disorder problem in ion irradiated pyrochlore compounds. Materials Research Society 2008 Fall Meeting (Symposium O), 1st – 5th December 2008. Boston, Massachusetts: Hynes Convention Center. In K. E. Sickafus, A. Navrotsky, and S. R. Phillpot (Eds.). Structure/Property Relationships in Fluorite-Derivative Compounds: *MRS Proceedings* (Vol. 1122E, Paper # 1122-O09-03). Pennsylvania, America: Materials Research Society.

Meyer, F. W., Galutschek, E., and Hotchkis, M. (2009). Low-energy grazing ion-scattering from Alkali-Halide surfaces: a novel approach to C-14 detection. 20th International Conference on the Application of Accelerators in Research and Industry (CAARI 2008), 10th – 15th August 2008. Fort Worth, Texas: Renaissance Worthington Hotel. In McDaniel, F. D. (Ed.). *AIP Conference Proceedings: Application of Accelerators in Research and Industry* (Vol. 1099). College Park, Maryland: American Institute of Physics.

Mo, L., Bignell, L. J., Steele, T., and Alexiev, D. (2009). Activity measurements of 3h using the TDCR method and observation of source stability. International Committee on Radionuclide Metrology (ICRM) 2009 Conference, 7th – 11th September 2009. Bratislava, Slovak Republic: Slovak Institute of Metrology. In *Applied Radiation and Isotopes,* 68 (7-8), 1540-1542.

Pedro, J., Smith, A., Duldig, M. L. Klekociuk, A., Simon, K., Curran, M., et al. (2009). 10Be concentrations in snow at Law Dome, Antarctica, following the 29 October 2003 and 20 January 2005 solar cosmic ray events. Asia Oceania Geosciences Society 4th Annual Meeting (AOGS2007), 30th July – 4th August 2007. Bangkok, Thailand: Queen Sirikit National Convention Centre. In M. Duldig (Ed.). *Advances in Geosciences: Solar Terrestrial* (Vol. 14, pp. 285-303). Toh Tuck Link, Singapore: World Scientific Publishing Company.

Peterson, M. A., Waring, C. L., and Mitry, W. H. (2009). Discrete interval sampling and pressure measurements in uncased boreholes using a zone-of-interest groundwater sampler (zoigs). Groundwater in the Sydney Basin Symposium, 4th – 5th August 2009. Sydney, Australia: Australian Technology Park. In W. A. Milne Home (Ed.). *Groundwater in the Sydney Basin Symposium: Proceedings* (CD-ROM). Sydney, Australia: IAH NSW Branch.

Scarff, S. A., Hughes, C. E., and Morrison, T. N. (2009). Use of isotopic and chemical tracers to determine water flow pathways in a small agricultural catchment during a rain event. Groundwater in the Sydney Basin Symposium, 4th – 5th August 2009. Sydney, Australia: Australian Technology Park. In W. A. Milne Home (Ed.). *Groundwater in the Sydney Basin Symposium: Proceedings* (CD-ROM). Sydney, Australia: IAH NSW Branch.

Short, S. A., Waring, C. L., Peterson, M. A., Hammond, M. S., and Wood, J. (2009). Studies of near-surface hydrology and hydrogeology of the Woronora plateau. Groundwater in the Sydney Basin Symposium, 4th – 5th August 2009. Sydney, Australia: Australian Technology Park. In W. A. Milne Home (Ed.). *Groundwater in the Sydney Basin Symposium: Proceedings* (CD-ROM). Sydney, Australia: IAH NSW Branch.

Vance, E. R., Perera, D. S., Hanna, J. V., and Aly, Z. (2009). Metakaolinite geopolymers for immobilization of nuclear waste. 33rd International Conference on Advanced Ceramics and Composites, 18th – 23rd January 2009. Daytona Beach, Florida: Hilton Daytona Beach Resort and Ocean Center. In the American Ceramic Society (2009), *Proceedings on the 33rd International Conference on Advanced Ceramics and Composites* (CD-ROM). Westerville, Ohio: The American Ceramic Society.

Waring, C. L., Stepanyants, Y. A., Hankin, S., Airey, P. L., and Peterson, M. A. (2009). Measurement of hydraulic conductivity, porosity and lithology by neutron activation borehole logging at high spatial resolution increments. Groundwater in the Sydney Basin Symposium, 4th – 5th August 2009. Sydney, Australia: Australian Technology Park. In W. A. Milne Home (Ed.). *Groundwater in the Sydney Basin Symposium: Proceedings* (CD-ROM). Sydney, Australia: IAH NSW Branch.

Whittle, K. R., Blackford, M. G., Lumpkin, G. R., Smith, K. L., and Zaluzec, N. J. (2009). In situ radiation damage studies of Ca3Zr2FeAlSiO12 and Ca3Hf2FeAlSiO12. Materials Research Society 2008 Fall Meeting (Symposium Q), 1st – 5th December 2008. Boston, Massachusetts: Hynes Convention Center. In N. C. Hyatt, D. A. Pickett and R. B. Rebak (Eds.). Scientific Basis for Nuclear Waste Management XXXII: *MRS Proceedings* (Vol. 1124, Paper #1124-Q10-08). Pennsylvania, America: Materials Research Society.

Whittle, K. R., Smith, K. L., Blackford, M. G., Redfern, S. A. T., Harvey, E. J., Zaluzec, N. J., et al. (2009). Ion irradiation of ternary pyrochlores. Materials Research Society 2008 Fall Meeting (Symposium O), 1st – 5th December 2008. Boston, Massachusetts: Hynes Convention Center. In K. E. Sickafus, A. Navrotsky, and S. R. Phillpot (Eds.). Structure/Property Relationships in Fluorite-Derivative Compounds: *MRS Proceedings* (Vol. 1122E, Paper # 1122-O08-03). Pennsylvania, America: Materials Research Society.

Whittle, K. R., Smith K. L., Blackford, M. G., Redfern, S. A. T., Harvey, E. J., Zaluzec, N. J., et al. (2009). Pyrochlore to fluorite transitions – ordering in fluorites? Materials Research Society 2008 Fall Meeting (Symposium O), 1st – 5th December 2008. Boston, Massachusetts: Hynes Convention Center. In K. E. Sickafus, A. Navrotsky, and S. R. Phillpot (Eds.). Structure/Property Relationships in Fluorite-Derivative Compounds: *MRS Proceedings* (Vol. 1122E, Paper # 1122-O03-01). Pennsylvania, America: Materials Research Society.

ANSTO Acknowledgements 2009

Abrasonis, G., Kovacs, G. J., Ryves, L., Krause, M., Mucklich, A., Munnik, F., et al. (2009). Phase separation in carbon-nickel films during hyperthermal ion deposition. Journal of Applied Physics, 105(8), 8.

Eppel, G. A., Lo Jacono, D., Shirai, M., Umetani, K., Evans, R. G., and Pearson, J. T. (2009). Contrast angiography of the rat renal microcirculation *in vivo* using synchrotron radiation. *American Journal of Physiology-Renal Physiology, 296(5),* F1023-F1031.

Gehman, J. D., and Provis, J. L. (2009). Generalized biaxial shearing of MQMAS NMR spectra. *Journal of Magnetic Resonance, 200(1*), 167-172.

Guilfoyle, A., Maher, M. J., Rapp, M., Clarke, R., Harrop, S., and Jormakka, M. (2009). Structural basis of GDP release and gating in g protein coupled fe2+ transport. *EMBO Journal, 28*(17), 2677-2685.

Hogg, A., Ramsey, C. B., Turney, C., and Palmer, J. (2009). Bayesian evaluation of the southern hemisphere radiocarbon offset during the Holocene. *Radiocarbon, 51(4),* 1165-1176.

Jacques, D. A., Streamer, M., Rowland, S. L., King, G. F., Guss, J. M., Trewhella, J., et al. (2009). Structure of the sporulation histidine kinase inhibitor SDA from bacillus subtilis and insights into its solution state. *Acta Crystallographica Section D-Biological Crystallography, 65,* 574-581.

Kondev, F. G., Dracoulis, G. D., Lane, G. J., Ahmad, I., Byrne, A. P., Carpenter, M. P., et al. (2009). Multi-quasiparticle isomers in lu-174. *Physical Review C, 80(1),* 9.

McConnachie, A. W., Irwin, M. J., Ibata, R. A., Dubinski, J., Widrow, L. M., Martin, N. F., et al. (2009). The remnants of galaxy formation from a panoramic survey of the region around m31. *Nature, 461*(7260), 66-69.

Page, M. G., and Warr, G. G. (2009). Influence of the structure and composition of mono- and dialkyl phosphate mixtures on aluminum complex organogels. *Langmuir, 25(15),* 8810-8816.

Sniderman, J. M. K., Finn, J., and Denham, T. P. (2009). A late-Holocene palaeoecological record from Ambra Crater in the highlands of Papua New Guinea and implications for agricultural history. *Holocene, 19(3),* 449-458.

Watanabe, H., Lane, G. J., Dracoulis, G. D., Byrne, A. P., Nieminen, P., Kondev, F. G., et al. (2009). Identification of j(pi)=19/2(+) and 23/2(+) isomeric states in sb-127. *European Physical Journal A, 42(2),* 163-169.

Watanabe, H., Lane, G. J., Dracoulis, G. D., Byrne, A. P., Nieminen, P., Kondev, F. G., et al. (2009). Multi-quasiparticle isomers involving proton-particle and neutron-hole configurations in i-131 and i-133. *Physical Review C,* 79(6), 8.

Watanabe, H., Lane, G. J., Dracoulis, G. D., Kibedi, T., Byrne, A. P., Nieminen, P., et al. (2009). Decay properties of high-spin isomers and other structures in sb-121 and sb-123. *Physical Review C, 79(2),* 15.

Wroe, A., Schulte, R., Fazzi, A., Pola, A., Agosteo, S., and Rosenfeld, A. (2009). RBE estimation of proton radiation fields using a Delta E-E telescope. *Medical Physics, 36(10),* 4486-4494.

ANSTO

SCIENCE AND TECHNOLOGY

AUSTRALIAN NUCLEAR SCIENCE AND TECHNOLOGY ORGANISATION

www.ansto.gov.au

June 2010